The influence of particle size and devolatilisation conditions on the CO_2 gasification of Highveld coal

GL van der Merwe, B.Eng (Chemical Engineering)

Dissertation submitted in fulfilment of the requirements for the degree Magister in Engineering at the School of Chemical and Minerals Engineering at the North-West University, Potchefstroom campus.

Supervisor: Prof. HWJP Neomagus

Co-supervisors: Prof. RC Everson and Prof. JR Bunt

Declaration

I, Gerhard Léon van der Merwe, hereby declare that the dissertation entitled: **"The influence of particle size and devolatilisation conditions on the CO_2 gasification of Highveld coal",** submitted in fulfilment of the requirements for the degree M.Eng is my own work, except where acknowledged in the text, and has not been submitted to any other tertiary institution in whole or in part.

Signed at Potchefstroom.

_____ _____

Gerhard L. van der Merwe Date

Synopsis

The influence of particle size and devolatilisation conditions on the CO_2 reactivity of Highveld seam 4 run of mine coal were investigated in a large particle thermo-gravimetric system. Particle sizes of 5 mm, 10 mm, 20 mm and 40 mm were chosen for both the devolatilisation and the gasification experiments. The devolatilisation experiments were done by placing the coal particles in an electrically preheated tube furnace at isothermal temperatures of 450°C, 700°C and 850°C. The reactivity of the resulting chars was subsequently determined at 900°C using 100% CO_2.

Coal samples were characterised in terms of proximate analysis, ultimate analysis, calorific value as well as SSNMR. The characterisation results indicated that there is no significant difference across the particle size range in terms of the chemical composition and the structural parameters obtained from SSNMR.

Devolatilisation results showed that an increase in temperature resulted in an increase in both devolatilisation rate and volatile yield, with the volatile yield at 850°C being similar to that obtained from proximate analysis for all particle sizes. An increase in particle size resulted in an increase in devolatilisation time and a decrease in devolatilisation rate. For devolatilisation of all particle sizes at 450°C, a distinct plateau in the weight loss curves was observed. The plateau is indicative that the devolatilisation is controlled by heat transfer through the coal particle. This phenomenon is less pronounced at higher temperatures.

Due to significant particle fragmentation of large particles at high temperatures, the gasification kinetics of 40 mm chars obtained at 700°C and 850°C could not be determined. The rate of gasification increased with a decrease in particle size while the devolatilisation temperature showed no significant effect for 5 mm and 10 mm particles. Some scatter in the gasification results was observed for 20 mm particles. This might be due to a higher degree of particle fragmentation occurring at the onset of gasification. Different conversion times were found to have a linear relation to the particle size. The gasification results were modelled using a shrinking unreacted core model in the kinetic controlled regime. The reaction kinetic constant showed some particle size dependence that could be due to particle fragmentation and the temperature profile inside the oven. The model showed a good fit for all results.

Acknowledgements

This work is dedicated to Léon van der Merwe.

A loving father and friend who always inspired me to greater things.

The author hereby wishes to acknowledge and thank all the people who played a major role through the course of this project and would especially like to send out a wish of gratitude to the following:

- Professors Hein Neomagus, John Bunt and Ray Everson for their excellent guidance and assistance. Without their critical evaluation and insightful suggestions this work would not have been a reality.
- Sasol for their financial support with regards to this investigation.
- Mr Jan Kroeze and Mr Adrian Brock for their technical advice and assistance with regards to experimental equipment and procedures.
- All the personnel of the School of Chemical and Minerals Engineering.
- The coal research group for valuable input during group discussions and meetings.
- Heidi Assumption for doing the SSNMR analysis as well as valuable discussions.
- All the people who shared the office with me over the last two years, for always making the office an interesting and stimulating working environment.
- My parents, sisters and my brother for their continued support and motivation.
- And lastly to my better half, Cazandra for her much appreciated love and support.

Table of Contents

Declaration ii
Synopsis iii
Acknowledgements iv
Table of Contents v
List of Tables ix
List of Figures x
Symbols xii
Abbreviations xiii
Chapter 1: Introduction 1
1.1. Background and Motivation 1
1.2. Objectives 5
1.3. Scope 6
Chapter 2: Literature Survey 7
2.1. Introduction 7
2.2. Coal Properties 7
2.2.1. Coal formation and chemical properties of coal 7
2.3. Devolatilisation 10
2.3.1. Mechanism of devolatilisation 12
2.3.2. Extent of devolatilisation 16
2.3.3. Devolatilisation time and rate 18
2.3.4. Effect of particle size 20
2.4. Gasification 23
2.4.1. Introduction 23
2.4.2. Gasification temperature 24
2.4.3. Devolatilisation temperature 24

2.4.4. Heating rate during devolatilisation 25
2.4.5. Coal rank 25
2.4.6. Effect of particle size 26
2.4.7. Mineral matter content 27
2.4.8. Other factors influential to gasification 28
2.4.9. Gasification modelling 28
2.5. Solid State Nuclear Magnetic Resonance 31
2.5.1. Introduction 31
2.5.2. Different SSNMR techniques 32
2.5.3. Accuracy and reliability of results 35
2.5.4. Different carbon fractions 32
Chapter 3: Experimental 37
3.1. Introduction 37
3.2. Materials 37
3.3. Sample Preparation from ROM coal 37
3.4. Characterisation 39
3.4.1. Conventional analyses 39
3.4.2. Solid state NMR 40
3.5. Devolatilisation 43
3.5.1. Particle selection 43
3.5.2. Devolatilisation equipment 46
3.5.3. Devolatilisation procedure 48
3.6. Gasification 49
3.6.1. Particle selection 49
3.6.2. Gasification equipment 49
3.6.3. Gasification procedure 50
3.7. Error calculations 51

Chapter 4: Results and Discussion 52
4.1. Introduction 52
4.2. Characterisation 52
4.2.1. Conventional analyses 52
4.2.2. Solid state NMR 54
4.3. Devolatilisation 60
4.3.1. Experimental results representation 61
4.3.2. Effect of particle size 63
4.3.3. Effect of devolatilisation temperature 69
4.4. Gasification 72
4.4.1. Experimental results representation 72
4.4.2. Effect of devolatilisation temperature 75
4.4.3. Effect of particle size 79
4.5. Initial reactivity 83
4.6. Gasification modelling 88
4.6.1. Determining reaction mechanism 88
4.6.2. Determining reaction constants 89
Chapter 5: Conclusions and Recommendations 92
5. Conclusions 92
5.1. Coal characterisation 92
5.2. Devolatilisation results 93
5.3. Gasification results 93
5.4. Gasification modelling 93
5.5. Recommendations 94
References 96
Appendix A: Devolatilisation 105
Appendix B: Gasification 111

Appendix C: Modelling 115

List of Tables

Table 1: Ultimate analyses of South African coal fields (England, 2002). 9
Table 2: Average heating rates at 95% devolatilisation times. 17
Table 3: SSNMR integration regions and notations 34
Table 4: Carbon fractions from NMR analyses. 34
Table 5: List of materials. 37
Table 6: Sieve size ranges and mass yield for each size range. 38
Table 7: Conventional analysis standards 39
Table 8: Devolatilisation TGA setup specifications. 47
Table 9: Devolatilisation experimental work sheet. 49
Table 10: Gasification experimental work sheet. 51
Table 11: Proximate analyses results over particle size range (adb) 52
Table 12: Ultimate analyses results over particle size range (daf – wt%) 53
Table 13: Calorific values for different particle sizes 54
Table 14: Region integration values for three size ranges 59
Table 15: Solid state NMR characteristic carbon types for three size ranges 59
Table 16: Percentage volatiles released at different experimental conditions. 71
Table 17: Initial reactivity of different size char particles prepared at different devolatilisation temperatures. 87
Table 18: Reaction rate constants at different experimental conditions. 91

List of Figures

Figure 1: Coal consumption in South-Africa. 2
Figure 2: Different gasifier configurations (taken from Kristiansen (1996)). 4
Figure 3: Different stages of coal formation. 8
Figure 4: Molecular representation of a high volatile bituminous coal as given by Shinn (1984). 13
Figure 5: Coal structure (Serio *et al.*, 1987).....14
Figure 6: Primary devolatilisation (Serio *et al.*, 1987). 15
Figure 7: Secondary devolatilisation (Serio *et al.*, 1987).....16
Figure 8: Illustration of fragmentation during particle heating adopted from Dacombe *et al.*, (1999). 22
Figure 9: Identified functional groups on SSNMR spectra with integration regions from Suggate & Dickinson (2004).....33
Figure 10: Demineralisation setup.....41
Figure 11: Filtration setup for HF acid 42
Figure 12: Example of 5 mm particles after preparation. 44
Figure 13: Example of 10 mm hand selected particles. 44
Figure 14: Example of a 20 mm hand selected particle. 45
Figure 15: Example of a 40 mm hand selected particle. 45
Figure 16: Large particle TGA setup. 46
Figure 17: Bucket system for large particle devolatilisation. 47
Figure 18: Quartz sample holder used for gasification.....50
Figure 19: CPMAS spectrum and integration regions for the +3.35 mm to -6.3 mm size range. 55
Figure 20: CPMAS spectrum and integration regions for the +12.5 mm to -25 mm size range. .55
Figure 21: CPMAS spectrum and integration regions for the +25mm to -53 mm size range. 56
Figure 22: DD spectrum and integration regions for the +3.35 mm to -6.3 mm size range. 57
Figure 23: DD spectrum and integration regions for the +12.5 mm to - 25 mm size range. 57
Figure 24: DD spectrum and integration regions for the +25 mm to - 53 mm size range. 57
Figure 25: Raw mass loss data for devolatilisation of 40 mm particles at 700°C. 61
Figure 26: Repeatability for devolatilisation experiments for 40 mm particles at 700°C. 62
Figure 27: Representation of average devolatilisation result (for 40 mm particles at 700°C). 63

Figure 28: Particle size devolatilisation at 450°C. 64
Figure 29: Schematic for devolatilisation of large coal particles. 65
Figure 30: Particle size devolatilisation at 700°C. 66
Figure 31: Particle size devolatilisation at 850°C. 67
Figure 32: Fragmentation of 40 mm particle at a devolatilisation temperature of 850°C. 68
Figure 33: Devolatilisation of 5 mm particle at different temperatures. 70
Figure 34: Raw mass loss data for 10 mm chars prepared at 450°C. 72
Figure 35: Normalised mass loss data for 10 mm char particles prepared at 450°C. 73
Figure 36: Carbon conversion for 10 mm chars prepared at 450°C. 74
Figure 37: Averaged carbon conversion for 10 mm chars. 75
Figure 38: CO_2 gasification of 5 mm particle at different devolatilisation temperatures 76
Figure 39: CO_2 gasification of 10 mm particle at different devolatilisation temperatures 77
Figure 40: CO_2 gasification of 20 mm particle at different devolatilisation temperatures 77
Figure 41: CO_2 gasification of 40 mm particle with devolatilisation temperature of 450°C. 79
Figure 42: CO_2 gasification of different particle sizes prepared at 450°C. 80
Figure 43: CO_2 gasification of different particle sizes prepared at 700°C. 81
Figure 44: CO_2 gasification of different particle sizes prepared at 850°C. 82
Figure 45: Influence of particle size on time to reach 30%, 50%, 70% and 90% conversion. 83
Figure 46: Initial CO_2 reactivity for 5 mm char particles prepared at different devolatilisation temperatures. 84
Figure 47: Initial CO_2 reactivity for 10 mm char particles prepared at different devolatilisation temperatures. 85
Figure 48: Initial CO_2 reactivity for 20 mm char particles prepared at different devolatilisation temperatures. 86
Figure 49: Initial CO_2 reactivity for 40 mm char particles prepared at devolatilisation temperature of 450°C. 87
Figure 50: Conversion models for gasification at 900°C. 89
Figure 51: SUCM for different sized chars prepared at 450°C. 90

Symbols

Symbol	Description	Units
A	Gas reagent	-
B	Solid reagent	-
b	Solid reagent stoichiometric coefficient	-
	Biot number	-
C_{Ag}	Concentration of reactant gas	mol/m^3
C-al	Total aliphatic carbon	-
C-ar	Total aromatic carbon	-
D_e	Effective ash layer diffusion coefficient	m^2/s
fa	Fraction aromatic carbon	-
faB	Fraction bridgehead carbons	-
faCO	Fraction carbonyl & carboxyl carbons	-
faH	Fraction protonated aromatic carbons	-
fal	Fraction aliphatic carbons	-
falH	Fraction methyl aliphatic carbons	-
falN	Fraction non-protonated aliphatic carbons	-
falO	Fraction aliphatic carbons attached to oxygen	-
faN	Fraction non-protonated aromatic carbons	-
faP	Fraction phenolic aromatic carbons	-
faS	Fraction of alkylated aromatic carbons	-
	Convective heat transfer coefficient	W/m^{2}K
k''	First order rate constant	m/s
	Thermal conductivity of solid	W/mK
	Characteristic length	m
	Mass loss at given time	g
	Initial mass of sample/particle	g
	Initial mass of sample after devolatilisation	g
	Mass ash remaining after gasification	g
	Mass loss from devolatilisation with onset of gasification	g
ρ	Particle density (molar)	mol/m^3
R	Particle radius	m
Ri	Initial reactivity	-/min
R^2	Goodness of fit value	-
t	Time	s
t_{90}	Time for 90% conversion	s
τ	Time for complete conversion	s
	Conversion	-
	Mass of particles (Images)	g

Abbreviations

Abbreviation	Description
ACE	Associated Chemical Enterprises
adb	Air dry basis
Afrox	African Oxygen Limited
BET	Brunauer-Emmer-Teller
BGL	British Gas and Lurgi
BHEL	Bharat Heavy Electricals Limited
CAF	Central Analytical Facility
CP	Cross-polarisation
CPM	Cylindrical pellet model
daf	Dry ash free
db	Dry basis
DD	Dipolar dephasing
HCl	Hydrochloric acid
HF	Hydrofluoric acid
HV	High volatile
KRW	Kellogg-Rust-Westinghouse
KZN	KwaZulu-Natal
LV	Low volatile
MAS	Magic angle spinning
NMR	Nuclear magnetic resonance
Mt	Million tonnes
PTFE	Polytetrafluoroethylene
RCM	Random capillary model
ROM	Run of mine
RPM	Random pore model
SABS	South-African bureau of standards
Sasol®FBDB™	Sasol fixed bed dry bottom
SP	Single pulse
SSB	Spinning side band
SSNMR	Solid state nuclear magnetic resonance
SU	Stellenbosch University
SUCM	Shrinking unreacted core model
TGA	Thermo gravimetric analyser
TMS	Tetramethylsilane
VM	Volumetric model

Chapter 1: Introduction

1.1. Background and Motivation

The proven recoverable world coal reserves for 2008 were estimated at 1 million ton (Mt), of which 730 000 Mt are hard coal (Coking and steam coals) and 270 000 Mt are brown coal (lignite and sub-bituminous coals). Major coal products produced worldwide include fuel, coke oven coke, gas coke, coal tar, brown coal briquettes, coke oven gas, blast furnace gas and oxygen steel furnace gas (IEA, 2010).

In spite of the limited availability of fossil fuels, with special regards to coal, many different types of coals are present within these reserves. The type of coal is dependent on the degree of coalification or carbonation. Three different types of coal are recognised between peat (substance from which coal is formed) and anthracite (the most extensive degree of coalification). These types or ranks are lignite, sub-bituminous and bituminous coals (World Coal Institute).

The coal reserves that are available in South-Africa mainly consist of anthracites and bituminous coals, with very little to no sub-bituminous coals and lignites. The production of coal in South-Africa in 2008 was over 200 Mtce, with 1 Mtce calculated as 7 million kilocalories (IEA, 2010). The reserve over production ratio for coal in South Africa is estimated at 121 years (BP, 2009) while the reserves for oil and gas are much smaller. Due to the limited availability of our fossil fuels it is very important to use these resources as efficiently as possible (World Coal Institute).

The main consumption of coal in South-Africa is summarised in Figure 1 (Data from IEA 2010).

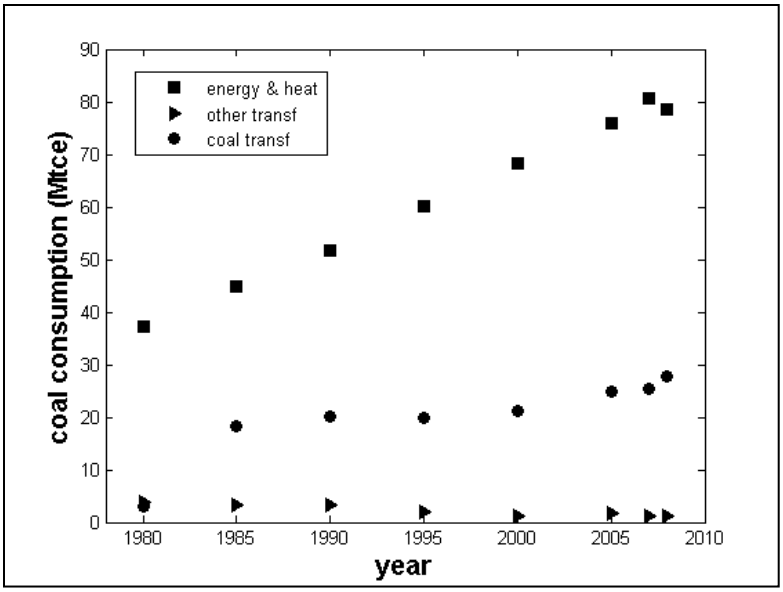

Figure 1: Coal consumption in South-Africa.

From Figure 1 it can be concluded that the demand for coal in South-Africa will continue to increase in order to meet increasing energy demands. Coal in South-Africa is mainly used for energy and heat production, followed by other types of transformations ("coal transf") including liquefaction. Secondary and tertiary coal transformations ("other transf") include coke, briquettes, coke oven gas and blast furnace gas and accounts for the lowest amount of coal usage (IEA, 2010).

The main areas for coal utilisation include steam generation via steam coal or lignite, and iron and steel productions via coking coal. With South-Africa being one of the top 5 coal producers in the world, and the fact that only 18% of all produced coal will reach the global market, it is clear that South-Africa produces enough coal to meet its own demand in terms of energy and fuel production (World Coal Institute).

South-Africa's synfuels and petrochemical industry rely greatly on coal feedstock for the production of CO and H_2. The Sasol® FBDB™ gasifiers are used in the conversion of coal for the production of fuels and chemicals via the Fisher-Tropsh process (van Dyk *et al.*, 2006 b; van Dyk & Waanders, 2007). During this conversion of coal into synthesis gas, multiple reactions such as devolatilisation, combustion and gasification take place. The properties of the coal will greatly influence these reactions and are therefore one of the deciding factors when selecting the type of gasifier.

Collot *et al.* (2006) listed the following parameters that will influence future design of gasifiers, both in terms of conversion and product spectrum.

- Coal composition and rank
- Coal preparation or particle size/density
- Gasification agents
- Gasification conditions such as temperature, heating rate, pressure and residence time
- Various plant configurations

According to Collot *et al.* (2006) and Kristiansen (1996) the three major gasifier configurations are entrained flow gasifiers, fluidised bed gasifiers and moving or fixed bed gasifiers. The configurations for these three gasifier types are shown in Figure 2 (Kristiansen, 1996).

Typically, entrained flow gasifiers operate at pressures from 2.7 MPa to 4.1 MPa and temperatures ranging from 600°C to 1650°C. Furthermore, small particles (<0.1 mm) are used resulting in very short particle residence time while still achieving high carbon conversions. The Shell and GE Energy gasification reactors are examples of entrained flow gasifiers (Chen *et al.*, 2001; Chen *et al.*, 2000; Zheng & Furinsky, 2005).

For fluidised beds the typical operating pressure ranges from 1.3 MPa to 2.1 MPa while operating temperatures range from 800°C to 1040°C. In most fluidised gasification systems, particles of less than 10 mm are used. Examples of fluidised bed gasifiers include the KRW and BHEL gasification systems (Collot *et al.*, 2006; Zheng & Furinsky, 2005; Higman & van der Burgt, 2008).

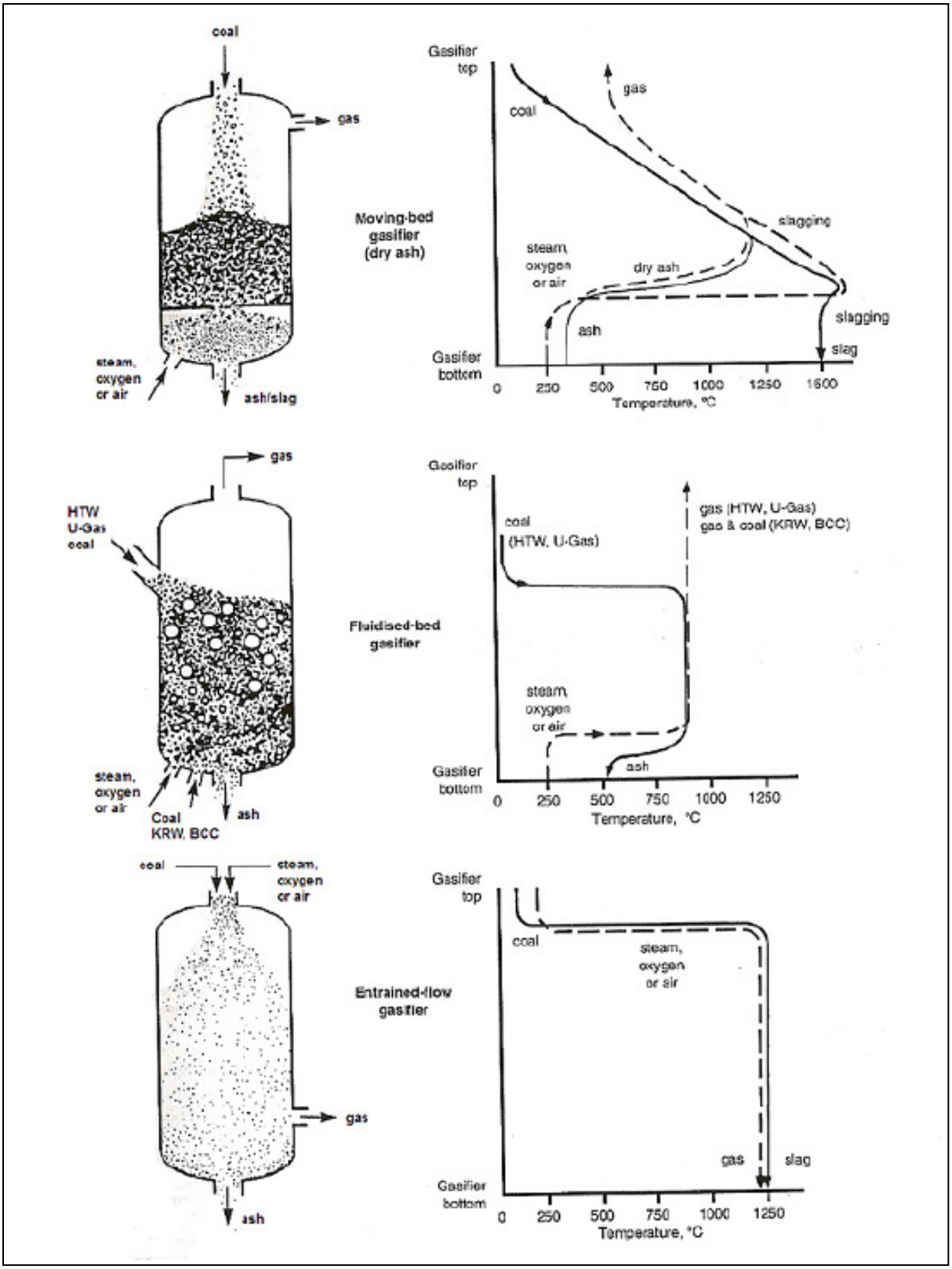

Figure 2: Different gasifier configurations (taken from Kristiansen (1996)).

Fixed or moving bed gasifiers typically operate at pressures between 1 MPa and 3 MPa with operating temperatures as high as 2000°C. The particle size used during gasification ranges from 5 mm to 80 mm (Collot *et al.*, 2006). During fixed bed gasification the gas flows upward in the reactor while the coal moves downwards as the ash is removed at the bottom of the reactor. The particle residence time in fixed bed gasification is the longest of the three major gasifier configurations. Systems with concurrent gas and coal flow are also available, but are not as commonly used as counter current systems. The Sasol® FBDB™ and BGL gasification systems are examples of fixed or moving bed gasifiers (Collot *et al.*, 2006; Zheng & Furinsky, 2005; Higman & van der Burgt, 2008).

In almost all coal processes the coal feed particles undergo an initial devolatilisation stage. During devolatilisation the coal is heated to a temperature at which the volatile components within the coal are driven off. Because of the heterogeneity of coal, the amount and nature of the volatiles vary according to coal type. While experimental work regarding devolatilisation reactions and products has been done, this work was mainly limited to particle sizes of less than 1 mm (Porada, 2004). Explorative work has been carried out on devolatilisation and gasification of particles ranging from 19 mm to 26 mm particles (du Plessis, 2007; van Wyk, 2007). The aim of this work is to do an extensive study of the influence of particle size and temperature on the devolatilisation of a typical Highveld coal, and also to investigate how the reactivity of the coal is influenced by these variables.

1.2. Objectives

The objectives of this study are:

- To study the devolatilisation process as a function of particle size and temperature for particles larger than 5 mm.
- To study and model the influence of particle size (larger than 5 mm) and devolatilisation temperature on the char-CO_2 gasification reactivity.

1.3. Scope

The following experimental scope was followed in order to meet the set objectives.

Obtain a ROM coal sample and sieve the sample into size fractions ranging from -1 mm to +53 mm.

From the sieved size fractions, representative samples will be used for conventional analyses. The conventional analyses will include the determination of calorific value, proximate analysis and ultimate analysis. For further characterisation, samples from three size fractions will be demineralised and analysed using SSNMR.

Hand selected large particles (5 mm to 40 mm) are to be devolatilised at temperatures of 450°C, 700°C and 850°C in an atmosphere of nitrogen in a large particle TGA. The results will then be compared using both particle size variation and different devolatilisation temperatures.

The CO_2 gasification reactivity of the resultant chars from the devolatilisation experiments will then be investigated at a temperature of 900°C in a large particle TGA. Results will then be compared in terms of particle size variation and different devolatilisation temperatures.

The gasification experiments will also be modelled using existing particle models that take the effect of particle size into account.

This report is divided into 5 Chapters. In Chapter 1 the background, motivation, scope and objectives of the project are discussed. In Chapter 2 a literature survey regarding coal devolatilisation, gasification and the use of SSNMR is presented. The experimental details are discussed in Chapter 3 and the results obtained are presented in Chapter 4. The conclusions and recommendations are given in Chapter 5.

Chapter 2: Literature Survey

2.1. Introduction

This chapter presents a review of literature with regards to the devolatilisation and the gasification of coal. The formation of coal and the chemical properties of coal are discussed in Section 2.2. Section 2.3 gives coal devolatilisation as a function of various parameters with specific regard to the extent of devolatilisation and the devolatilisation rate. The effect of particle size on devolatilisation is also considered in Section 2.3. In Section 2.4 literature regarding coal gasification as a function of various parameters and the modelling techniques used in literature is reviewed. In Section 2.5 a summary of SSNMR literature is given.

2.2. Coal Properties

2.2.1. Coal formation and chemical properties of coal

The coals that are presently used in South-Africa were formed from various plant materials (that are indigenous to South-Africa) approximately 200 million years ago. This, alongside the fact that different environmental conditions were present during the time that the coals were formed, could explain the different coal properties of northern and southern hemisphere coals. While the coals in the northern hemisphere (typically vitrinite) were formed in a humid coastal like environment, the southern hemisphere coals were formed during an era after the ice age during which to low prevailing temperature was increasing (England, 2002; Neavel, 1981).

Peat serves as the precursor for coal and is formed when leaves and plant debris collect in a swamp like environment. Most of the plant material making up the peat composition must have been growing on the site of formation. Materials such as logs could have

however drifted into the system by means of rivers or streams (as all the coal fields in South Africa were once fresh water collection points) (England, 2002). These layers of peat can then be covered by sediments of sandstone (Neavel, 1981). This process can be repeated, forming consecutive layers of peat and sandstone sediment so that the pressure on, and the temperature of the peat increases as these layers get buried deeper and deeper over time.

Under the influence of the increased pressure and temperature the biological degradation of the peat continues but the rate of the degradation process decreases with time. The reduced degradation rate is mainly due to the decrease in water and oxygen in the coal. The rank of the coal is determined from the degree of coalification. Coal rank ranges from lignite to anthracite, with anthracite being the highest coal rank (Neavel, 1981). The different stages of coalification are shown in Figure 3.

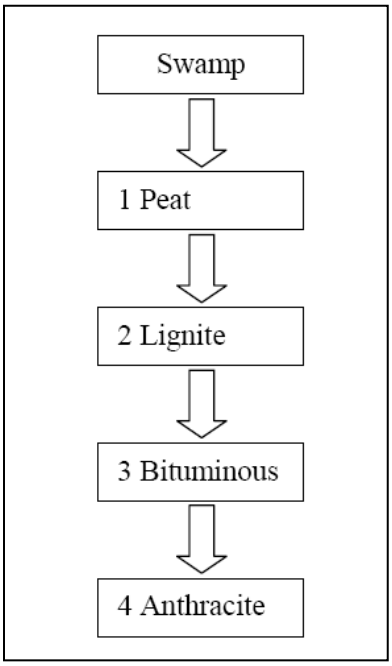

Figure 3: Different stages of coal formation.

The type of coal (rank) and properties of the coal present in a specific area will depend on the material from which the coal was originally formed as well as the degree of coalification that has occurred.

Various coal seams are mined for industrial use across South-Africa. These include principal coalfields in the Witbank-Middelburg area (seams 1-5); the Free-State; Northern KwaZulu Natal; Ermelo; Heidelberg; Waterberg; and the Soutpansberg area. The Witbank number 4 seam is of high economical value and is utilised by Sasol and major power stations. The chemical properties in terms of ultimate analysis for the mentioned coalfields are given in Table 1:

Table 1: Ultimate analyses of South African coal fields (England, 2002).

	Ultimate Analyses		
Coal field	**Carbon (Wt %)**	**Hydrogen (Wt %)**	**Oxygen (Wt %)**
Free-State	77 – 79	4.3 – 4.6	13.5 – 16.5
Heidelberg	79.5	4.2	13.5
Ermelo	80 – 82	5.0 – 5.2	10.5 – 12
Witbank No. 4 Seam	81 – 82.5	4.4 – 4.7	10 – 11.5
Witbank No. 5 Seam	83 – 84	5.1 – 5.4	8.5 – 9
Witbank No. 2 Seam	83 – 85	4.5 – 5.0	8 – 10
Natal Bituminous	84 – 88.5	4.5 – 5.3	4 – 8
KZN Anthracite HV	90 – 91	3.5 – 3.9	2 – 3
KZN Anthracite LV	92	3.0	2

Tang *et al.* (2005) found that coal rank related to coal properties such as volatile matter, hydrogen content, fuel ratio and fixed carbon content. It is also reported that the volatile matter and hydrogen content decreased with rank increase where as the fuel ratio and fixed carbon content increased as the coal rank increased.

The thermal stability of coals also changes with different rank. The intensity of the instability is determined by the quantity of volatiles released at a certain temperature. The volatile release can be used as a measure of decomposition of the coal components (van Heek, 2000). The devolatilisation behaviour of the coal can be widely influenced by the chemical structure of the parent coal (Fletcher *et al.*, 1992).

The O/C and H/C ratios for coals tend to decrease with increasing rank. During devolatilisation however Fletcher *et al.* (1992) showed that O and H are released at similar rates resulting in ratios for different rank coals to tend towards the ratios observed for high rank coals. Lu *et al.* (2000) also found a decrease in H/C and O/C

ratios with increase in devolatilisation temperature up to a maximum temperature of 1200°C.

Various amounts of other chemical properties, such as moisture and mineral matter content (both inherent and extraneous), also form part of the coal composition. Both these properties tend to decrease the heating value of the coal and the mineral matter results in the residue (ash) after the coal is reacted to completion (England, 2002). Some mineral transformations can occur during conversion processes resulting in the ash having different compositions than the original mineral matter content of the coal. Literature also shows that the influence of inorganic compounds within the coal during conversion processes cannot be ignored as these can have catalytic effects. Furthermore, products such as CO_2 and H_2O can be formed from decomposition reactions (Solomon *et al.*, 1992; van Dyk *et al.*, 2006 a).

2.3. Devolatilisation

The devolatilisation process is often characterised by the weight loss profile created over a period of time as a function of temperature. Most devolatilisation curves are identified by a fast initial weight loss until about 80% conversion followed by a much slower weight loss until complete devolatilisation (Solomon *et al.*, 1992).

Both physical and chemical changes within the coal or char particle occur during devolatilisation and have subsequent effects on the devolatilisation behaviour of the particle (Kim *et al.*, 2008). Chemical reactions that appear during devolatilisation include bond breaking and cross linking.

A wide variety of processes are affected by devolatilisation; including particle softening, swelling, and fragmentation. The physical structure and reactivity of the resultant char is also influenced by the devolatilisation process (Lee *et al.*, 2002; Solomon *et al.*, 1992). Furthermore, pressure and particle density can also have varying effects on the behaviour of coal or char particles during devolatilisation. Depending on parent coal properties, coal particles can show different swelling or contraction behaviour during devolatilisation with increase in pressure, while an increase in particle density will generally result in less swelling compared to low density particles (Strezov *et al.*, 2005).

Different devolatilisation conditions can also have varying effects on the chemical structure of the generated chars. Lu *et al.* (2000) investigated the change in properties such as average stacking height, aromaticity, crystallite size, graphitic sheet interlayer spacing and interchain spacing for aliphatic rings. They found that the crystallite size, aromaticity and average stacking height for the low rank coals increased with increase in devolatilisation temperature. The interlayer spacing for the graphitic sheets, interchain spacing for aliphatic rings and stacking height for the high rank coals decreased with increase in devolatilisation temperature (Lu *et al.*, 2000).

The large variation in devolatilisation results reported in literature can be caused by a multitude of factors such as different equipment used; different experimental conditions; different techniques; different definitions used to evaluate complete devolatilisation; coal type; particle size; batch size and degree of fragmentation (Stubington *et al.*, 1991; Stubington & Sasongko, 1998; Ross *et al.*, 2000; Solomon *et al.*, 1992).

Investigations into devolatilisation of coal particles can broadly be divided into two categories. The first being experiments done in fluidised bed reactors or drop tube furnaces where the coal particles can move unobstructed during the experiments. The second category comprises TGA systems and other experimental setups where the particles are stationary. Comparison of results from the two different setups is difficult due to the different heating environments. Devolatilisation times from stationary particle systems tend to exceed that obtained from fluidised bed systems (Stubington *et al.*, 1997).

Excessive movement of the particles in fluidised bed systems will cause the degree of fragmentation to be much higher than that for stationary particle systems, which could explain the enhanced devolatilisation rate (Peeler & Poynton, 1992). The observed trends with regards to aspects such as temperature and particle size do, however, seem to be consistent. Due to similar heating conditions in TGA systems and tube reactor systems the results obtained are more comparable (Stubington *et al.*, 1991).

The definition of devolatilisation time used in literature varies depending on the techniques used during experimentation. Different definitions are used because of the slow lagging behaviour of the final mass loss at the end of devolatilisation. Different devolatilisation time definitions include: mass loss equal to either 90% or 95% of volatile mass loss as determined from proximate analysis, flame extinction time and when mass

loss is less than 0.01% of volatile content determined from proximate analysis (Ross *et al.*, 2000; Stubington & Sasongko, 1998; Stubington *et al.*, 1991; Stubington *et al.*, 1997).

2.3.1. Mechanism of devolatilisation

Industrial processes such as liquefaction and gasification start with a wide range of reactions that cause molecular transformation of the feedstock (coal, biomass, oil, etc.) at different thermal conditions (Stock, 1989). The thermal decomposition of coal during devolatilisation processes makes up a major part of the coal chemistry investigated in literature. Research on a molecular level is rarely attempted due to the complexity of these reactions; for this reason coal research investigations are either done on the coal matrix as a whole or on pure compounds found in the coal (Stock, 1989).

A proposed representation of the molecular structure of high volatile bituminous coal is shown in Figure 4 (Shinn, 1984). Models are made up of thermally stable aromatic ring clusters that are randomly connected by less thermally stable aliphatic cluster attachments. Different functional groups make up the attachments found in coals/chars and include alkyl and oxygen functional groups. These attachments are bonded to the aromatic structure by means of bridges, side chains and loops.

Figure 4 shows how smaller molecules can be trapped inside the coal structure that can extend into a three dimensional molecular network. The extension of the model into a three dimensional structure is indicated by the (~) sign. When the structure is heated (during devolatilisation), the bonds connecting these clusters randomly break (release of volatile matter occurs) resulting in a multitude of simultaneously occurring reactions and transformation (Solomon & Serio, 1994; Fletcher *et al.*, 1992).

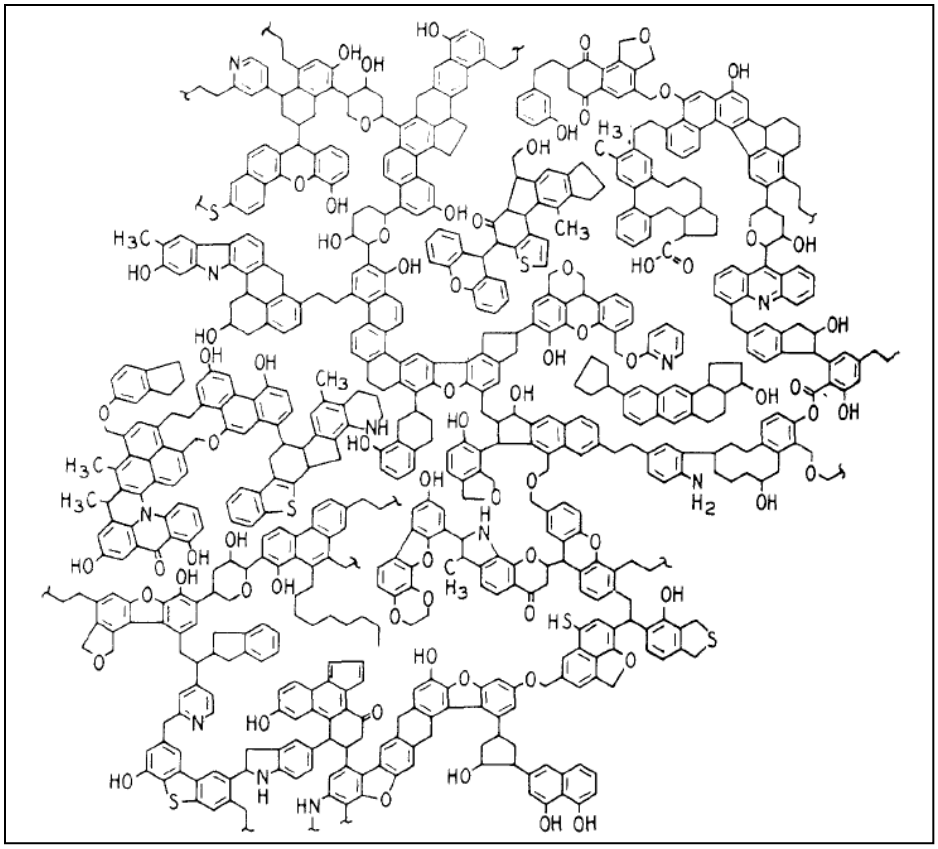

Figure 4: Molecular representation of a high volatile bituminous coal as given by Shinn (1984).

The decomposition of coal during devolatilisation is a complex matrix of reactions, some of which are not yet completely understood. With regards to the mechanism of devolatilisation, issues such as water release, gas and tar formation, transport to the exterior of the particle and the chemistry involved in this process need to be addressed. Some view devolatilisation as a depolymerisation reaction occurring parallel with thermal decomposition reactions all competing for the available hydrogen to form stable structures (Solomon & Hamblen, 1985).

Different mechanisms are used to describe various devolatilisation models. Most mechanisms however use combinations of bridge or bond breaking, cross linking and substitution reactions. Bond breakage reactions are divided into two groups; first, being breakage that results in the release of small molecular groups from the macromolecular network; and second, the breaking of bonds that keeps the network together resulting in structure fragments (Solomon & Serio, 1994).

A mechanistic overview of coal devolatilisation is given by Solomon *et al.* (1992). The mechanism is explained together with Figures 5 - 7 which are graphical representations of the coal structure (Figure 5), primary devolatilisation (Figure 6) and secondary devolatilisation (Figure 7) respectively.

The onset of devolatilisation begins with the breaking of hydrogen bonds; vaporisation and transport of non bonded molecules; and low temperature cross linking (not shown). The breakage of the weakest molecular bonds to cause fragmentation in the macromolecular structure is shown by label (1) and label (2) in Figure 5. The resulting molecular fragments withdraw hydrogen from the aliphatic structures and increase the aromaticity of the remaining structure. The light fragments are released from the structure as tars. The sources of tar molecules include the molecules that are not attached to the coal structure (entrapped) and small network fragments produced during devolatilisation (Solomon & Hamblen, 1985).

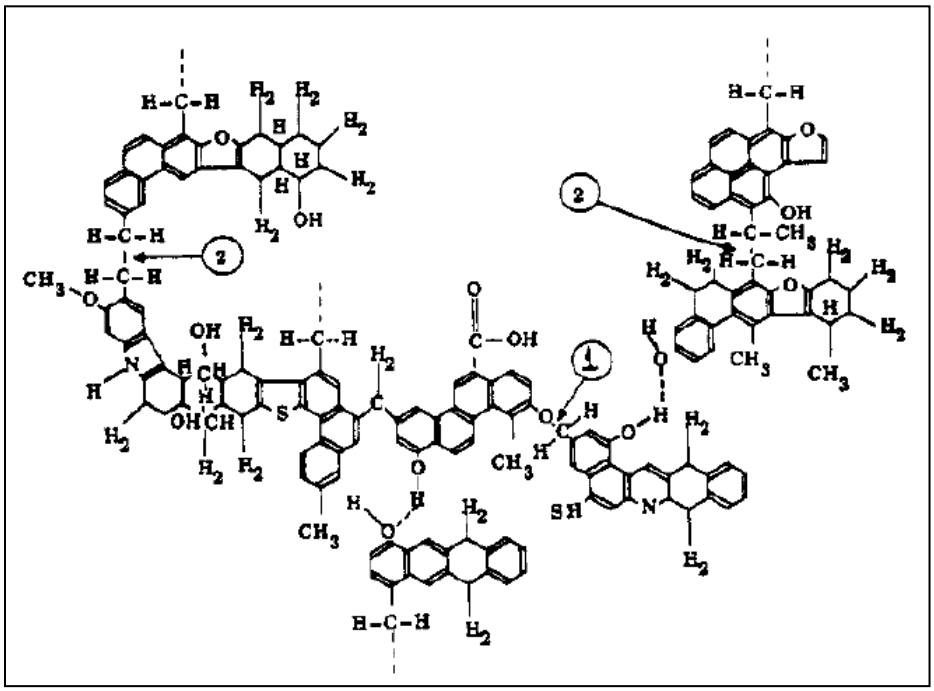

Figure 5: Coal structure (Serio *et al.*, 1987).

This is followed by the cross linking of the remaining structure and fragments that were not released as tar, as shown by label (3) in Figure 6, which is usually associated with the formation of gasses such as H_2O, CH_4 and CO_2. The release of these gasses in turn affects the O/C and H/C ratios of the resulting char. For bituminous coals this happens at temperatures just above the temperature required for maximum tar formation, weight loss and aliphatic H_2 release (Solomon & Serio, 1994).

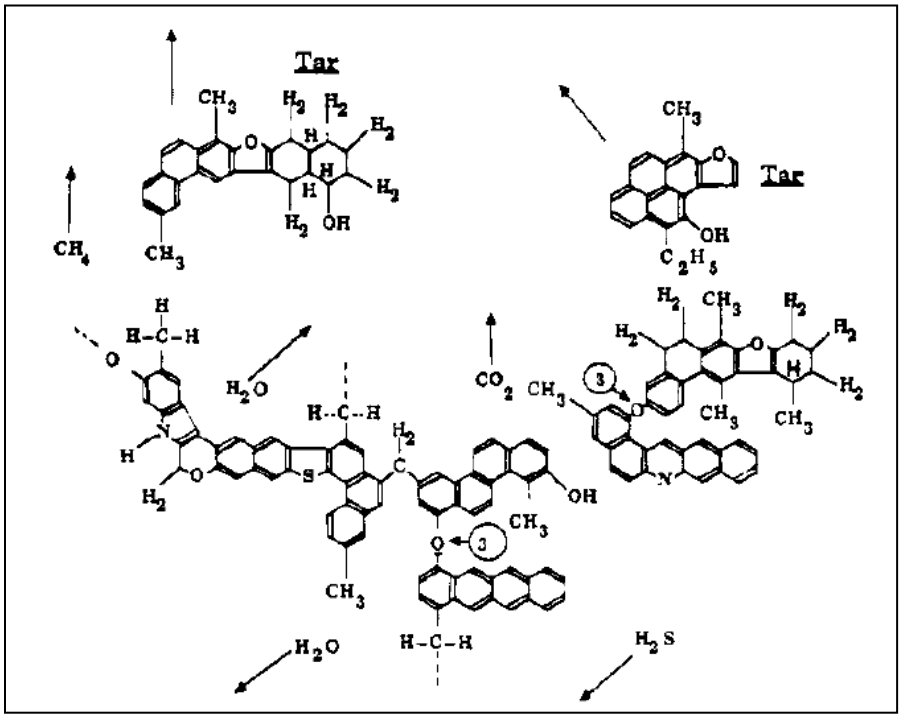

Figure 6: Primary devolatilisation (Serio *et al.*, 1987).

Secondary devolatilisation starts with gas release caused by functional group decomposition and ring condensation as shown in Figure 7.

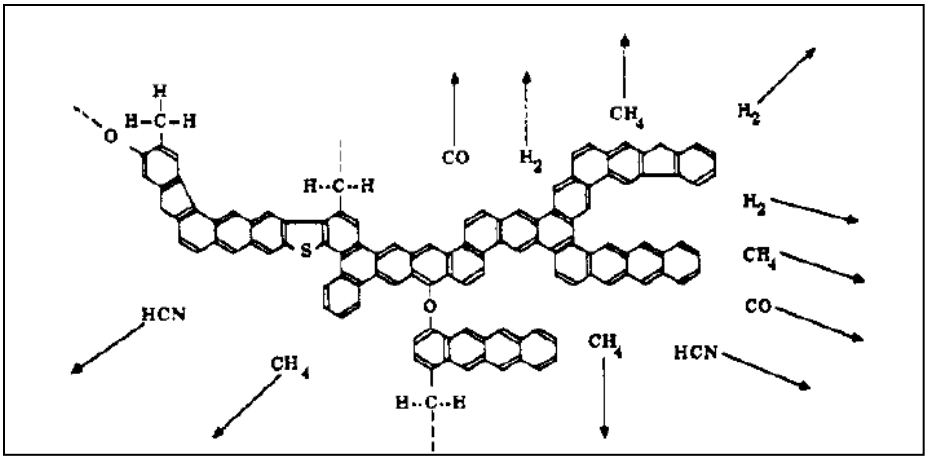

Figure 7: Secondary devolatilisation (Serio *et al.*, 1987).

The hydrogen relating to the formation reactions during secondary devolatilisation are believed to be originating from the aromatic hydrogen. Devolatilisation is considered to be complete once all the hydrogen that can be donated is depleted. Char is the structure remaining after the devolatilisation is complete (Solomon & Hamblen, 1985; Serio *et al.*, 1987). The different stages of devolatilisation summarised as low temperature devolatilisation (bulk of volatiles released) and moderate to high temperature devolatilisation (tar evolution followed by H_2 release), overlap for large particles due the large temperature gradients and cannot be clearly distinguished (Devanathan & Saxena, 1987). The tar evolution completes prior to gas evolution (Stubington & Sumaryono, 1984).

2.3.2. Extent of devolatilisation

The extent of devolatilisation can be defined as the maximum amount of volatiles released at a given set of conditions. The extent of devolatilisation is a function of various factors including temperature, pressure, residence time of volatile matter inside the particle, secondary reactions and heating rate (Stubington & Sumaryono, 1984).

The ultimate amount of volatile yield is usually determined from proximate analysis. It is however not uncommon to obtain results indicating an ultimate volatile yield higher than

that determined from proximate analysis. Stubington & Sasongko (1998) investigated devolatilisation of millimetre sized particles and found that at temperatures of 850°C the extent of devolatilisation was higher than the proximate value determined at 900°C. Stubington & Sasongko (1998) suggested that this phenomenon can be attributed to the procedures used to determine volatile yield during proximate analysis.

With increasing devolatilisation temperature the char yield decreases and the volatile yield proportionally increases (Stubington & Sumaryono, 1984). Devanathan *et al.* (1987) found that the bed temperature had a strong influence on volatile yield and a moderate influence on product distribution. Alonso *et al.* (2001) indicated that residual volatile matter can still remain inside the char even at high devolatilisation temperatures of 1000°C and 1300°C. Investigating coals with a variation of volatile content from 8.7% to 27.5% Kim *et al.* (2008) found that the extent of volatile content did not change significantly for devolatilisation temperatures ranging from 900°C to 1200°C and was close to the proximate analysis results. This indicates that a maximum temperature for volatile release can be obtained depending on the coal type.

Alongside temperature, the heating rate can also have an effect on the devolatilisation process. Typical heating rates on the surface and in the centre of the particle vary with particle size, as shown by Stubington & Sasongko (1998) who published results for surface and particle centre heating rates of different particle sizes. These results are shown in Table 2.

Table 2: Average heating rates at 95% devolatilisation times.

Coal particle diameter (mm)	Surface rate (°C/s)	Centre rate (°C/s)
2	153	124
5	39	28
10	14	9
15	7	4
20	5	3

From this publication, it was concluded that high heating rates are only obtainable for small particle sizes and higher heating rates resulted in an increased volatile yield compared to proximate analyses results. Devolatilisation results obtained at low heating

rates cannot be extrapolated to high heating rates without a considerable amount of error (Burnham *et al.*, 1989).

Furthermore, if the residence time of the volatile matter inside the particle increases a decrease in volatile yield can be expected due to secondary reactions. Secondary reactions are dependent on external pressure, temperature, heating rate, particle size, molecular size distribution of tar (which affects the diffusion of the tar out of the particle) and pore size distribution. The tar fraction of coal can be defined as the molecules that are heavy enough to condense at room temperature. The transport of these molecules out of the particle is controlled by mass transfer, vaporisation of the tar, diffusion and convective transport. The time of removal of tar from the particle is in competition with re-polymerisation reactions (Solomon & Serio, 1994). The effect of mass transport seems to be less significant on lignites and sub-bituminous coals.

Using a simulation model, Devanathan & Saxena (1987) investigated various factors that have an influence on the devolatilisation of Montana lignite coal particles. It was concluded that pressure had a moderate effect on product distribution while the effect of particle size was found to have little effect on both product distribution and volatile yield (Devanathan & Saxena, 1987; Hershkowitz, 1985).

When considering the cooling of the particle after devolatilisation is completed, it was found by Gibbins-Matham & Kandiyoti (1988) that for wire mesh reactors, the cooling had no significant effect on the weight loss when the cooling rate is less than 100 – 500 K/sec. The effect of more rapid cooling was not investigated. It was also found that the time that the particle spends at the desired temperature has a more significant effect on the final weight loss.

2.3.3. Devolatilisation time and rate

The rate of devolatilisation and the time for complete devolatilisation are very closely related and will be discussed simultaneously.

The rates of devolatilisation have been found to vary over more than two orders of magnitude. Various factors, such as differences between tested samples, different

heating rates, physical shape, heat capacities, heat conductivities and physical environments of the coal particles can all contribute to the observed differences in devolatilisation rate (Solomon *et al.*, 1992; Solomon & Hamblen, 1985).

Stubington & Sumayono (1984) investigated three coals with volatile content ranging from 19.4% to 43.5%. Their investigations showed that the devolatilisation rate increased and devolatilisation time decreased for 3 mm to 11 mm coal particles with an increase in pore diameter of the coal. The larger pore diameter increases mass transfer through the particle as well as the radiative heat transfer into the particle, resulting in more rapid heating of the particle. Furthermore the volatile flux out of the particle for medium to high volatile bituminous coals could affect the heat transfer through the particle and thus decrease the devolatilisation rate and subsequently increase devolatilisation time (Stubington & Sasongko, 1998; Ross *et al.*, 2000).

The effect of particle size and pressure was found to have a very strong influence in devolatilisation time (Devanathan & Saxena, 1987). Stubington & Sumaryono (1984) and Sasongko & Stubington (1996) also found that an increase in devolatilisation temperature resulted in increased devolatilisation rate and decreased devolatilisation time.

Some investigations indicated that an increase in fragmentation would increase initial devolatilisation rate and decrease devolatilisation time (particle sizes ranging from 1.4 mm to 29 mm) (Peeler & Poynton, 1992; Stubington & Linjewile, 1989), while others showed that fragmentation did not significantly influence devolatilisation (particle sizes ranging from 1 mm to 20 mm) (Stubington *et al.*, 1997; Sasongko & Stubington, 1996). This was because fragmentation either occurred near the end of devolatilisation or resulted in particle sizes close to the original particle size (only small pieces fragment from initial particle) (Sasongko & Stubington, 1996). This indicates that the degree of fragmentation as well as the time at which fragmentation occurs is very important during large particle investigations. The formations of cracks during early stages of devolatilisation also enhance the release of moisture from the particles (Wildegger-Gaissmaier & Agarwal, 1990).

Devolatilisation times for stationary particle systems can exceed that of fluidised bed reactors by 200% to 400% despite the fact that heat up times for particles larger than 6 mm were found to be similar. As devolatilisation is expected to be temperature controlled

this results is unexpected and is caused by the larger degree of fragmentation encountered in fluidised bed systems (Stubingon & Linjewile, 1989; Stubington *et al.*, 1997).

Kim *et al.* (2008) investigated the devolatilisation behaviour of five different coals (1 mm to 18 mm) at 900°C to 1200°C and found that the rate of devolatilisation increased with increasing volatile matter content of the parent coal. The volatile matter of the five coals ranged from 10% to 35%. The time for devolatilisation of coals with initial volatile content ranging from 8.7% to 27.5% was approximately the same. This again indicated that the devolatilisation of coal particles is controlled by heat transfer properties. It was also mentioned that the influence of coal properties on the devolatilisation rate decreased with increasing particle size (Kim *et al.*, 2008).

Stubington *et al.* (1991) found that coal type and gas flow rate had no significant influence on devolatilisation time. This indicates that the external convective heat transfer did not play a major role during devolatilisation.

2.3.4. Effect of particle size

Due to the relatively small particle sizes used in most investigations it was possible to assume isothermal conditions for most experiments and the resulting calculations would not be greatly influenced at moderate heating rates. However at high temperatures the devolatilisation reaction can be completed within a few seconds (depending on the particle size) and causes weight loss versus time measurements to be inaccurate due to the difficulty in measurements and to particle temperature gradients (Lazaro *et al.*, 1998). Even when the final temperature can be reached in very short times, the first few seconds can hardly ever be under isothermal conditions.

When investigating single large particles, a numerous number of experimental repeats need to be done in order to obtain representative results. As the particle diameter increases the controlling devolatilisation mechanism changes from reaction kinetics to a combination of reaction kinetics and heat transfer followed by predominantly heat transfer controlled (Stubington & Sumaryono, 1984; Solomon & Hamblen, 1985; Agarwal *et al.*, 1984; Stubington *et al.*, 1991; Wildegger-Gaissmaier & Agarwal, 1990).

Particle size has a considerate influence on the devolatilisation process. It affects, amongst other things; the degree of fragmentation; the intra-particle temperature profiles across the particle; the heating rate of the particle; the volatile residence time inside the particle; the final product distribution; the final char yield; the devolatilisation rate; and the devolatilisation time (Stubington & Sumaryono, 1984; Stubington & Sasongko, 1998; Chen *et al.*, 1994; Bunt & Waanders, 2009).

A pronounced factor in the rate of devolatilisation is the degree of fragmentation, which is, in turn, dependent on particle size, temperature gradient, particle shape, pore size distribution, devolatilisation temperature, structural flaws, volatile content and the coal's physical and chemical properties (Mitchell & Akanetuk, 1996; Chen *et al.*, 1994; Dacombe *et al.*, 1999; Lee *et al.*, 2002; Stubington *et al.*, 1991; Kim *et al.*, 2008). That some investigators observed no fragmentation for particles in the range of 3 mm to 4 mm (Lee *et al.*, 2002; Stubington & Sasongko, 1998) indicates that for each coal there is a critical particle diameter at which fragmentation start to occur.

Investigating the behaviour of fragmentation of millimetre sized particles, Dacombe *et al.* (1999) obtained results indicating that the degree of fragmentation was most significant for coals with a volatile content in the region of 22%. The fragmentation of particles during the initial heating stage is illustrated in Figure 8.

From Figure 8 it can be seen that as devolatilisation continues the inner part of the particles tends to fragment into fewer larger sized fragments while the outside layer of the particle results in a much higher number of smaller fragments. Van Dyk (2001) found that fragmentation occurred over the duration of devolatilisation (up to 60 minutes) and that the degree of fragmentation was, for particles between 6 mm and 19 mm, also a function of the time that the particle was within the devolatilisation conditions.

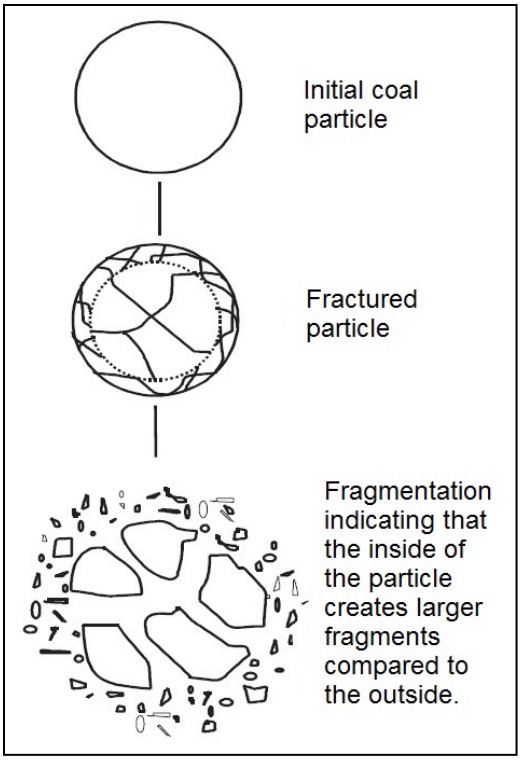

Figure 8: Illustration of fragmentation during particle heating adopted from Dacombe *et al.*, (1999).

A study on synthetic char particles (in order to vary the porosity of the particles) by Mitchell & Akanetuk (1996) indicated that coal fragmentation increases with an increase in volatile matter. Lee *et al.* (2002) similarly found that higher volatile content increases fragmentation.

As the volatile products inside large particles need to travel through the pore network inside the particle during devolatilisation, the reactive tar species start to undergo secondary reactions that result in carbon deposits forming inside the pores. Increased particle size therefore results in an increased char yield, as increasing particle size results in an increased volatile residence time (Stubington & Sumaryono, 1984; Devanathan & Saxena, 1987; Solomon & Hamblen, 1985).

At high temperature and heating rate, intra-particle temperature profiles can be present. These non-isothermal conditions are, however, seldom taken into account, and it is often assumed that the particles temperature equals the surrounding (gas) temperature (Solomon *et al.*, 1992).

By using average properties for coal Adesanya & Pham (1995) showed that for 1 mm particle the Biot number (Equation 1) can vary from 1 – 20, where isothermal conditions can only be assumed at a Biot number less than 0.2.

— (1)

Adesanya & Pham (1995) also indicated that an increase in particle size and volatile flux could result in a significant increase in the time needed for the particle centre temperature to reach that of the environment. By contrast the faster devolatilisation rate for small particles results from the faster heat up times (Bunt & Waanders, 2009).

2.4. Gasification

2.4.1. Introduction

Gasification is an important process step in the conversion of coal to gas and consequently to chemicals and liquid fuels. Knowledge of the gasification kinetics is needed to sufficiently design industrial processes such as gasifiers. The reaction rate of the coal with CO_2 is often used to characterise the reactivity of coal. Results of the CO_2 reactivity tests can be used to compare coals or chars *i.e.* resulting from different devolatilisation conditions. The CO_2 reactivity tests are normally carried out with powders. Relatively little work has been dedicated to the gasification of particles larger than 1 mm in the reactivity analysis of coal. Different experimental rigs and conditions as well as the char formation conditions have been used, which results in limited comparability (Matsui *et al.*, 1987). The factors that can influence gasification of coal char particle can span over a wide range of physical properties as well as experimental conditions such as coal rank, pressure, temperature, particle size, gas composition of oxidising agent, mineral content, heating rates, etc (Irfan *et al.,* 2011; Cousins *et al.,* 2006).

2.4.2. Gasification temperature

The temperature at which gasification is carried out can have a significant effect on the controlling mechanism during conversion process. An increase in temperature generally increases the resulting conversion rate of the CO_2 – char gasification reaction (Kwon *et al.*, 1988; Liu *et al.*, 2006 a; Liu *et al.*, 2008). At relatively low temperatures, the reactivity is highly temperature sensitive, since the conversion is primarily occurring in the reaction kinetics controlled regime (Kwon *et al.*, 1988). Investigating lignite and sub-bituminous coals, Sawettaporn *et al.* (2009) found that for particles of the same size and devolatilisation temperature, the reactivity increased with increasing gasification temperature. The temperature dependence is diminished at higher temperatures because of a transition from the chemical reaction controlled regime to the diffusion controlled regime. At very high temperatures, when the temperature is above the ash fusion temperature, the reactivity can even decrease significantly with temperature (Liu *et al.*, 2006 a).

2.4.3. Devolatilisation temperature

Alonso *et al.* (2001) investigated the CO_2 gasification of chars prepared at 1000°C and 1300°C at gasification temperatures of 500°C, 700°C, 900°C and 1100°C. Their results showed that at gasification temperatures of 500°C and 700°C the reactivity of the char prepared at 1300°C was lower than the char prepared at 1000°C, while at gasification temperatures of 900°C and 1100°C the reactivity of the chars prepared at 1300°C was higher than the chars prepared at 1000°C (Alonso *et al.*, 2001). Wu *et al.* (2008, 2009 b) found that an increase in devolatilisation temperature decreases the BET surface area of the resulting char (possibly due to a more ordered char structure) and subsequently reduce the gasification reactivity of the char. While investigating lignites, however, Bozkurt *et al.* (2008) found that an increase in devolatilisation temperature resulted in an increase in the gasification reactivity with CO_2. Erincin *et al.* (2005) obtained results showing that the reactivity of chars increased with increase in devolatilisation temperature up to 700°C above which the reactivity decreased.

2.4.4. Heating rate during devolatilisation

Investigating different ranks of coal chars prepared at slow and rapid heating rates at different gasification temperatures (450°C to 1100°C), Feng *et al.* (2004) obtained results indicating that at temperatures below 810°C to 850°C the reactivity of chars prepared at slow heating rates was higher than the chars prepared at rapid heating rates. While at gasification temperatures above 810°C to 850°C the reactivity of the chars prepared at rapid heating rates was higher than the reactivity of the chars prepared at slow heating rates (Feng *et al.*, 2004). Wu *et al.* (2008), who investigated the gasification of chars at temperatures from 950°C to 1150°C, similarly found that chars prepared at high heating rates have higher gasification reactivity than chars prepared at slow heating rates. The differences in reactivity were found to be less pronounced at higher temperatures (Liu *et al.*, 2006 a; Wu *et al.*, 2008). Liu *et al.* (2008) found that the reactivity of the chars prepared at high heating rates with different final temperatures showed very little deviation over the temperature range. The increased char reactivity due to increased heating rate during devolatilisation is more significant for high volatile bituminous coals, than for medium volatile bituminous coals (Luo *et al., 2001)*. Roberts *et al.* (2003) suggested that higher devolatilisation pressures and heating rates indirectly affected the reaction rate of the char as the physical structure and surface area of the char was most affected by the different conditions (leading to higher reaction rates) rather than the intrinsic reactivity. Luo *et al.* (2001) linked the increased char reactivity to an increase in char porosity at higher devolatilisation heating rates.

2.4.5. Coal rank

Despite of the fact that the chars from different parent coals show similar chemical structures, the reactivity of the chars shows a trend of decreasing reactivity with increasing rank. This suggests that the reactivity determining property of the chars might relate to physical properties and not to the chemical nature (Fletcher *et al.*, 1992). Similar results were obtained from the work done by Park & Ahn (2007) that showed that

the reactivity of the chars increased with decreasing parent coal rank. Macro and meso pores were considered to be one of the factors that significantly influenced the reactivity as this created channels through which the reactant gas could diffuse into the reactive surface area. Mangena *et al*. (2011) compared gasifier operation with different types of feed coal. A lignite and a bituminous coal were used during this investigation, and it was found that despite the possible differences in chemical and structural characteristics of the two coals, both could successfully be used for gasifier operations. The lignite coal did however show a much larger drying and devolatilisation zone in the gasifier (due to higher volatile and water content) and a much smaller reduction and combustion zone (due to the higher reactivity) compared to the bituminous coal (Mangena *et al.*, 2011). Liu *et al.* (2010) studied the gasification behaviour of three different types of coal, and found that for both CO_2 and steam gasification; the gasification temperature ranging from 1400°C to 1500°C did not have a significant influence on the gasification reactivity. Results did however indicate that the reactivity of the three coals varied significantly compared to each other.

2.4.6. Effect of particle size

Stubington *et al.* (1997) did experimental work on the combustion of large particles (up to 11 mm) and concluded that combustion rate is a function of particle size, and that fragmentation resulted in smaller particles and subsequently increased the burning rate of the sample. A reduction in particle size has been found the increase the conversion rate of the CO_2 – char reaction (Kwon *et al.*, 1988; Bunt & Waanders, 2009). The degree of fragmentation during gasification is a function of the coal properties as well as gasification conditions (Struis *et al.*, 2002). Matsui *et al.* (1987) indicated that for particle size smaller than 710 µm, particle size effects become negligible at temperatures between 885°C and 980°C. Hanson *et al.* (2002) investigated the gasification behaviour of two high vitrinite content coals in both air and CO_2. Results showed that variation in particle size (< 2.8 mm) did not show significant difference in reactivity for gasification in either air or CO_2 environment. Kovacik *et al.* (1991) conducted research on bituminous and sub-bituminous coal particles smaller than 2.4 mm and found that for char particle sizes smaller than 105 µm the gasification reaction occurs in the chemical reaction

controlled regime for temperatures between 700°C and 950°C. CO_2 diffusion effects were observed for particle sizes smaller than 105 µm at temperatures above 900°C and at lower temperatures for larger particle sizes. Zhu *et al.* (2008) found that the decreased reactivity with increase in particle size (up to 250 µm) was less pronounced for demineralised coals than for raw coals. The reactivity has also been found to be influenced by secondary reactions of volatiles inside the particles as well as mineral matter distribution.

2.4.7. Mineral matter content

The catalytic effect of mineral matter content has a varied effect depending on the coal type used. Sawettaporn *et al.* (2009) showed that an increase in ash content resulted in an increase in char – CO_2 reactivity for lignite and sub-bituminous coals. Ochoa *et al.* (2001) found that the effect of mineral matter content is more pronounced for sub-bituminous chars and was detected up to 1060°C. This effect, however, decreases with increasing gasification temperature. Bunt & Waanders (2010) monitored the behaviour of non-volatile trace elements such as Ba, Co, Cr, Mn, and V during gasification in an industrial gasifier. Their results showed that the elemental concentration changed due to different compounds (containing the specific element) forming during the gasification process. This could possibly cause the catalytic effect of certain minerals to change during the gasification process. For bituminous coals it was found that structural effects had a greater influence on the char reactivity than the mineral matter content (Ochoa *et al.*, 2001). The effect of ash fusion and ash accumulation that occurs at the reaction surface of the char particle has been found to be a significant factor contributing to lower the gasification reactivity obtained for chars gasified at high temperatures (Liu *et al.*, 2006 b). Luo *et al.* (2001) found that the difference in gasification rates for different coals became less distinct at higher temperatures (1400°C - 1600°C) due to the increased resistance to gas diffusion originating from ash fusion taking place.

Comparing the results from two parent coals (lignite and bituminous) to the results of a demineralised coal, Zhu *et al*. (2008) showed that the crystalline structure increased for demineralised coal during devolatilisation (opposed to a decrease in crystalline structure

for the non-demineralised coals), indicating that the mineral matter could be the cause of different char structures after devolatilisation.

2.4.8. Other factors influential to gasification

Roberts *et al.* (2010) has shown that an increase in partial CO_2 pressure will slightly increase the reaction rate, while the increase in total pressure has shown to have no significant influence in the measured kinetics.

The influence of pressure during devolatilisation has also been found to decrease the char reactivity for devolatilisation pressures up the 1.5 MPa where after the reactivity increased. The maximum reactivity was achieved at the highest pressure investigated which was at 5 MPa (Yang *et al.,* 2007)

Zhang *et al.* (2006) investigated anthracites with variation in volatile content and experimental results indicated that an increase in the coal's volatile matter content resulted in an increase in char reactivity.

The devolatilisation time the chars encounter in the temperature history during char preparation also affects the reactivity of the resulting chars. Liu *et al.* (2004) showed that an increase in devolatilisation time reduced the reactivity of the resulting chars. The effect of devolatilisation time became less significant at extended devolatilisation time. Increased devolatilisation time resulted in a more ordered structure of the char and subsequently lowers reactivity. This was more pronounced in high volatile coals. Similar results were obtained by Cousins *et al.* (2006) who found that reactivity decreased with increase in devolatilisation time due to the increase in the extent of graphitisation that has occurred.

2.4.9. Gasification modelling

The modelling of CO_2 gasification reactions is largely dependent on the experimental conditions. Predominately the temperature, and to a lesser extent, the pressure and the

CO_2 fraction of the gas determine the controlling conversion regime (kinetically controlled versus diffusion control (internal and external) or a combination of these). Several models have been derived over the last few decades, such as the shrinking unreacted core model (SUCM); the volumetric model (VM); the cylindrical pellet model (CPM); the random pore model (RPM); and the random capillary model (RCM).

The chemical reaction controlled regime (CO_2 gasification) has generally been found to occur at temperatures below 1100°C, while at temperatures between 1100°C to 1400°C the reaction is mainly controlled by factors such as ash diffusion (Gu *et al.*, 2009; Zhang *et al.*, 2006; Wu *et al.*, 2008). These temperature ranges are dependent on coal properties as well as devolatilisation conditions. Bozkurt *et al.* (2008) concluded that the char-CO_2 reaction for lignite particles up to 3 mm gasified at less than 1000°C was still within the chemical reaction controlled regime while for high volatile bituminous coals Hodge *et al.* (2010) found that at gasification temperatures below 900°C the gasification reaction still occurred in the reaction kinetics controlled regime. For the combustion of large coal particles (in the range of 7mm), Scala (2011) found that the particles burned under boundary layer diffusion conditions for experiments done at 800°C to 900°C.

Ochoa *et al.* (2001) found that for sub-bituminous and high volatile bituminous coals gasified at temperatures below 1060°C, the reaction still occurred in the chemical kinetics controlled regime. Above this temperature diffusion started to play a more significant role. The results at temperatures above 1060°C were modelled using the RPM and RCM with the RPM giving the best fit to experimental results.

Kwon *et al.* (1988) compared the CPM, VM and the SUCM for different rank coal particle sizes ranging from 0.18 mm to 1 mm at gasification temperatures of 700°C to 900°C and found that the SUCM gave the best fit to experimental results. Results indicated that at gasification temperatures below 900°C the reaction occurs in the chemical reaction controlled regime. Matsui *et al.* (1987) also compared the VM and the SUCM at temperatures ranging from 885°C to 980°C for particle sizes from 44 µm to 710 µm. Their results showed that the VM gave the best fit to experimental results and that particle size had no influence on the reactivity. Wu *et al.* (2009 a) showed that for low temperature gasification (950°C) the SUCM gave a reasonably good fit while the accuracy of the fit decreased significantly at higher gasification temperatures (1400°C). Liu *et al.* (2003) modelled the gasification of coal particles smaller than 0.21 mm with

both the shrinking unreacted core model and a modified RPM for gasification at temperatures between 1000°C and 1600°C. Their results indicated that at these temperatures the SUCM did not give an adequate fit to experimental results while a modified RPM gave good fit to experimental results.

The SUCM can be described to occur in the following manner (Levenspiel, 1999): The reaction first occurs on the outer shell or skin of the particle, after which the reaction zone moves into the solid particle leaving behind a layer of ash. The ash layer is made up of once reactive material that has been completely converted as well as inert material that is present in the particle. This implies that at any time during the reaction, an unreacted core that will shrink in size as the reaction continues will be present inside the particle.

The SUCM, as described in (Levenspiel, 1999) is derived from the equation of the reaction gas or fluid (A) reacting with the solid (B). This equation is given in Equation 2:

(2)

The equation gives the stoichiometric relation of the reaction gas to the solid in terms of *b*. The reaction equation for CO_2 with coal particles (assuming that only the carbon inside the particle reacts with the CO_2) is given in Equation 3:

(3)

The governing equations that are used for the purpose of modelling the gasification results are taken from Levenspiel (1999).

When the reaction is chemical reaction controlled, the ash layer diffusion has no significant effect and the rate of the reaction is a function of the surface area of the unreacted core with the governing equation shown in Equation 4.

– (4)

With calculated using Equation 5.

(5)

When the resistance to gas diffusion through the ash layer increases beyond a certain point the controlling reaction mechanism shifts over into the ash diffusion controlled regime. The governing equation for the SUCM in the diffusion controlled regime is given in Equation 6.

(6)

With calculated using Equation 7:

(7)

2.5. Solid State Nuclear Magnetic Resonance

2.5.1. Introduction

Solid-state NMR (SSNMR) was chosen as a method of analysis due to the fact that this technique can be used for fuels or materials that are structurally undefined and not readily soluble (Sethi *et al.*, 1988; Suggate & Dickinson, 2004). This technique gives a wide range of structural parameters (some only estimated) of the carbon skeleton (Solum *et al.*, 1989) that can be very useful in the modelling of complex processes such

as devolatilisation. For spectra with very distinct peaks the results obtained have been found to be very reliable (Solum *et al.*, 2001).

Even though the NMR analysis is less sensitive than other well known analyses such as chromatography and mass spectroscopy, it provides new information with regards to structural analysis and characterisation of chars and devolatilisation products.

2.5.2. Different SSNMR techniques

The main techniques that will be looked into for this study include the following:

- ^{13}C CP/MAS NMR (Cross polarisation magic angle spinning)
- DD/MAS NMR (Dipolar dephasing magic angle spinning)
- Variable contact time experiments
- Integration of obtained spectra

The DD technique is used to subdivide the fraction of aromatic carbons (fa – obtained from CPMAS curve integration) into protonated and non-protonated fractions.

2.5.3. Different carbon fractions

The amount of information that can be determined from SSNMR analyses has increased significantly over the years, where originally only the aromatic and aliphatic ratios were investigated; numerous parameters have been calculated in recent studies.

The parameters that can be obtained from SSNMR analyses are taken from the integration regions as indicated by Suggate & Dickinson (2004). The chemical shift (ppm) integration regions as shown in Figure 9 are described in Table 3 which shows the integration regions with the specific type of carbon or carbon bonds associated with each region as well as the notation used in the literature and the representative notation used in this study.

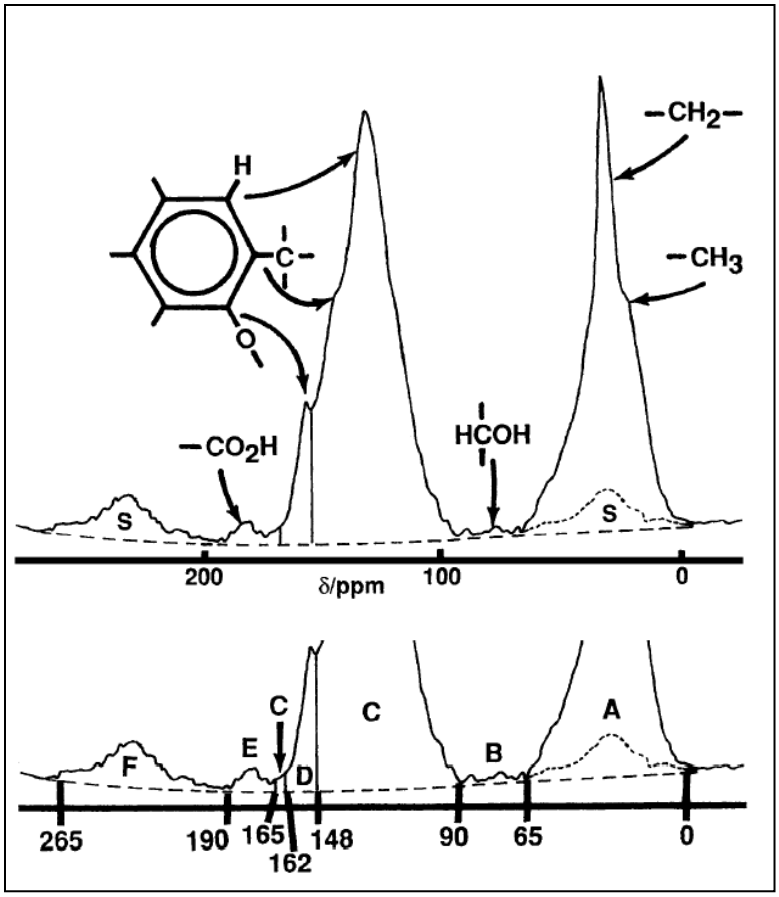

Figure 9: Identified functional groups on SSNMR spectra with integration regions from Suggate & Dickinson (2004).

For each of the integration regions mentioned in Table 3, CPMAS and DD integral values are determined. In calculating the values of each type of carbon present in the sample it is assumed that the area under the frequency peak of each type of carbon is directly proportional to the amount of the specific type of carbon in the sample (Suggate & Dickinson, 2004).

Table 3: SSNMR integration regions and notations

Integration region	Carbon Assignment	Notation (As per publication)	Representative notation
280 – 232	Spinning sideband	F*	SSB
232 – 170	Carbonyl carbons	E*	faCO
170 – 161	Aromatic	C*	fa
161 – 147	Phenolics	D*	faP
147 – 133	Alkylated Aromatics	G**	faS
133 – 90	Aromatic	C*	fa
90 – 50	Aliphatic O	B*	falO
50 – 0	Aliphatic C	A*	fal
	Total Aromatic Carbon	C + D + G + 2F	
	Total Aliphatic Carbon	A + B - F	

* Notation taken from Suggate & Dickinson (2004).

** Notation taken from Solum *et al.*, (1989).

The carbon fraction parameters are given in (Table 4).

Table 4: Carbon fractions from NMR analyses.

Aromatic carbon fractions	
fa	Total aromatic carbon
faCO	Carbonyl and carboxyl
faH	Protonated aromatic ring carbons
faN	Non-protonated aromatic carbons
faP	Phenolic aromatic carbons
faS	Alkylated aromatic carbons
faB	Aromatic bridgehead carbon fraction
Aliphatic carbon fractions	
fal	Total aliphatic carbon
falH	Fraction of methyl aliphatic carbons
falN	Non-protonated aliphatic carbon
falO	Aliphatic carbons attached to oxygen

To ensure that all subsequent analyses are comparable, a standard is inserted into the sample with each analysis and the resultant spectra is then adjusted to fit that of the standard used. Various standards can be used, such as tetramethylsilane (TMS) as

used by Suggate & Dickinson (2004) and Wilkie & Haworth (1978) or Adamantane with a peak reference of 38.3 ppm, as used in this study.

Solum *et al.* (1989) investigated these parameters over a wide range of coal ranks (lignite to low volatile bituminous coals), and found that fa, faN and faB increase with increasing rank while other factors like fal, falH and falO decrease with increasing rank. It should be noted that the integration over the aliphatic range is the least accurate of all the integrations (Solum *et al.*, 2001).

Comparing only aromatic and aliphatic fractions of the same sample Wilkie & Haworth (1978) found that for anthracite the aromatic fraction exceeded that of the aliphatic fraction, and the aromatic fraction was equal and smaller than the aliphatic fraction in bituminous and sub-bituminous coals respectively.

Chars prepared from different parent coals tend to have similar aromaticity after complete devolatilisation. Fletcher *et al.* (1992) found that the aromaticity of the chars prepared from parent coals ranging from lignite to low volatile bituminous coals varied over a small range from 79% to 88%. The parent coal aromaticity for these coals varied from 53% for the sub-bituminous coals to 77% for the high rank coals.

2.5.4. Accuracy and reliability of results

With regard to different methods of NMR analysis, van Niekerk (2008) showed that for high-inertinite coals, the difference of data obtained by cross polarisation (CP) and single pulse (SP) experiments were negligible for both original and demineralised coals. The range of aromatic values (fa) obtained for CP and SP experiments with both original and demineralised coals was 0.85 – 0.86 (van Niekerk, 2008). The differences for other structural parameters are of the same order when comparing demineralised and original coal samples. Single pulse experiments are used when low amounts of carbon are present in the sample and are much more time consuming than CP experiments. Wilkie & Haworth (1978) found that fewer pulses are required to analyse anthracite samples as anthracites have a more ordered structure than coals of lower rank.

The accuracy of SSNMR data depends on a variety of factors including the quality of the samples, the contact time used during analyses and the extent of signal polarisation. The quality of the sample depends on the amount of magnetic material in the sample, as this influences the visibility of carbons in the sample. A variable contact time experiment can be done to find the optimum contact time for the analyses. Using the optimum contact time will ensure that full polarisation of most signals is obtained resulting in a more accurate NMR analysis (Suggate & Dickinson, 2004; Solum *et al.*, 1989). When comparing results for SSNMR analyses found in literature, special care must be taken to consider the equipment and techniques used as no standard has yet been set (Suggate & Dickinson, 2004).

In their investigation to quantify different carbon types in high rank coals Sethi *et al.* (1988) used three types of bands representing benzene-like, condensed and substituted carbons and found that the results obtained from DD NMR analysis correlated very well with different techniques of measurement such as spectroscopic and elemental analyses.

Chapter 3: Experimental

3.1. Introduction

In this chapter work relating to the different chemicals, procedures and setups for each set of experiments is discussed. In Section 3.2 a list of materials is tabulated while in Section 3.3 and 3.4 procedures for coal preparations and coal characterisation are given. Section 3.5 and 3.6 pertain to the procedures followed during the devolatilisation and the gasification experiments respectively. Lastly, the error calculations are given in Section 3.7.

3.2. Materials

The materials used during this investigation are listed in Table 5.

Table 5: List of materials.

Material	Purity	Origin/Supplier
Coal	-	Highveld – Seam 4
HCl	~ 32 (Vol %)	ACE
HF	~ 48 (Vol %)	ACE
N_2	> 99.999 (Vol %)	Afrox
CO_2	> 99.995 (Vol %)	Afrox

3.3. Sample Preparation from ROM coal

One ton Highveld coal was received ROM in batches of approximately 250 kg and sent to SABS Secunda. The coal was taken as is and air dried for two hours by spreading the coal over a large concrete floor. With the use of a rotary splitter the initial sample was reduced to 125 kg. This was done by taking containers on opposite sides of the rotary

splitter and adding them together, and then repeating the splitting process with the new batch formed from adding opposite containers. This procedure was followed to ensure that a representative sample was obtained from the ROM coal.

This sample was then sieved into different size fractions. Each size fraction was then weighed and stored in black plastic bags. The sieve ranges as well as the yield for each size are shown in Table 6:

Table 6: Sieve size ranges and mass yield for each size range.

Sieve ranges	Mass Yield (Wt %)
+ 53 mm	12.9
+ 25 mm to - 53 mm	17.0
+ 12.5 mm to - 25 mm	20.2
+ 6.3 mm to - 12.5 mm	9.7
+ 3.35 mm to - 6.3 mm	11.0
+ 1 mm to - 3.35 mm	16.3
- 1 mm	12.7

The 12.5 mm to 25 mm size fraction resulted in the largest percentage mass yield of 20.2% while the 6.3 mm to 12.5 mm size fraction showed the lowest percentage mass yield of 9.7%. No definite trend with regards to mass yield percentage and particle size can be observed.

Investigating the coal size distribution for 3 different top size scenarios for coal of similar properties as the coal used in this investigation, Bunt & Waanders (2009) showed that the smaller size fractions (< 6.7 mm) tended to result in smaller yields (<4.4%) compared to larger size fraction (> 6.7 mm) yields (up to 17.6% for +53 mm fraction). These results were obtained using an initial mass of 240 kg for all three scenarios. Investigating ten different pulverised coals for variation in coal properties with different size fractions (-38 µm to +212 µm) Cloke *et al.* (2002) found that the mass yield for each size fraction is coal specific and that no definite trend could be found relating to mass yield and size fraction.

After sieving, representative samples from each size fraction were obtained via a series of rotary splitting. The samples were then reduced to a size of -212 µm using a combination of jaw crushers and a pulveriser. The pulverised samples were placed in small sealable plastic containers and proximate, ultimate and calorific value analyses

were done at the SABS laboratories in Secunda. The coal samples obtained from sieving the initial representative ROM sample was then transported to the coal research laboratories at North-West University.

3.4. Characterisation

The coal characterisation techniques used during this study include proximate and ultimate analyses as well as the determination of calorific values (conventional analyses). Furthermore SSNMR was used to characterise three different size fractions.

3.4.1. Conventional analyses

The conventional analyses were done on raw coal samples only and were done by the South-African Bureau of Standards (SABS) in Secunda, South - Africa. The standards used are listed in Table 7:

Table 7: Conventional analysis standards

Proximate analysis	
Inherent moisture (Inh. H_2O)	SABS 925
Ash	ISO 1171
Volatile matter content (Vol. Mat.)	ISO 562
Fixed carbon (Fix. Car.)	By difference
Ultimate analysis	
Carbon	ASTM 5373
Hydrogen	ASTM 5373
Nitrogen	ASTM 5373
Total Sulphur	ASTM D4239
Oxygen	By difference
Calorific value	
Calorific value	ISO 1928

3.4.2. Solid state NMR

For SSNMR analysis further preparation of the samples was needed. Due to the possible influence of mineral matter content in the parent coal during analysis, the coal samples were demineralised. The presence of paramagnetic centres in coal samples may cause carbon resonance to be invisible during SSNMR analyses (Solum *et al.*, 1989).

The demineralisation process was done using a combination of HF and HCl solutions. Both the HF and HCl acids were supplied by Sigma Aldrich. The mean particle size for all samples was reduced to - 75 µm prior to demineralisation. The HCl was diluted to a 5 molar solution, while the HF acid was used as received. The demineralisation procedure consisted of four steps:

Step 1:

The pulverised coal was weighed and placed in acid-resistant PTFE beakers. The HCl acid was then introduced into the beaker using a ratio of 400 ml acid for every 100 g of coal. The coal was then left to leach the solution at room temperature for the duration of 24 hours while the mixture was continuously stirred with a magnetic stirrer. The beaker was covered with a Perspex lid to reduce spillage due to the rotation of the magnet within the fluid as well as to prevent the acid solution from evaporating during the process. The setup is shown in Figure 10.

Step 2:

The mixture was then removed from the magnetic stirrer and poured into a ceramic Büchner funnel lined with a double layer of filter paper. The Büchner funnel drained into a glass container. The vacuum on the Büchner funnel was held for a couple of minutes to ensure that the residue dried sufficiently. Once dry, the residue was scraped from the filter paper and again placed in the PTFE beaker.

The HF acid was added to the residue in a ratio of 400 ml of acid for every 100 g of coal originally used in Step 1. From here Step 2 followed a similar procedure as Step 1.

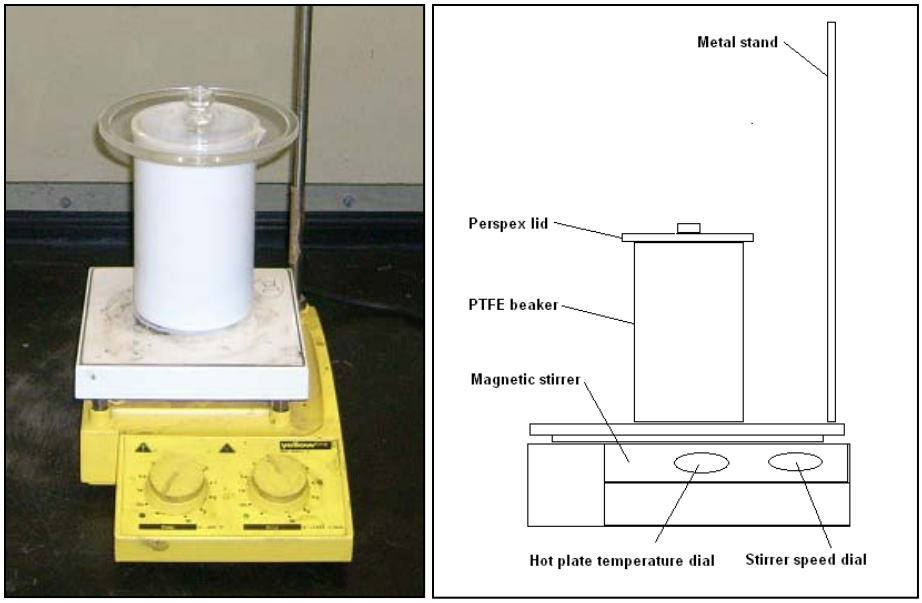

Figure 10: Demineralisation setup

Step 3:

In the third step the mixture was again removed from the magnetic stirrer but was poured into a plastic Büchner funnel with double layer filter paper, as the HF acid will react with the glassware. The funnel drained into a plastic container as shown in Figure 11 (In the case of HCl and HF the funnel and container are ceramic/glassware and plastic respectively):

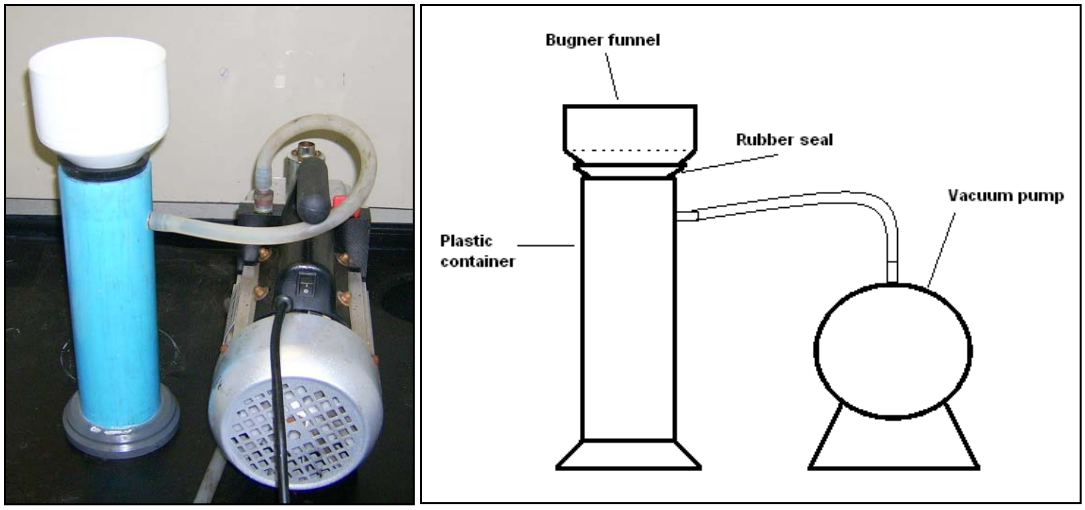

Figure 11: Filtration setup for HF acid

The residue was filtered for a couple of minutes to ensure that it dried sufficiently. The residue was scraped from the filter paper and placed in the PTFE beaker. HCl was added into the beaker in the ratio of 400 ml acid for every 100 g coal originally weighed. The mixture was again covered and stirred at room temperature for 24 hours.

Step 4:

Similar to Steps 2 and 3 the mixture was filtered with double layer filter paper in a glass Büchner funnel. The final residue remaining in the Büchner funnel was washed by pouring distilled water into the funnel and letting it filter through the residue. After the product was washed the residue was scraped from the filter paper and placed in an oven proof container. The container was then placed in a convection oven at 105°C for 24 hours to dry.

SSNMR analyses were outsourced to the CAF (Central Analytical Facility) NMR laboratory at the Stellenbosch University (SU). The three particle size ranges selected for SSNMR are the +3.35 mm to -6.3 mm, +12.5 mm to -25 mm and the +25 mm to -53 mm size fraction.

The SSNMR spectra were acquired on a Varian VNMRS 500 MHz two-channel spectrometer using 4 mm zirconia rotors and a 4 mm Chemagnetics^{TM} T3 HXY MAS probe. All CP spectra were recorded at ambient temperature with proton decoupling; a

relaxation delay of 3 s and 4000 scans were collected for adequate signal-to-noise. The power parameters were optimised for the Hartmann-Hahn match; the radio frequency fields were $Y_C B_{1C} = Y_H B_{1H} \approx 55$ kHz. The contact time for CP was 2 ms. The free induction decay was 3500 points, Fourier transformed with a 50 Hz line broadening. MAS was performed at 15 kHz and Adamantane was used as an external chemical shift standard where the downfield peak referenced to 38.8 ppm. The dipolar dephasing (DD) experiments were carried out under similar conditions with the interrupted decoupling time constant t1Xidref set to 40 µs after evaluating an array of time constants. The integration reset points were taken from the publications of Solum *et al.* (1989) and Suggate & Dickinson (2004).

3.5. Devolatilisation

3.5.1. Particle selection

The devolatilisation experiments required that the coal samples (particles) be roughly the same size. The chosen size ranges were 5 mm, 10 mm, 20 mm and 40 mm. This was done by hand picking all the particles except for the 5 mm particle size range. The 5 mm particles were obtained by sieving the + 3.35 mm to - 6.3 mm size fraction between the ranges of +4.75 mm and - 5.6 mm.

The hand selected particles were selected on a dimension basis. This implies that the particles were characterised in term of three dimensions: the length, width and height of the particle. A 20 mm particle for example would have all three dimensions in the range of 20 mm. Particles that had edges far exceeding the given dimensions were slightly altered by chiseling off the protruding edges.

Figures 12 to 15 indicate how these particles were characterised into the different size fractions.

Figure 12: Example of 5 mm particles after preparation.

As the 5 mm size fraction (Figure 12) was sieved, some particles are slightly smaller with regards to one or more of the size dimensions.

Figure 13: Example of 10 mm hand selected particles.

Figure 14: Example of a 20 mm hand selected particle.

With regards to 10 mm, 20 mm and 40 mm particle selection (Figures 13 - 15), the particles were selected by inspection with regards to the three dimensions needed (Length, Width and Height). In the Figures 14 and 15 the Width is indicated by B and the mass of the particles by W.

Figure 15: Example of a 40 mm hand selected particle.

It was not always possible to obtain large particles that fit precisely into the given dimensions. In some cases (Figure 15), one or more of the dimensions slightly exceed the required size, even after alteration. The intention was not to alter the ROM raw coal too much. Due to the fact that the particles were handpicked by inspection, it was possible to avoid particles with very high ash content or with a rock like texture.

3.5.2. Devolatilisation equipment

All particle devolatilisation experiments were done on the large particle TGA shown in Figure 16. This setup utilising a LENTON TSH15/50/180 tube furnace was developed in-house for specific use in large particle analysis.

The furnace was mounted on vertical rails to facilitate vertical movement of the oven during experiments. The top end of the furnace tube was covered with a metal cap, through which the gas was introduced into the system. The metal cap also housed the thermocouple that extended into the tube to measure the temperature directly above the sample.

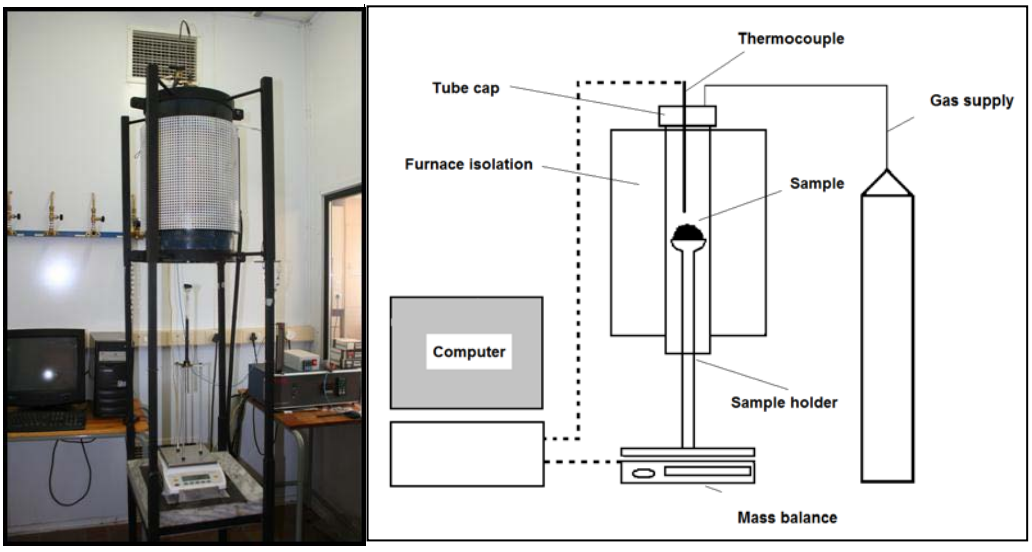

Figure 16: Large particle TGA setup.

The specifications for this tube furnace are given in Table 8:

Table 8: Devolatilisation TGA setup specifications.

Furnace specifications	
Model	LENTON - TSH15/50/180
Max Temp (°C)	1500
Heated Length (mm)	180
Volts	240
Ext Dimensions Incl. Console (mm) H x L x D	600 x 600 x 420
Mass (kg)	22
Work tube (mm) I.D x Length	50 x 600
Mass balance specifications	
Model	Sartorius® ED4202S
Max Weight Capacity (g)	4200

The sample was placed in a stainless steel cup like sample holder with ventilation holes at the bottom to ensure adequate flow of gas around the particle during devolatilisation. For the 40 mm particles, an additional mesh bucket was added to ensure that the particle did not touch the inside of the oven during measurements. The bucket system and the stand housing the bucket are shown in Figure 17.

Figure 17: Bucket system for large particle devolatilisation.

The bucket system was heated prior to placing the sample inside the furnace, to avoid excessive heat loss due to heating of the bucket. The sample holder was attached to a tri-pod stand to ensure stability of the particle. A K-type thermocouple was used to measure the temperature above the particles inserted into the system. The gas supply to the furnace was controlled by a rotameter that was calibrated prior to experimentation.

3.5.3. Devolatilisation procedure

Initially the oven was set to the required temperature using a Eurotherm 808 programmable temperature controller fitted with a Eurotherm 92 over-temperature protection unit. While the oven was being heated, the nitrogen gas was supplied at a flow rate of 12.5 dm^3(STP)/min.

Once the oven reached the required temperature, the furnace was lowered over the empty bucket system in order to heat the bucket system. The mass balance was then tared and the computer software was initialised.

After particle selection, the data login software on the computer was started and set to log the mass and temperature reading on the thermocouple above the particle at 5 second intervals.

The furnace was lifted and the particle was immediately placed into the bucket system, the furnace was then lowered again with the particle placed in the required heating zone. The initial mass of the 5 mm and 10 mm particles was in the order of 3 g (25 to 30 particles) and 7 g (8 to 10 particles) respectively while single particles were used for 20 mm and 40 mm particles. The temperature and mass were then measured for the duration of devolatilisation. The results were displayed on the computer monitor for visual inspection of the experiment.

Once the mass loss stabilises the experiment was terminated and the logging software was stopped. The oven was then lifted slightly to move the particle to a cooler region in the tube. The gas flow was maintained until the particle cooled to below 200°C. The particle was then removed from the furnace and left to cool to room temperature.

The experimental work and parameters are summarised in Table 9.

Table 9: Devolatilisation experimental work sheet.

Devolatilisation experimental work sheet	
Particle sizes	5 mm 10 mm 20 mm 40 mm
Devolatilisation Temperatures	450°C 700°C 850°C
Gas	N_2
Gas flow rate	12.5 dm^3(STP)/min

Char particles created during devolatilisation experiments were placed in marked containers and some were subsequently used during the gasification experiments.

3.6. Gasification

3.6.1. Particle selection

The particles (chars) generated during the devolatilisation experiments were used for the gasification investigation. The gasification of the 5 mm and 10 mm samples was done on minimum sample weight of 3 g. This was done in order for the weight of the remaining ash after gasification to be in the range of 1 g, to reduce the noise caused by the mass balance with very small weight changes.

3.6.2. Gasification equipment

The large particle TGA system was also used for the gasification experiments. In the case of gasification, some alterations on the setup were made due to the reactive nature

of CO_2. The K-type thermocouple placed above the particle was fitted with a ceramic sleeve to prevent the CO_2 from coming into contact with the metal surface of the thermocouple.

The stainless steel sample holder used during devolatilisation was replaced for gasification experiments. The new sample holder was constructed from quartz with the same ventilation holes and basic geometry as the stainless steel setup. The quartz sample holder is shown in Figure 18.

Figure 18: Quartz sample holder used for gasification.

The gas was again controlled with a rotameter that was calibrated for CO_2 gas prior to the start of the gasification experiments.

3.6.3. Gasification procedure

The gasification procedure was started by heating the furnace to 900°C and waiting for the temperature to stabilise. While the furnace was heating, the CO_2 gas was introduced into the system at a flow rate of 7.5 dm^3(STP)/min. This flow rate ensures an excess of CO_2.

For the gasification experiments of 5 mm and 10 mm particles, approximately 35 and 15 particles were used respectively while single particles were used for 20 mm and 40 mm particles. After the temperature stabilised the samples were placed in the sample holder and the logging software was initialised. The software was set to record the mass as well as the temperature above the sample at 5 second intervals. Once the data started logging the furnace was lowered over the sample. The experimental conditions and parameters are summarised in Table 10.

Table 10: Gasification experimental work sheet.

Gasification experimental work sheet	
Particle sizes	5 mm 10 mm 20 mm 40 mm
Gasification temperature	900°C
Gas	CO_2
Gas flow rate	7.5 dm^3(STP)/min

The mass loss was continuously monitored until no change in mass was observed for a significant amount of time. This indicated that gasification of the sample was complete and that the experiment could be terminated.

The ash formed during gasification was then removed from the sample holder and placed in marked containers. The ash was removed from the furnace without being cooled.

3.7. Error calculations

In the case where multiple runs were used to obtain an average value from experiments, the error of the experiment was determined based on a statistical 95% confidence interval.

Chapter 4: Results and Discussion

4.1. Introduction

In this section the experimental results are presented and discussed. In Section 4.2 the characterisation results obtained from conventional analyses and SSNMR are presented. This is followed by Section 4.3 where the devolatilisation results for different particle sizes and temperatures are discussed. The results from the gasification experiments are given in Section 4.4 and relate gasification reactivity to particle size and devolatilisation temperature. In Section 4.5 the CO_2 gasification modelling is presented and discussed.

4.2. Characterisation

4.2.1. Conventional analyses

All conventional analyses were carried out at SABS Secunda according to the standards listed in Table 7. The results for the proximate analyses are given on an air dry basis (adb) in Table 11.

Table 11: Proximate analyses results over particle size range (adb)

Particle size range	Inh. H_2O	Vol. Mat.	Ash	Fix. Car.
+25 mm -53 mm	3.6	22.2	29.2	45.0
+12.5 mm -25 mm	3.8	22.1	26.5	47.6
+6.3 mm -12.5 mm	3.8	21.2	27.9	47.1
+3.35 mm -6.3 mm	3.9	21.2	26.2	48.7
Average	**3.8 ± 0.3**	**21.7 ± 1.1**	**27.5 ± 2.6**	**47.1 ± 3.1**

From the results in Table 11 it can be seen that the inherent moisture and volatile matter content do not differ significantly over the size ranges investigated. The inherent

moisture varies between 3.6% and 3.9% while the volatile matter content varies from 21.2% to 22.2%. The ash content and the amount of fixed carbon show a slightly higher degree of variation over the size range. The largest size fraction (+25 mm – 53 mm) has the highest mineral matter content and subsequently the lowest amount of fixed carbon, with the other size fractions having similar amounts of ash and carbon. Although small variations occur, it can be concluded that the proximate analysis does not show significant differences between the different particle sizes.

Opposing trends with regards to volatile matter content and fixed carbon content have been found by Yu *et al.* (2005) who investigated three coal particle size fractions (-63 µm, -100 µm and -200 µm). Their results showed that the volatile matter content decreased from 41.49% to 35.98% from the smallest particle size fraction to the largest particle size fraction while the fixed carbon content increased from 39.24% to 44.22% from the smallest to the largest particle size fractions.

Comparing coal property changes with particle size variations (-38 µm to +212 µm) of a South African coal from the Middelburg region, Cloke *et al.* (2002) showed a variation of 3.8% for ash(db) percentage over nine size fractions as well as a variation of 7.1% for both volatiles (daf) and fixed carbon (daf) percentages. No significant trend correlating the mentioned parameters and particle size could be observed for this coal.

The results from ultimate analyses are given on a dry ash free basis (daf) percentage in Table 12.

Table 12: Ultimate analyses results over particle size range (daf – wt%)

Particle size range	Carbon	Hydrogen	Nitrogen	Tot. Sul.	Oxygen
+25 mm -53 mm	84.9	5.0	2.4	1.6	6.1
+12.5 mm -25 mm	85.1	4.9	2.0	2.3	5.8
+6.3 mm -12.5 mm	85.2	5.0	2.0	0.9	6.9
+3.35 mm -6.3 mm	82.9	4.8	2.0	1.2	9.2
Average	**84.5 ± 2.2**	**4.9 ± 0.2**	**2.1 ± 0.4**	**1.5 ± 1.2**	**7 ± 3.1**

The ultimate analysis results also indicate that no significant differences in chemical properties are present with size variation. The carbon ranges from 82.9% to 85.2% over the size ranges investigated while the hydrogen and oxygen values range from 4.8% to 5.0% and 6.1% to 9.2% respectively. The sulphur content varies from 0.9% to 2.3% over

the size range but shows no significant trend with regards to particle size. The variation in sulphur content can be due to coal heterogeneity. The large variation in oxygen content may be attributed to the fact that this value is calculated by difference. These results correlated very well with the Witbank coal seams as shown in Table 1 (England, 2002). The proximate and ultimate values obtained are similar to the values reported by Higman & van der Burgt (2008) for typical South African bituminous coals.

The calorific values for different particle sizes are presented in Table 13. The calorific value also does not differ significantly (20.9 – 21.9 MJ/kg) over the particle size range. The lower calorific values obtained in-house are probably due to differences in moisture content that might have arisen in the time between the initial analysis that was done at SABS and the analysis that was repeated in-house.

Table 13: Calorific values for different particle sizes

Particle size range	SABS (MJ/kg)	In-house (MJ/kg)
+25 mm -53 mm	20.9	19.8
+12.5 mm -25 mm	21.7	20.6
+6.3 mm -12.5 mm	21.2	20.4
+3.35 mm -6.3 mm	21.9	20.6
Average	**21.9 $\pm$ 0.9**	**20.9 $\pm$ 0.8**

4.2.2. Solid state NMR

The CPMAS spectra and integration regimes for the +3.35 mm to -6.3 mm, +12.5 mm to -25 mm and +25 mm to -53 mm particle size ranges are shown in Figures 19, 20 and 21 respectively.

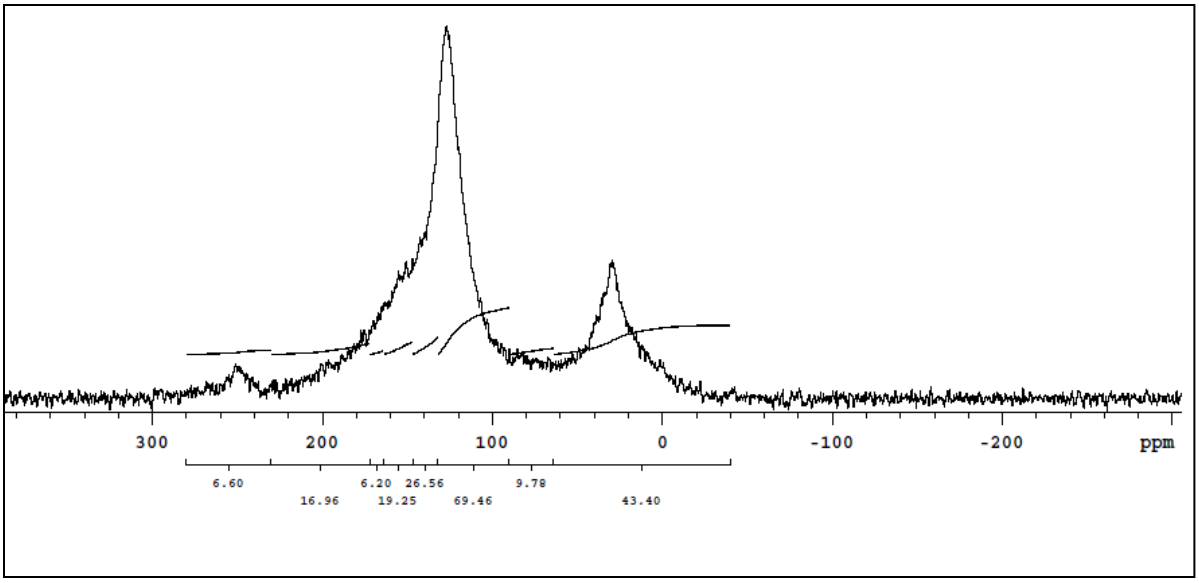

Figure 19: CPMAS spectrum and integration regions for the +3.35 mm to -6.3 mm size range.

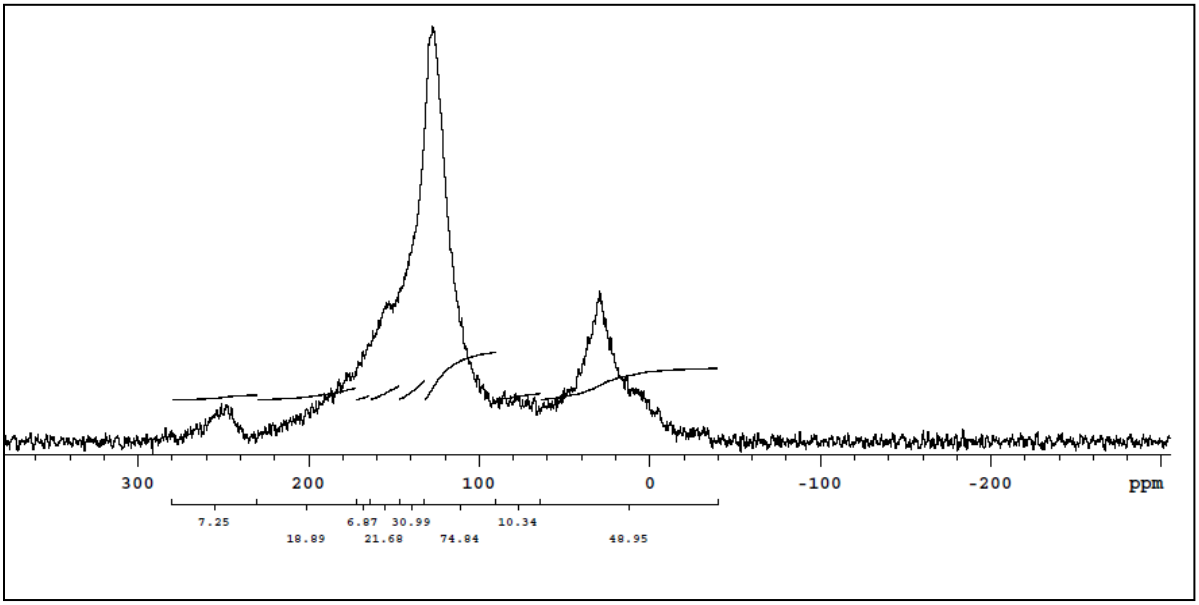

Figure 20: CPMAS spectrum and integration regions for the +12.5 mm to -25 mm size range.

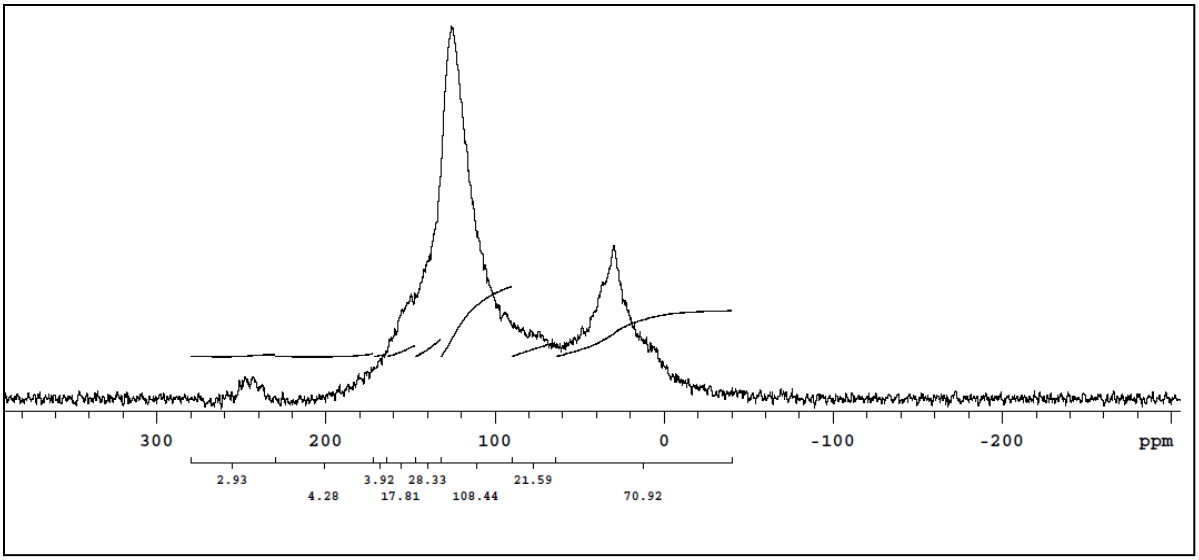

Figure 21: CPMAS spectrum and integration regions for the +25 mm to -53 mm size range.

From these figures, it can be observed that similar spectra were obtained for all three size fractions with the SSB peak appearing at approximately 250 ppm. The two most prominent peaks representing mostly aromatic carbons (at approximately 130 ppm) and mostly aliphatic carbons (at approximately 30 ppm) are also similar for all three particle size ranges. No significant differences can be observed from the CPMAS spectra of the three size fractions.

The DD spectra for the +3.35 mm to -6.3 mm, +12.5 mm to -25 mm and +25 mm to -53 mm particle size ranges are shown in Figures 22, 23 and 24 respectively. The integration regions are also indicated.

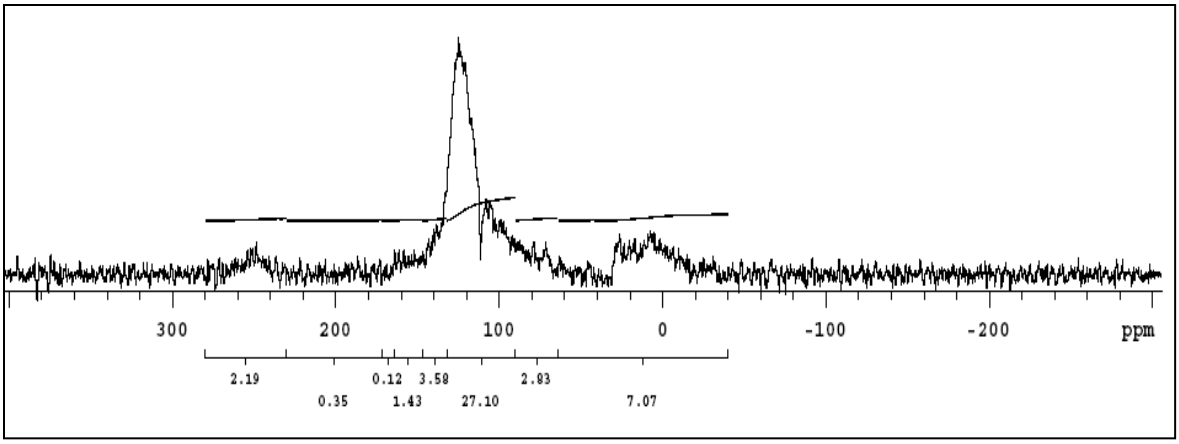

Figure 22: DD spectrum and integration regions for the +3.35 mm to -6.3 mm size range.

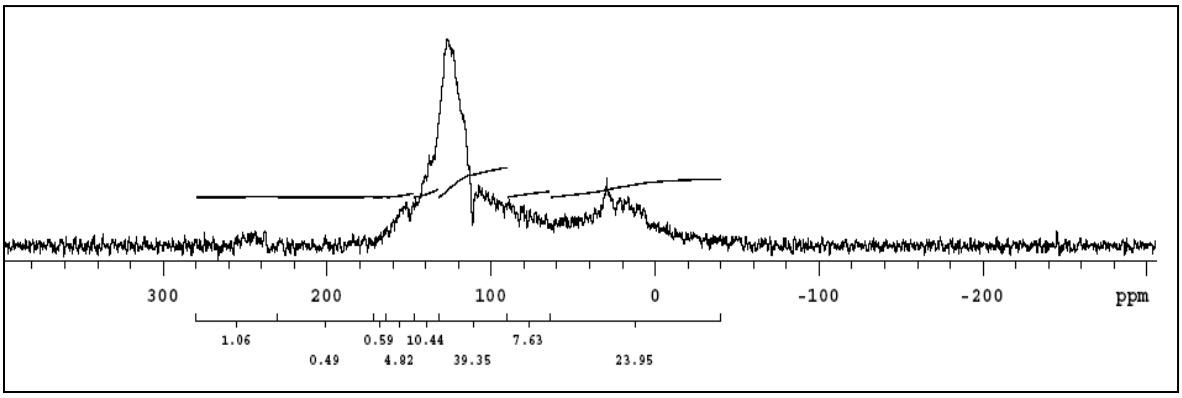

Figure 23: DD spectrum and integration regions for the +12.5 mm to - 25 mm size range.

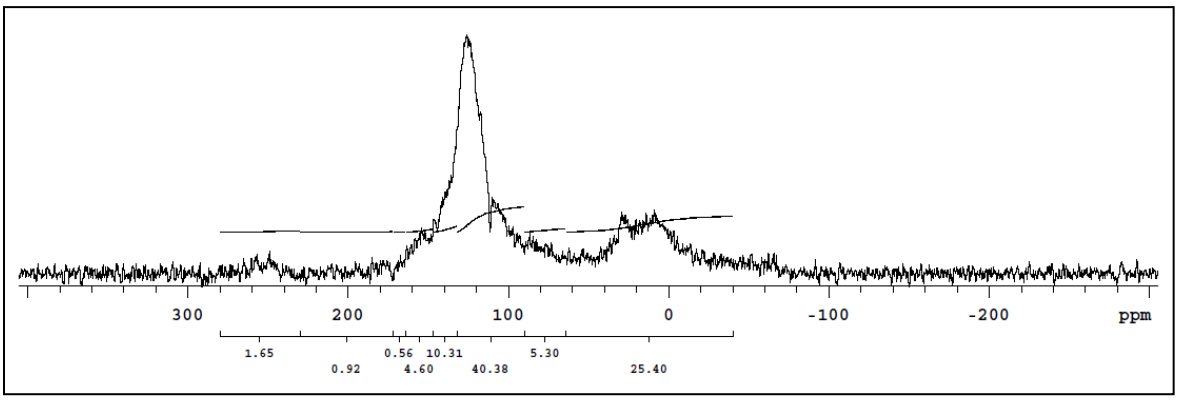

Figure 24: DD spectrum and integration regions for the +25 mm to - 53 mm size range.

For all three size fractions, significant peaks at 30 ppm and 10 ppm can be observed. A less pronounced peak at 250 ppm can also be observed for all three size fractions.

The DD dephasing spectrum obtained for the +3.35 mm to -6.3 mm size fraction differs from the other two in the way that the left shoulder of the peak around 10 ppm is very sharp in comparison to the left shoulder of the same peak for the other two size fractions. Furthermore, the integration values obtained from the DD spectrum for the +3.35 mm to -6.3 mm size range are significantly lower than those of the other two size fractions. The signal to noise ratio is also much higher for the +3.35 mm to -6.3 mm size fraction than for the other two size fractions.

The difference may be a result of a collection of various factors including: actual difference in the sample; demineralisation effects; signal to noise ratio in the DD spectrum; and analysis conditions. As all samples were analysed using the same method and at the same time, the effect of analytical conditions is believed to be minimal. An automated algorithm was used for baseline correction as well as region integration in order to ensure that all samples were analysed in a similar manner. Since the characterisation has only been carried out once, a definitive reason for this difference in the DD spectrum was not found.

From the region integration results shown in the CPMAS and DD spectra the total amount of aromatic carbons (C-ar), total amount of aliphatic (C-al) carbons and the total amount of various other carbon types can be determined for each size fraction. The integration results for these two experiments over three size ranges are shown in Table 14.

The integration regions used to obtain the values in Table 14 were discussed in Section 2.5. The region integration values from Table 14 were used to determine the characteristic parameters as described in Section 2.5. The characteristic parameters of each size fraction as well as the variation of these parameters as found in literature are shown in Table 15.

Table 14: Region integration values for three size ranges

	+3.35 mm to -6.3 mm		+12.5 mm to -25 mm		+25 mm to -53 mm	
Region	**CPMAS**	**DD**	**CPMAS**	**DD**	**CPMAS**	**DD**
1 (F)*	6.60	2.19	7.25	1.06	8.36	1.77
2 (E)	16.96	0.35	18.89	0.49	21.78	1.46
3 (C)	6.20	0.12	6.87	0.59	7.60	0.90
4 (D)	19.25	1.43	21.68	4.82	25.47	6.21
5 (G)	26.56	3.58	30.99	10.44	35.36	13.28
6 (C)	69.46	27.10	74.84	39.35	87.95	42.65
7 (B)	9.78	2.83	10.34	7.63	12.89	6.67
8 (A)	43.40	7.07	48.96	23.95	54.89	21.95
Total	**198.20**	**44.68**	**219.81**	**88.32**	**254.30**	**94.89**
C-ar	**134.67**	**36.61**	**148.89**	**57.32**	**173.10**	**66.58**
C-al	**46.58**	**7.71**	**52.04**	**30.52**	**59.42**	**26.85**

***** Notation in brackets taken from Suggate & Dickinson (2004) and Solum *et al.* (1989).

Table 15: Solid state NMR characteristic carbon types for three size ranges

Parameter	+3.35mm -6.3mm	+12.5mm -25mm	+25mm -53mm	Literature**
fa	0.74	0.74	0.74	0.61 – 0.86
fal	0.26	0.26	0.26	0.14 – 0.39
faCO	0.08	0.08	0.08	0.00 – 0.10
faP	0.11	0.11	0.11	0.02 – 0.09
faS	0.15	0.15	0.15	0.13 – 0.21
faN	0.27	0.38	0.38	0.28 – 0.53
faH	0.47	0.36	0.36	0.16 – 0.33
faB	0.02	0.12	0.12	0.09 – 0.34
falN *	0.04	0.13	0.10	0.06 – 0.17
falH	0.22	0.13	0.15	0.08 – 0.27
falO	0.05	0.05	0.05	0.01 – 0.12

* Results for non-protonated aliphatic normalised to fraction of aliphatic carbon

** Literature results taken from Solum *et al.* (1989).

From the results shown in Table 15 it can be concluded that there is no significant difference in the fraction of aromatic (74%) and aliphatic carbon (26%) for all three samples investigated. It is furthermore observed that the fractions of aromatic carbonyl and carboxyl carbons (8%), of aromatic phenolic carbons (11%), of alkylated aromatic

carbons (15%) and aliphatic carbons bonded to oxygen (5%) do not differ over the three particle size ranges investigated.

Parameters for the +3.35 mm to -6.3 mm size fraction calculated using the results obtained from the DD experiments differ from the other two size fractions to various extents due to the differences noticed in the DD spectra. The accuracy of the results calculated from the direct or indirect use of integration DD results are also less precise due to the high signal to noise ratio observed during DD experiments for all particle sizes.

The fractions of protonated aromatic carbons (27% to 38%), non-protonated aromatic carbons (36% to 47%), non-protonated aliphatic carbons (4% to 13%) and methyl aliphatic carbons (13% to 22%) are reasonably comparable over the investigated size ranges. The fraction of bridgehead carbons ranges from 2% to 12% across the three size ranges.

The results obtained from the SSNMR analyses are in good correlation with the results found by Solum *et al.* (1989) for coals ranging from lignite to low volatile bituminous coals.

From the proximate, ultimate and SSNMR characterisation results it can be concluded that no significant difference with regards to the chemical composition as well as carbon types are present over the investigated particle size range.

4.3. Devolatilisation

As devolatilisation experiments were carried out with different particle size and devolatilisation temperature the results are first discussed in general in Section 4.3.1 in order to show experimental repeatability and data processing. Thereafter the effects of particle size and devolatilisation temperature are discussed in Section 4.3.2 and 4.3.3 respectively.

4.3.1. Experimental results representation

As experiments were done on single particles (for particle sizes of 20 mm and 40 mm) or on a small number of particles (for particle sizes of 5 mm and 10 mm), each set of experiments had to be repeated several times to ensure that the results obtained were representative for the entire batch (Stubington & Sumaryono, 1984). A series of repeats carried out for the devolatilisation of 40 mm particles at 700°C is shown in Figure 25.

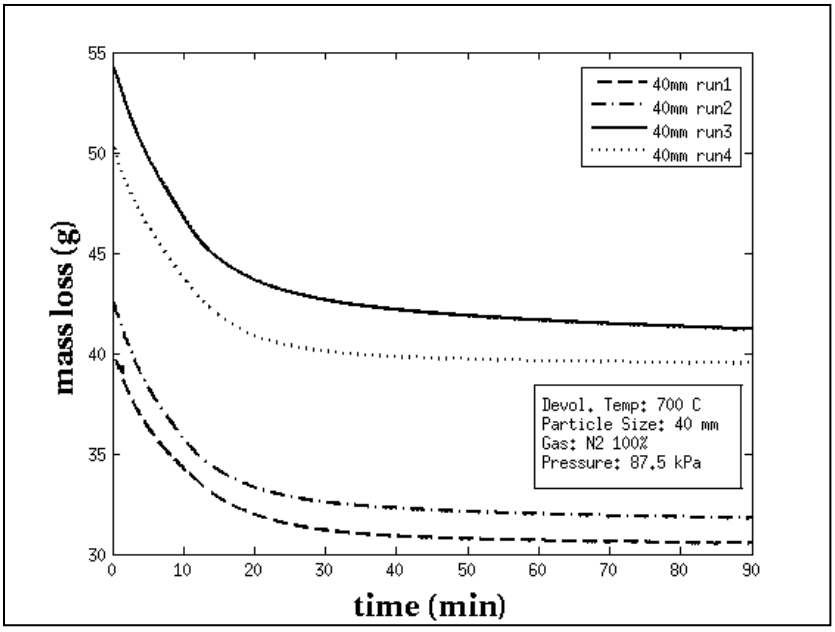

Figure 25: Raw mass loss data for devolatilisation of 40 mm particles at 700°C.

From Figure 25 it can be seen that each particle has a different initial mass after which the corresponding mass loss takes place. The shape of the 4 runs is identical, starting with a fast initial mass loss followed by a slower mass loss towards the end of devolatilisation. Since single particles were used for each experiment, the final amount of mass loss differed for each run. This was due to the difference in initial mass and volatile matter content for each particle. The experiments were terminated once the mass loss versus time was constant. In order to make results more comparable, the mass loss data was normalised with respect to time using Equation 8.

—— (8)

The normalised data for the devolatilisation of 40 mm particles at 700°C is shown in Figure 26. (The complete set of devolatilisation experiments are shown in Appendix A).

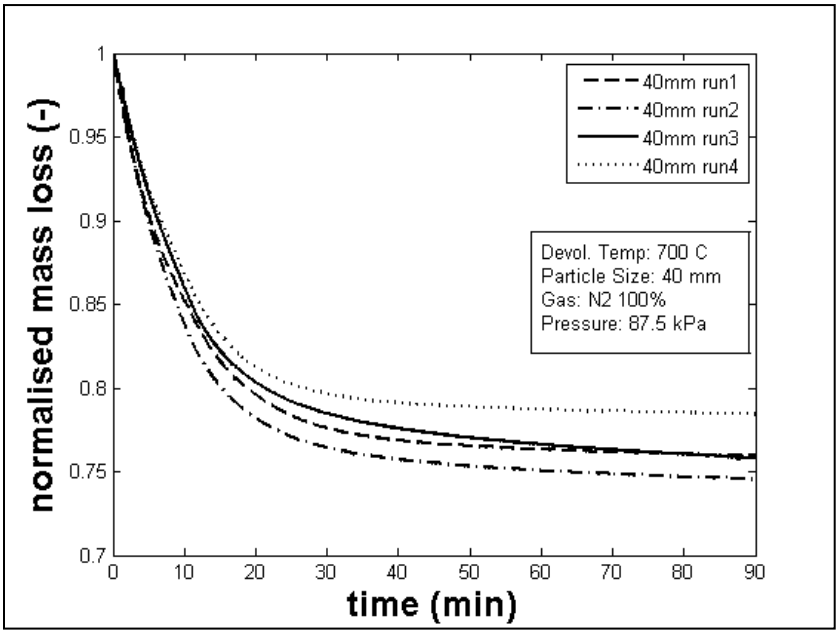

Figure 26: Repeatability for devolatilisation experiments for 40 mm particles at 700°C.

From Figure 26 it can be seen that the repeatability of the devolatilisation experiments for large particles is relatively good.

The average of these four lines (Figure 26) was used to represent the 40 mm particles devolatilised at 700°C and this single line is shown in Figure 27.

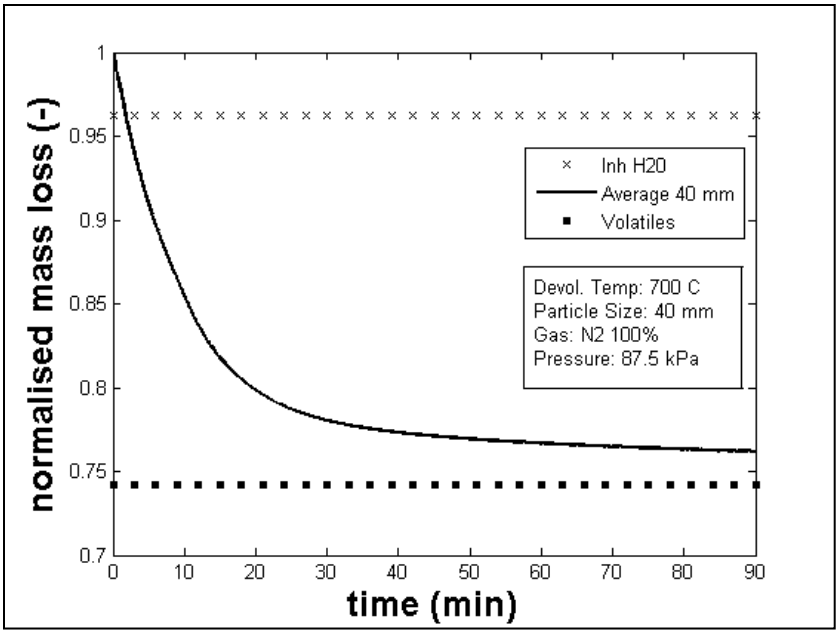

Figure 27: Representation of average devolatilisation result (for 40 mm particles at 700°C).

The devolatilisation figures in the remainder of this dissertation all show the averaged normalised mass loss (m/m_0) versus time results and contain information pertaining to experimental conditions as well as proximate analysis results. The inherent moisture determined from the proximate analysis is indicated as Inh. H_2O, while the sum of total volatile matter content and inherent moisture is indicated as Volatiles. The Inh. H_2O and Volatiles measures are used to compare the extent of devolatilisation achieved at different experimental conditions. Furthermore the devolatilisation temperature, particle size, devolatilisation atmosphere and pressure are indicated in the figure. The experimental errors for each set of results are reported in Table 16 (page 71).

4.3.2. Effect of particle size

The effect of particle size on the devolatilisation kinetics is given in Figure 28.

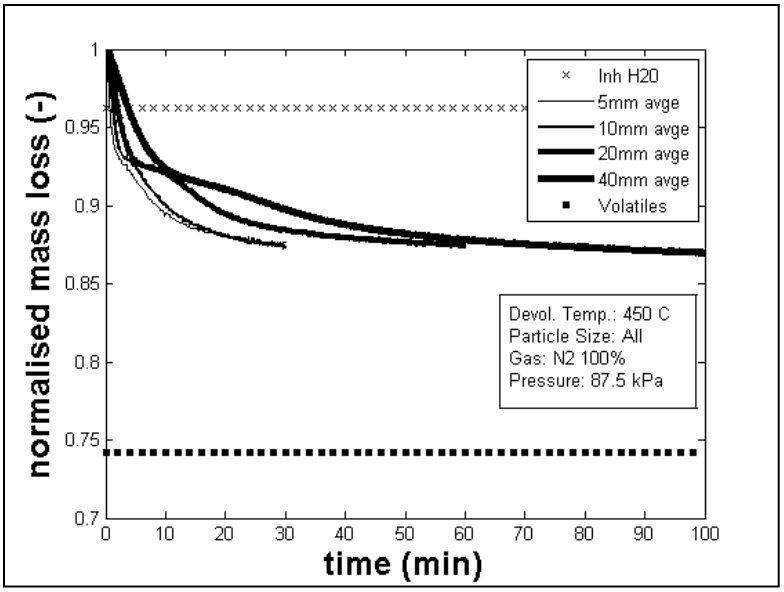

Figure 28: Particle size devolatilisation at 450°C.

From Figure 28 it can be seen that the mass loss curves for all particle sizes show a fast initial mass loss followed by a slower final section. During the initial mass loss period, two distinct regions can be identified with the significant bend separating the two regions.

While comparing devolatilisation for different particle sizes at 450°C, it was found that the initial rate of normalised mass loss decreases from the small particles to the larger particles. The time needed for complete devolatilisation also increases with increase in particle size. The 40 mm particles take approximately 100 min for complete devolatilisation while the devolatilisation of 5 mm particles is complete in approximately 20 min. The total volatile yield for devolatilisation at 450°C over the investigated particle sizes ranges from 12.1% to 14.5% and does not differ significantly. These values are significantly lower than the values from the proximate analysis, indicating that at this relatively low temperature not all volatiles are released.

The shape of the normalised mass loss graph of the larger particles (20 mm and 40 mm) shows a characteristic feature between about 90% and 95% normalised loss in the form of a bend. This bend is believed to be caused by the fact that the moisture release period and the devolatilisation period for larger particles can more clearly be

distinguished due to a larger temperature profile. The separate moisture and volatile release is illustrated in Figure 29.

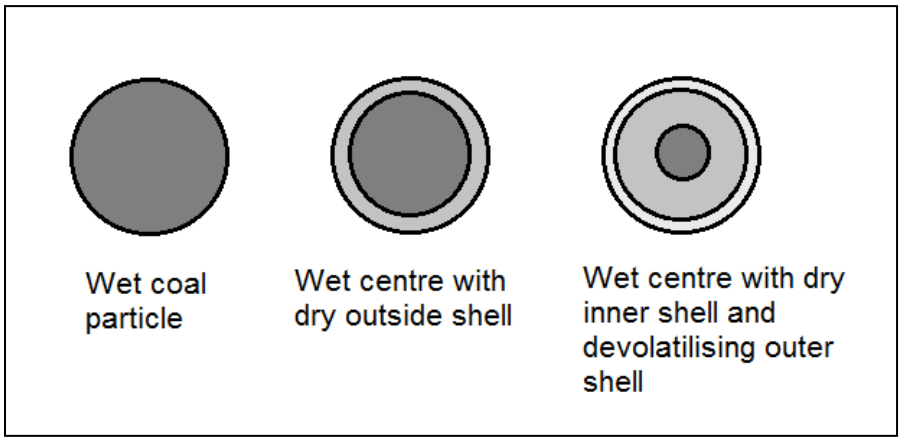

Figure 29: Schematic for devolatilisation of large coal particles.

From the devolatilisation schematic shown in Figure 29 it is proposed that the entire coal particle initially has inherent moisture (wet). After some heat treatment the outside of the particle reaches a temperature at which inherent moisture is released and forms a dry shell (moisture free). As the temperature of the particle core increases the moisture from the centre continues to be released while the dry outside shell reaches sufficient temperatures for devolatilisation. When the initial moisture release occurs separately from volatile release two distinct regions of mass loss will be present. The separate release of moisture and volatile matter will become less pronounced at higher temperatures as the inside shells reach devolatilisation temperature faster. This bend in the volatile release curves could also be due to the change over from the fast devolatilisation to slow devolatilisation. But due to the fact that the precise heating rate to the inside of the particle and volatile release rate from the centre of the particle are not known, it is difficult to distinguish the main contributing factor for the bend in the mass loss curves.

The normalised mass loss for different particle sizes at a devolatilisation temperature of 700°C is shown in Figure 30.

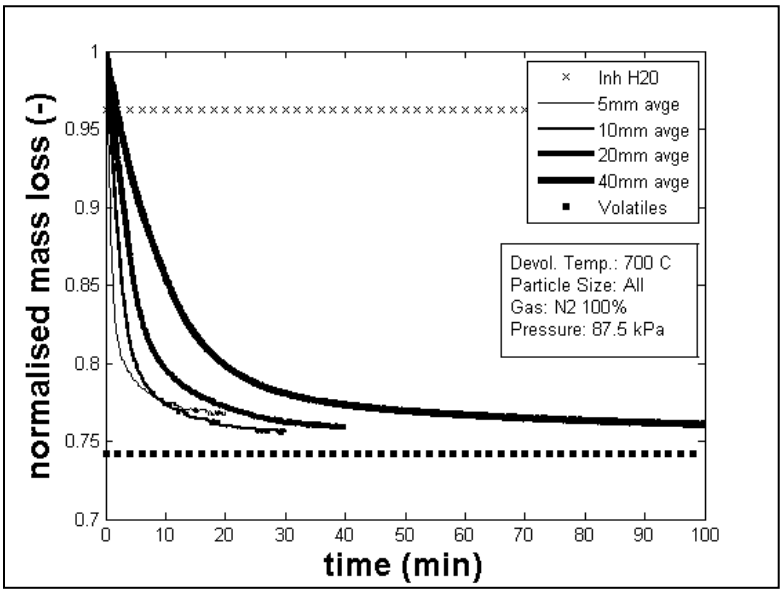

Figure 30: Particle size devolatilisation at 700°C.

From Figure 30 it can again be observed that the initial rate of normalised mass loss increases with decrease in particle size. The separate periods of mass loss, as seen for devolatilisation at 450°C, are not observed anymore. An increase in particle size results in an increase in time needed for complete devolatilisation with the final volatile yield varying from 23.6% to 24.6% over the entire particle range. This final amount of volatile release is close to the total amount of volatiles determined from proximate analysis (25.8%).

The devolatilisation results for different particle sizes at 850°C are shown in Figure 31. From Figure 31 it can again be seen that the initial rate of normalised mass loss increases with a decrease in particle size.

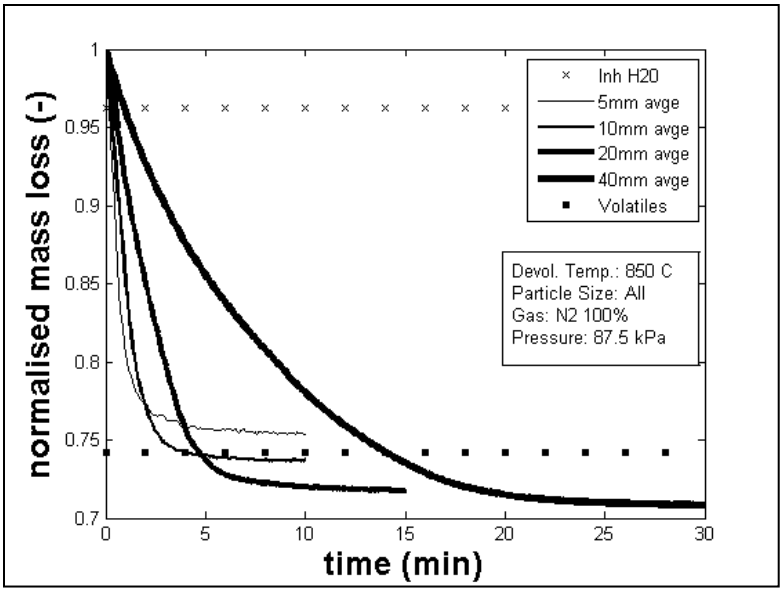

Figure 31: Particle size devolatilisation at 850°C.

Furthermore the time for complete devolatilisation increases (8 min to 30 min) with an increase in particle size. The devolatilisation times for 5 mm and 10 mm particles are almost similar (approximately 8 min).

The final amount of volatile yield seems to increase with increase in particle size and ranged from 26.8% to 29.3%; the observed increase in volatile yield with particle size is, however, within the calculated precision. Borah *et al.* (2008) investigated the devolatilisation behaviour of coal from five different collieries with particle sizes ranging from 4 mm to 9 mm at 850°C. Their results showed significant scatter over the particle size range with regards to final amount of volatile release to proximate values. Volatile matter release to proximate volatile matter value ratios ranged from 0.83 to 1.86 with no definite trend with regards to particle size. Zhu *et al.* (2008) however showed that an increase in particle size resulted in an increase in char yield, and it was suggested that this increase in char yield could possibly by caused by the increase in secondary reactions with larger particles. Results indicate that devolatilisation time as well as rate of devolatilisation is strongly influenced by particle size, which confirms results obtained by Borah *et al.* (2008). Stubington & Sumaryono (1984) have related the increased devolatilisation time for large particles to the increased heating time.

The separate mass loss regions found during devolatilisation at 450°C are not visible at higher devolatilisation temperatures (700°C and 850°C). This is believed to be caused by the more rapid heating rate of the particle at higher devolatilisation temperatures, which causes moisture and volatile release to occur simultaneously.

A significant amount of particle fragmentation occurred during the devolatilisation of the 40 mm particles at elevated temperatures (700°C and 850°C). Fragmentation was also observed for other particle sizes but was not as pronounced. An example of fragmentation of a 40 mm particle during devolatilisation at 850°C is shown in Figure 32.

Figure 32: Fragmentation of 40 mm particle at a devolatilisation temperature of 850°C.

From Figure 32 it can be seen that the single large 40 mm particle fragmented into 4 relatively large pieces and multiple smaller pieces (not all shown). The amount of fragmentation occurring during the devolatilisation of the 40 mm particles prepared at devolatilisation temperatures above 450°C was so significant that no 40 mm chars remained intact for gasification. This is to be expected as higher temperature gradients (caused by higher devolatilisation temperatures) in the coal particle could cause a more pronounced pressure gradient leading to greater fragmentation (Sasongko & Stubington, 1996). Chen *et al.* (1994), making use of a statistical model, were able to simulate a higher probability of fragmentation with increase in particle size and obtained similar

results pertaining to larger particles leading to a higher degree of fragmentation. The char particles were very brittle after devolatilisation and some fragmentation occurred during the removal of the char from the TGA. The fragmentation characteristics differed from particle to particle, with some only fragmenting into two large pieces and others into multiple smaller pieces. The observed degree of fragmentation increased with increase in particle size as well as increase in devolatilisation temperature. Investigating the devolatilisation section of a commercial gasifier Bunt & Waanders (2008) concluded that a significant amount of particle breakage occurs during the devolatilisation of large (+25 mm) particles. The +25 mm particle abundance decreased from 50% to 15% while the finer particle (-25 mm to +6.3 mm) abundance increased from 37% to 64% in the devolatilisation section.

4.3.3. Effect of devolatilisation temperature

To show the effect of temperature on the rate of devolatilisation, the same particle size was compared at different temperatures as shown in Figure 33 for the devolatilisation of 5 mm particles.

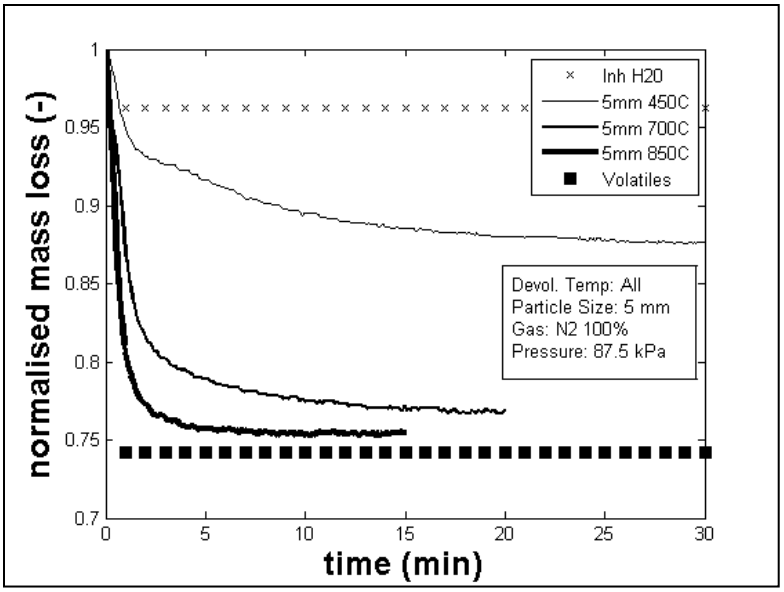

Figure 33: Devolatilisation of 5 mm particle at different temperatures.

From Figure 33 it can be seen that the initial rate of normalised mass loss decreases with a decrease in devolatilisation temperature, while the time required for complete devolatilisation decreases with an increase in devolatilisation temperature. The maximum obtainable volatile yield increases with an increase in devolatilisation temperature. A maximum volatile yield of 14% is achieved for 5 mm particles at 450°C while at devolatilisation temperatures of 700°C and 850°C, a maximum volatile yield of 23.6% and 26.8% is achieved respectively. Similar devolatilisation trends were observed for all particle sizes.

Stubington & Sumaryono (1984) investigated temperature ranges from 750°C, 850°C and 950°C and similarly found a decrease in char yield accompanying an increase in devolatilisation temperature. The prominent mass loss curve bend is noticed only for devolatilisation at 450°C for all particle sizes. The amount of volatile release at 850°C exceeds the amount determined from proximate analysis for all particle sizes except for 5 mm particles. Borah *et al.* (2008) and Stubington & Sasongko (1998) also found higher volatile release values (devolatilisation at 850°C) than predicted by proximate analyses (done at 900°C) and ascribed these differences to the technique used to determine air dried proximate values. The volatiles determined from proximate analyses are only a number determined from a standard used and do not necessarily include all volatiles.

For all particle sizes, the time for devolatilisation decreased with increase in temperature. This is consistent with the findings of Sasongko & Stubington (1996) who studied coal devolatilisation for particle sizes ranging from 1 mm to 20 mm.

A summary of the total amount of volatiles as a function of particle size and devolatilisation temperature is given in Table 16.

Table 16: Percentage volatiles released at different experimental conditions.

Particle size (mm)	Temp 450°C	Temp 700°C	Temp 850°C	Proximate (Inh. H20 + Vol.)
5	14.0 ± 2.3	23.6 ± 2.0	26.8 ± 2.5	25.8 ± 1.2
10	14.5 ± 3.2	24.6 ± 3.7	26.4 ± 3.6	
20	13.3 ± 3.4	24.2 ± 5.9	28.1 ± 7.3	
40	12.1 ± 4.3	23.9 ± 3.3	29.3 ± 6.9	

The extent of secondary reactions is believed to increase with temperature and volatile residence time within the coal (indicating that particle size plays a significant role) (Stubington & Sumaryono, 1984). This would result in larger particles retaining more secondary reaction material and consequently a decrease in volatile yield. This was, however, not noticed during this study. The fragmentation might cause some of the deposited materials to be released again, resulting in an increase in volatile yield with increase in fragmentation.

Investigations by Zajdlik *et al.* (2001) showed that up to 4% volatile matter could still be retained in coal particles (72.3 wt% carbon) after devolatilisation at 800°C. For all particle sizes investigated in this study the final percentages of mass loss obtained at a devolatilisation temperature of 850°C were within 5% of proximate analysis results, which is a strong correlation considering the fact that only small amounts of particles were used during some experiments. While investigating particle sizes ranging from 3 mm to 10 mm, Stubington & Sasongko (1998) also found a variation of approximately 4% in final volatile yields and explained that the scatter could have been caused by the use of single particles with properties different from the batch.

4.4. Gasification

In order to compare the reactivity of chars obtained at different devolatilisation conditions, the CO_2 reaction rates of the different chars were compared. The effects of particle sizes were also investigated. The results are discussed in terms of experimental results representation (Section 4.4.1) followed, in Section 4.4.2 and 4.4.3, by the effect of devolatilisation temperatures and particle size respectively.

4.4.1. Experimental results representation

The chars prepared during devolatilisation experiments still contain some volatile matter (specifically the ones prepared at 450°C) that is released during the early stages of gasification. The fast initial mass loss (volatile release) for 10 mm char particles prepared at 450°C is shown in Figure 34.

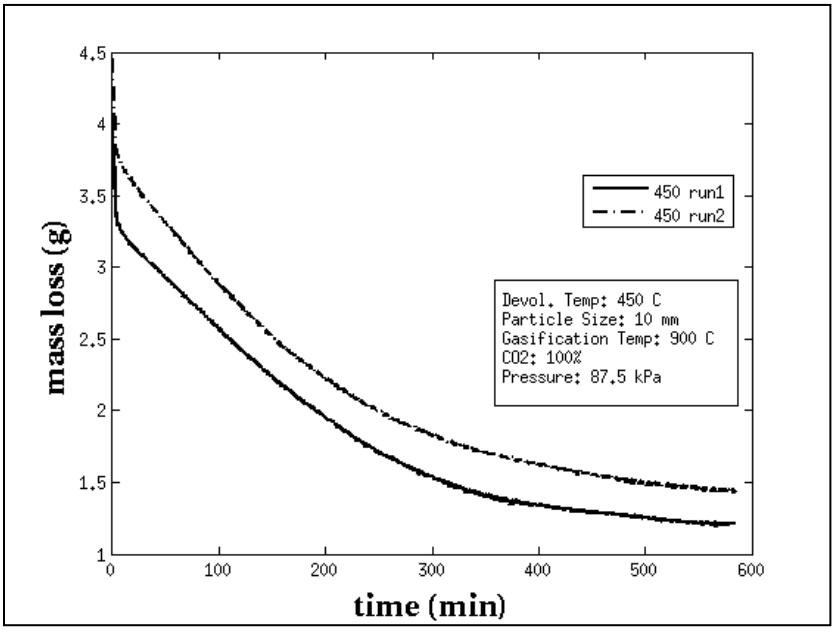

Figure 34: Raw mass loss data for 10 mm chars prepared at 450°C.

From Figure 34 it can be seen that for both repeats the residual volatile content was released in a very short time from onset of gasification. Furthermore the reactions were carried out until the mass loss was constant, leaving assumably only ash as remaining product.

The raw mass loss data is normalised according to Equation 8, and shown in Figure 35 for the gasification of 10 mm chars devolatilised at 450°C. From this figure it can be seen that both runs have similar shape and that the final amount of mass loss does not differ significantly and compare well with the ash values from the proximate analysis (Table 11).

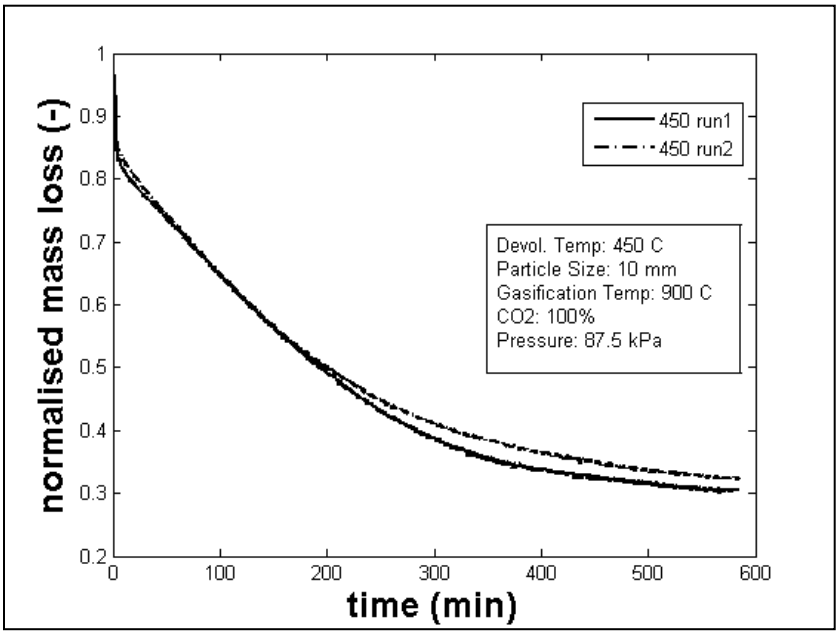

Figure 35: Normalised mass loss data for 10 mm char particles prepared at 450°C.

To account for remaining volatiles and different ash values the data are normalised to a dry ash free basis in order to compare gasification kinetics only, according to Equation 9.

(9)

The gasification carbon conversion results for 10 mm chars prepared at 450°C are shown in Figure 36.

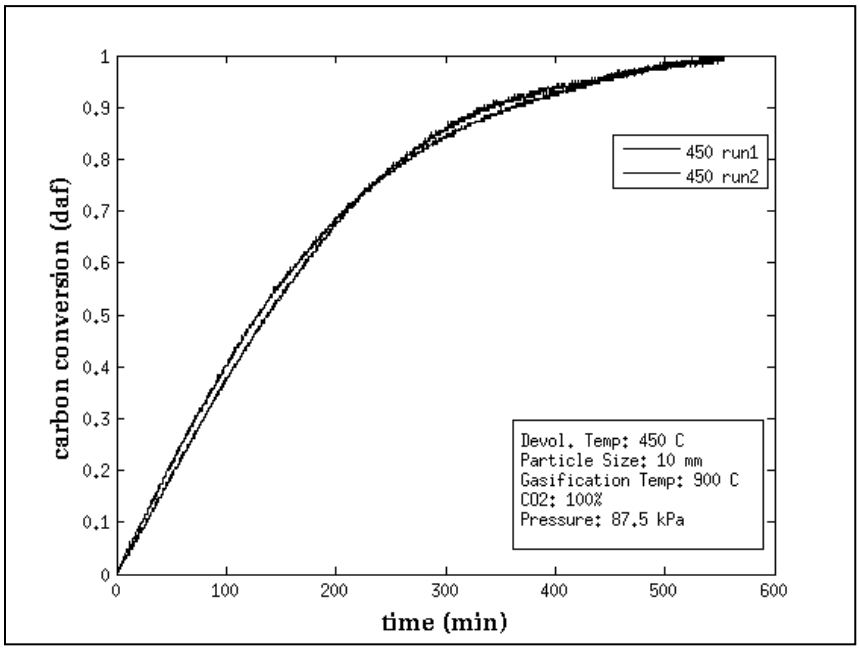

Figure 36: Carbon conversion for 10 mm chars prepared at 450°C.

From Figure 36 it can be seen that the results are comparable once the data have been normalised to an ash and volatile free basis. For the gasification reactions, the repeatability of the experiments was determined by doing two experiments and averaging the results. From Figure 36 it can also be seen that the time for the reaction to reach completion, approximately 550 minutes, is similar in both experiments. This procedure was followed for all subsequent gasification analyses. The labels on the figures indicate the experimental conditions at which the chars were prepared and gasified. These include; the devolatilisation temperature; particle size; gasification temperature; CO_2 concentration; and the pressure at which the experiments were done.

The average of the two experiments was taken to be representative of the gasification reaction at these specific conditions. The calculated average for the gasification of 10 mm particles prepared at 450°C is shown in Figure 37. (A complete set of carbon

conversion data showing the two individual runs as well as the calculated average is given in Appendix B.)

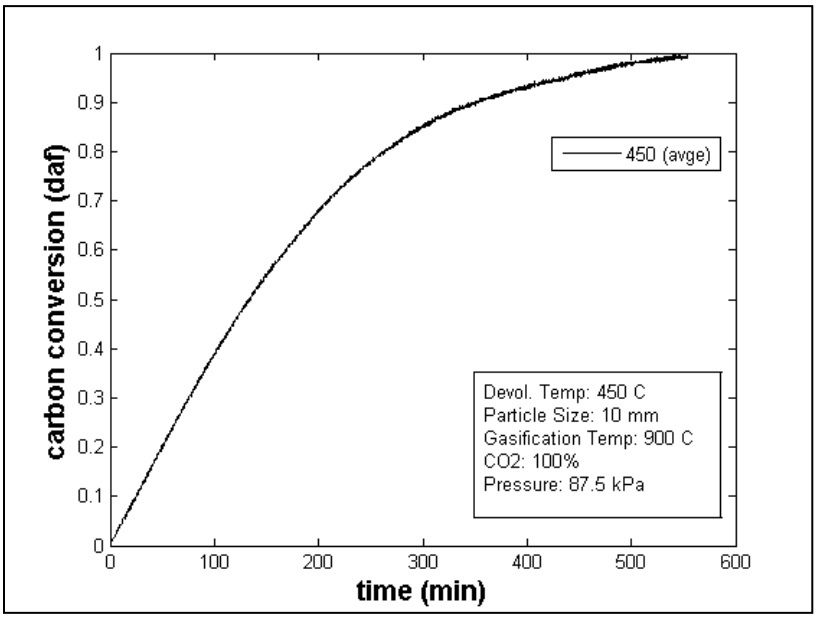

Figure 37: Averaged carbon conversion for 10 mm chars.

4.4.2. Effect of devolatilisation temperature

In order to investigate the influence of devolatilisation temperature on the gasification of char particles, similar sized char particles prepared at different temperatures (450°C, 700°C and 850°C) were gasified at a constant temperature of 900°C.

The results obtained for the gasification of 5 mm char particles prepared at different devolatilisation temperatures are shown in Figure 38.

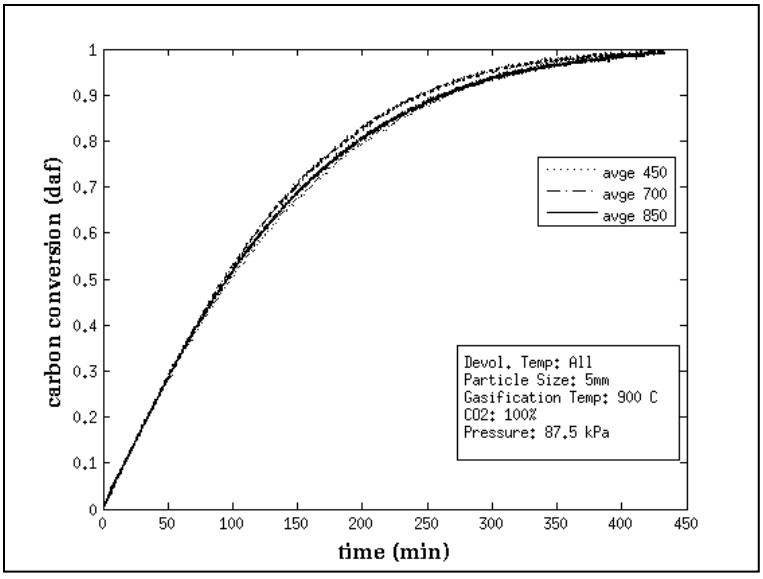

Figure 38: CO_2 gasification of 5 mm particle at different devolatilisation temperatures.

From Figure 38 it can be seen that the initial rate of carbon conversion for 5 mm particles are similar for different devolatilisation temperatures. It can further be seen that the time needed for complete conversion (approximately 430 min) does not differ significantly on the basis of devolatilisation temperature. This indicates that the devolatilisation temperature does not significantly influence the CO_2 gasification rate of 5 mm particles at 900°C.

The gasification results for 10 mm char particles prepared at different devolatilisation temperatures are shown in Figure 39. From this figure it can be observed that the carbon conversion rate for 10 mm char particles prepared at different temperatures also does not differ significantly. The 10 mm chars prepared at 450°C show a slightly faster initial carbon conversion compared to chars prepared at 700°C and 850°C. Furthermore the time required for complete carbon conversion (approximately 550 min) is similar for all devolatilisation temperatures.

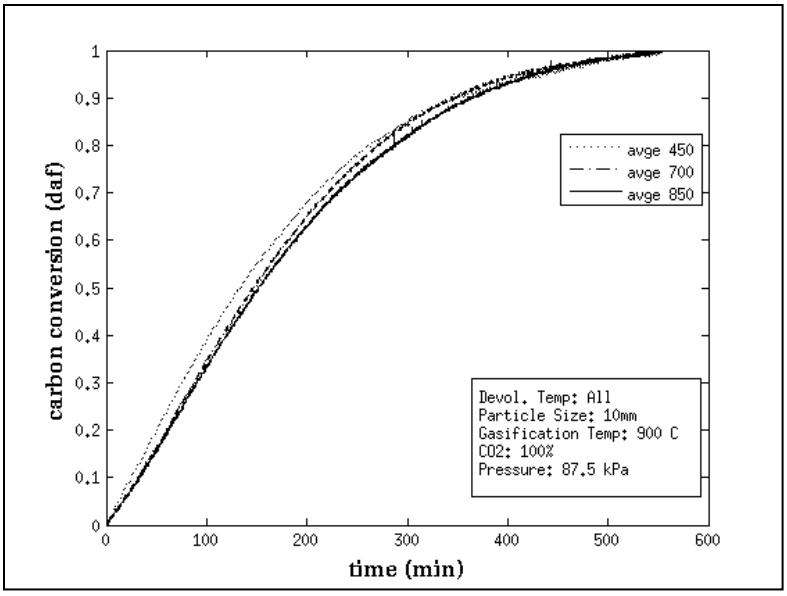

Figure 39: CO_2 gasification of 10 mm particle at different devolatilisation temperatures.

The gasification results obtained for 20 mm particles are shown in Figure 40.

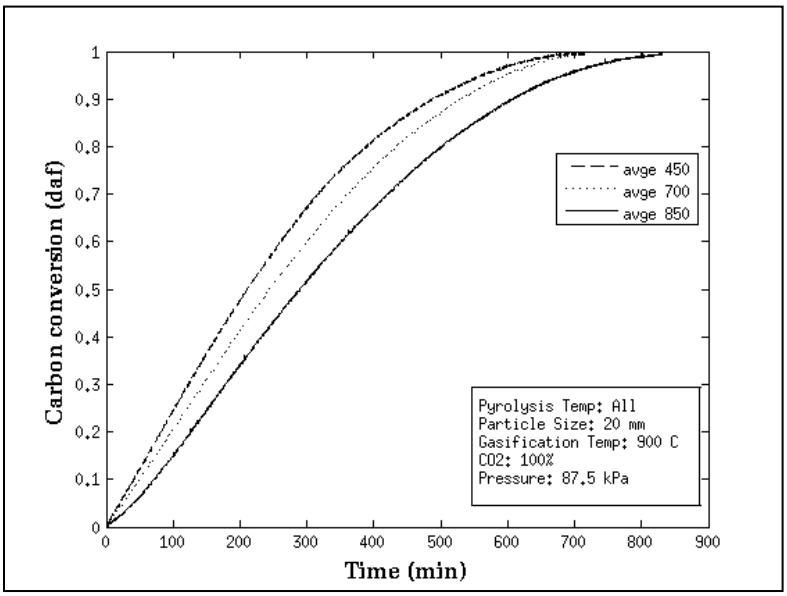

Figure 40: CO_2 gasification of 20 mm particle at different devolatilisation temperatures.

For the gasification of 20 mm particles, Figure 40 indicates that a relatively large variation in initial carbon conversion occurs. The reactivity increases with decrease in devolatilisation temperature. Furthermore it can be observed that the time for complete conversion (approximately 720 min) is similar for chars prepared at 450°C and 700°C while the 10 mm chars prepared at 850°C require approximately 820 min for complete conversion.

This wider distribution of initial carbon conversion for 10 mm and 20 mm particles could be caused by the probability that larger particles will fragment more. As fragmentation is a function of internal pressure building up due to the release of volatile matter, it can be expected that a larger amount of volatile matter could increase the possibility of fragmentation (Sasongko & Stubington, 1996). Also as the amount of volatiles remaining in the particle decreases with increasing devolatilisation temperature, it could be expected that the degree of fragmentation of char particles will decrease with an increase in devolatilisation temperature. As the 20 mm chars prepared at 450°C had the highest residual volatile content, these chars would fragment more resulting in a carbon conversion rate greater than that of the chars prepared at 700°C and 850°C respectively. The 20 mm chars prepared at 850°C have the lowest amount of residual volatile matter. This possibly results in little or no fragmentation and may explain the lower carbon conversion rate. The particles devolatilised at high temperatures have seen higher temperatures for longer periods of time which can also cause a decrease in the CO_2 reactivity (Everson *et al.*, 2008).

The result for the gasification of 40 mm char particles prepared at 450°C is shown in Figure 41 from which it can be seen that the time taken for the reaction to reach completion was approximately 1100 minutes.

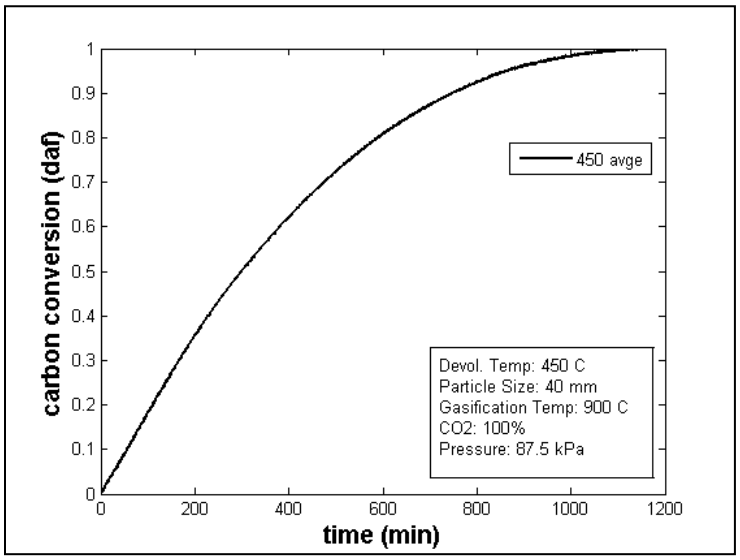

Figure 41: CO_2 gasification of 40 mm particle with devolatilisation temperature of 450°C.

From these results it is concluded that the devolatilisation results do not significantly influence the reactivity of the resulting char particles, although some variation is found for the 20 mm particles. These findings correlate with that of Lui *et al.* (2008) who investigated the influence of devolatilisation temperatures ranging from 1000°C to 1400°C on the CO_2 gasification of bituminous coal particles (175 µm to 355 µm). Investigating the CO_2 reactivity of four lignites Cakal *et al.* (2007) also found that the devolatilisation temperature was not the main cause for increased gasification reactivity.

4.4.3. Effect of particle size

In order to investigate the effect of particle size on the gasification rate of char particles, different sized char particles prepared at the same devolatilisation temperature were compared.

The results for CO_2 gasification of different particle sizes (5 mm to 40 mm) prepared at 450°C are shown in Figure 42.

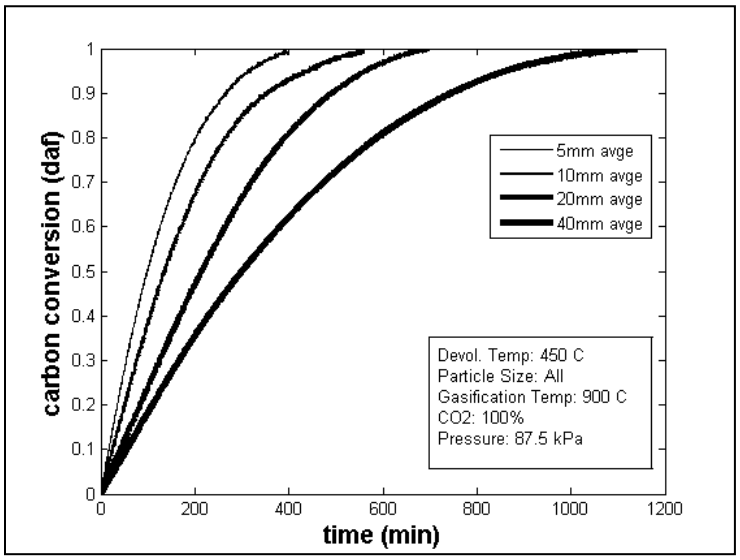

Figure 42: CO_2 gasification of different particle sizes prepared at 450°C.

From Figure 42 it can be seen that the initial rate of carbon conversion decreases with an increase in particle size. Furthermore it can be seen that the time required for complete conversion increases with an increase in particle size. A conversion time of approximately 430 min is required for complete carbon conversion of 5 mm particles while the conversion times for 10 mm, 20 mm and 40 mm particles are 550 min, 720 min and 1100 min respectively.

The effects of particle size for devolatilisation temperatures of 700°C and 850°C were only investigated for particle sizes of 5 mm, 10 mm and 20 mm as no 40 mm particles remained intact during devolatilisation.

The results obtained for the gasification of different char particle sizes prepared at 700°C are shown in Figure 43.

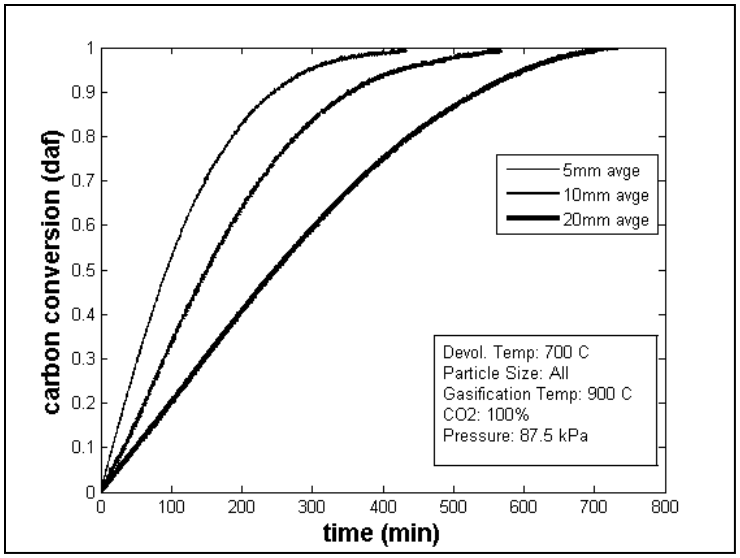

Figure 43: CO_2 gasification of different particle sizes prepared at 700°C.

For different char particle sizes, it can be seen from Figure 43 that a decrease in particle size results in an increase in initial carbon conversion rate for the gasification of chars prepared at 700°C. The time required for complete carbon conversion increased from 430 min for 5 mm particles to 550 min and 720 min for 10 mm and 20 mm particles respectively.

The gasification results for different char particle sizes prepared at 850°C are shown in Figure 44. The carbon conversion rate also decreases with increasing char particle size, as can be seen from Figure 44. The time for complete conversion increases from 430 min for 5 mm particle to 550 min and 820 min for 10 mm and 20 mm particles respectively.

For all devolatilisation temperatures, the conversion time increases with increase in particle size. Furthermore the carbon conversion rate decreases with an increase in particle size. Bunt & Waanders (2009) obtained similar results with regards to carbon conversion rate as a function of particle size (-75 mm to -35 mm), observing an increase in carbon conversion rate associated with a reduction in reactor feed particle size. Investigating particle sizes between the ranges of 0.18 mm and 1 mm, Kwon *et al.* (1988) also obtained results indicating a decrease in carbon conversion rate with an increase in particle size.

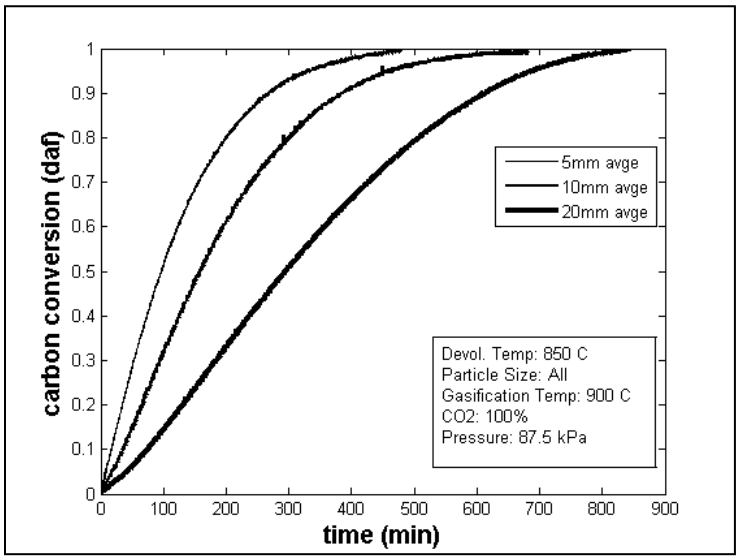

Figure 44: CO_2 gasification of different particle sizes prepared at 850°C.

On the basis of these results it is believed that the devolatilisation temperature has no significant effect on the gasification rate of the 5 mm and 10 mm particles, while an indirect effect on the reactivity of the 20 mm is observed. The decreased reactivity for the 20 mm particles with an increase in devolatilisation temperatures could be caused by the higher degree of fragmentation resulting from the lower devolatilisation temperatures. For char particles smaller than 105 µm, Kovacik *et al.* (1991), obtained a CO_2 gasification time in excess of 1.5 hours (150 minutes) for particles gasified at 950°C. This would indicate that a longer gasification time for larger particles can be expected at gasification temperature of 900°C, as shown by the results obtained.

To indicate the influence of particle size on the reaction time, the time to reach different conversions as a function of particle size is shown in Figure 45 for the particles devolatilised at 450°C (The graphs for this influence at 700°C and 850°C is shown in Appendix B). From Figure 45 it can be seen that the conversion time is proportional to the particle diameter.

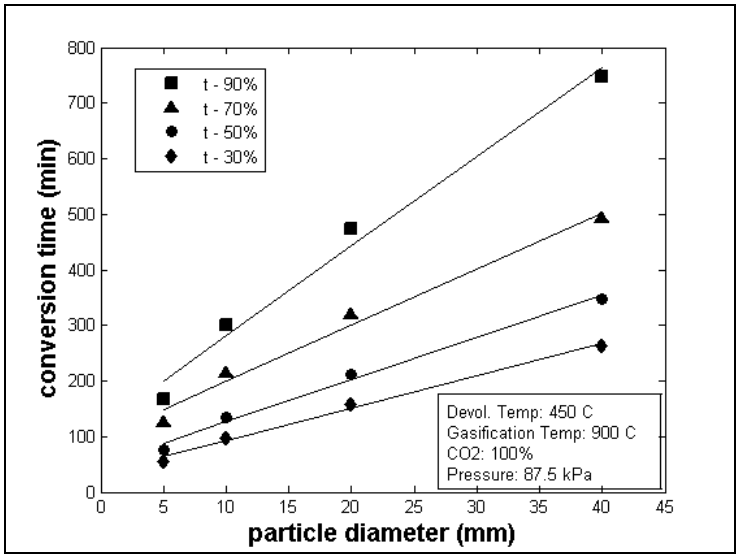

Figure 45: Influence of particle size on time to reach 30%, 50%, 70% and 90% conversion.

The influence of particle size on reaction kinetics, are less significant at very small particle sizes (149 µm vs. 545 µm) as shown by Matsui *et al.* (1987). Their results indicated that the carbon conversion rate for these two particle sizes were very identical for CO_2 gasification at 980°C. Zhu *et al.* (2008) however found that char reactivity decreased with increase in particle size. From the results obtained, it can be concluded that the influence of particle size is more significant with increase in particle size.

4.5. Initial reactivity

In order to conclude on the influence of particle size and devolatilisation temperature on the CO_2 reactivity, the initial reactivity (*Ri)* at each condition was calculated. The initial reactivity is determined from the slope of the reaction curve at the start of the reaction.

The initial reactivity for the gasification of 5 mm char particles prepared at the different devolatilisation temperatures are shown in Figure 46. From Figure 46 it can be seen that the initial reactivity for the 5 mm char particles are similar and range from 5.64×10^{-3} to 5.77×10^{-3}.

Figure 47 is used to show the initial CO_2 reactivity for 10 mm char particles prepared at different devolatilisation temperatures. From Figure 47 it can be seen that the initial reactivity for the char particles prepared at different temperatures are scattered in a narrow band. The char particles prepared at 450°C however show a slightly higher initial reactivity compared to the chars prepared at 700°C and 850°C respectively.

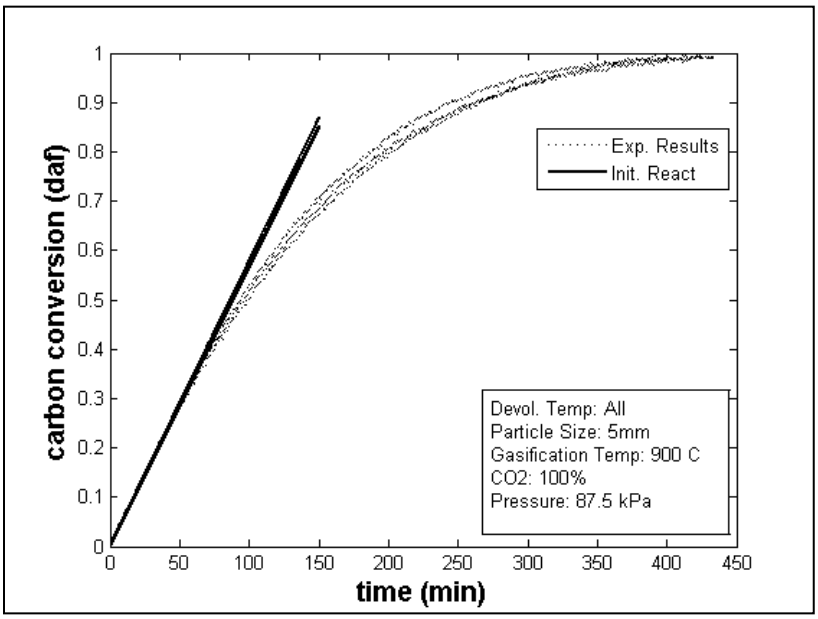

Figure 46: Initial CO_2 reactivity for 5 mm char particles prepared at different devolatilisation temperatures.

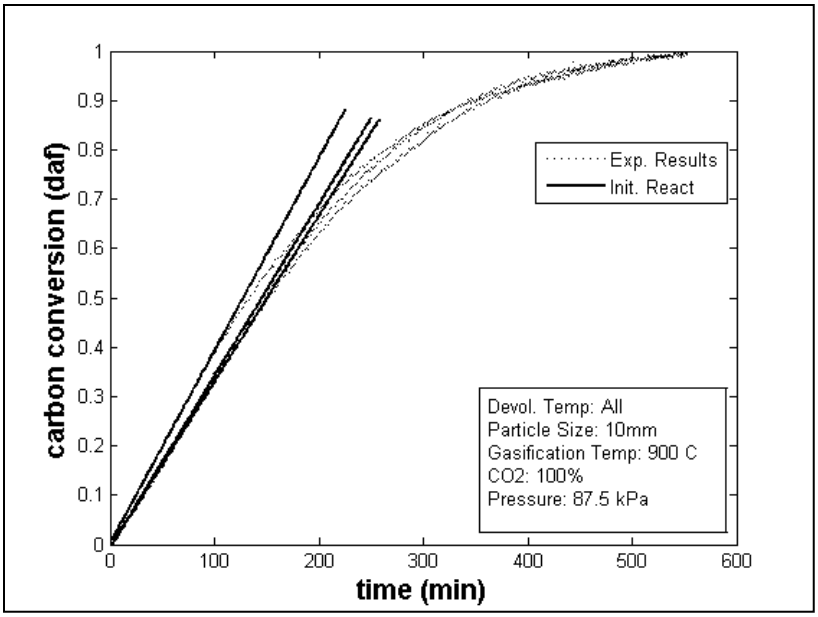

Figure 47: Initial CO_2 reactivity for 10 mm char particles prepared at different devolatilisation temperatures.

For the initial CO_2 reactivity for 20 mm char particles prepared at different devolatilisation conditions as shown in Figure 48, it can be seen that the initial reactivity decreases with increasing devolatilisation temperature. Ranging from 2.43 x 10^{-3} to 1.87 x 10^{-3} for chars prepared at 450°C and 850°C respectively (Table 17).

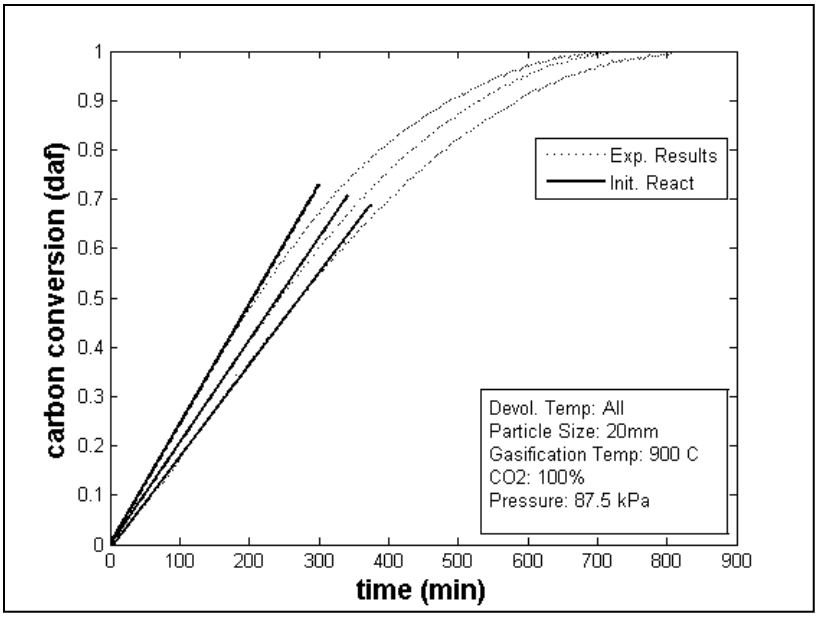

Figure 48: Initial CO_2 reactivity for 20 mm char particles prepared at different devolatilisation temperatures.

The initial CO_2 reactivity for 40 mm char particles prepared at 450°C are shown in Figure 49. The initial reactivity was determined to be 1.82 x 10^{-3} and is the lowest for all particle sizes and devolatilisation temperatures.

It is interesting to note that the initial reactivity for the 20 mm particles prepared at 850°C as very similar to the initial reactivity of the 40 mm particles prepared at 450°C. The initial reactivity of the different char particle sizes and the different devolatilisation temperatures are compared in Table 17.

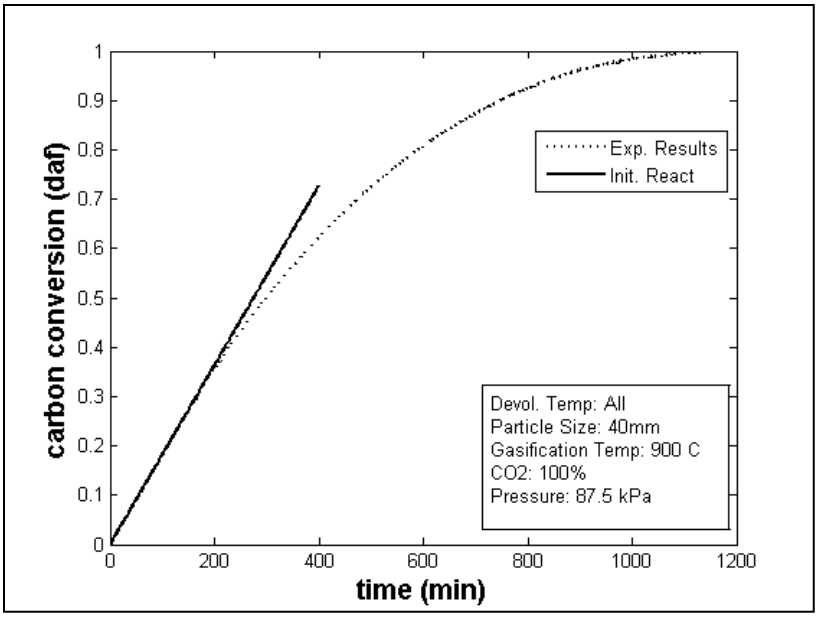

Figure 49: Initial CO_2 reactivity for 40 mm char particles prepared at devolatilisation temperature of 450°C.

Table 17: Initial reactivity of different size char particles prepared at different devolatilisation temperatures.

Devolatilisation Temperature	Particle Size (mm)			
	5 mm	10 mm	20 mm	40 mm
450°C	5.65×10^{-3}	3.90×10^{-3}	2.43×10^{-3}	1.82×10^{-3}
700°C	5.77×10^{-3}	3.48×10^{-3}	2.08×10^{-3}	-
850°C	5.64×10^{-3}	3.34×10^{-3}	1.87×10^{-3}	-

From Table 17 it can be seen that the initial CO_2 reactivity for the 5 mm particles prepared at different devolatilisation temperatures had no significant difference, while a decreasing initial reactivity trend can be observed for both the 10 mm and the 20 mm particles with increase in devolatilisation temperatures. Furthermore, at all devolatilisation temperatures, the initial CO_2 reactivity decreases with increase in particle size. Similarly Zhu *et al.* (2008) found that the initial reactivity decreased with increase in particle size. This effect was less pronounced with demineralised chars.

4.6. Gasification modelling

The shrinking unreacted core model (SUCM) was used to model CO_2 gasification results for different char particle sizes prepared under different devolatilisation conditions. The SUCM is described in Section 2.4.3.

4.6.1. Determining reaction mechanism

Since sufficiently low reaction temperatures, and hence long reaction times, were used during the gasification reactions, it was assumed that the gasification was carried out in the kinetic controlled regime. Since the conversion was still a function of particle size, as was shown in Figure 45, the experiments cannot be explained by the RPM (reaction controlled regime). Therefore, the SUCM was chosen to model the gasification results.

To further confirm that the chemical reaction controlled SUCM (Equation 4) is preferred above the ash diffusion controlled SUCM (Equation 6), the carbon conversion was plotted as a function of the (t/t_{90}) (this is the reaction time, normalised for the reaction time to reach 90% conversion) In Figure 50, the results are shown and it can be concluded that the experiments better agree with the chemical reaction controlled SUCM than the ash diffusion controlled SUCM.

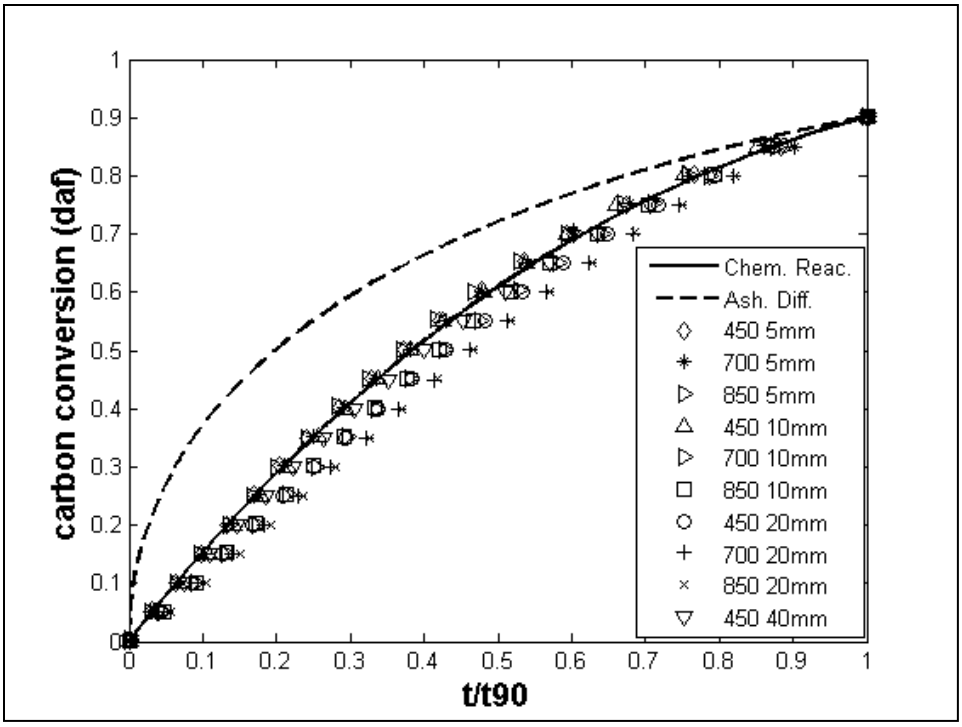

Figure 50: Conversion models for gasification at 900°C.

Investigating the CO_2 gasification of different rank chars at different temperatures ranging from 700°C to 900°C for particles having a diameter in the range of millimetres, Kwon *et al.* (1988) also found that the conversion is mainly chemical reaction controlled. From these observations, it was decided to quantify the gasification rate with the chemical reaction controlled SUCM.

4.6.2. Determining reaction constants

The gasification results were modelled with the shrinking unreacted core model by using the kinetic rate constant (*k"*) as the only fitting parameter. The kinetic constant (*k"*) is determined from Equation 4 by fitting the experimental conversion time with the modelled ones using the least square method.

The modelling of the average conversion as a function of particle size for particles devolatilised at 450°C is shown in Figure 51. The complete set of modelling curves for the other temperatures is shown in Appendix C.

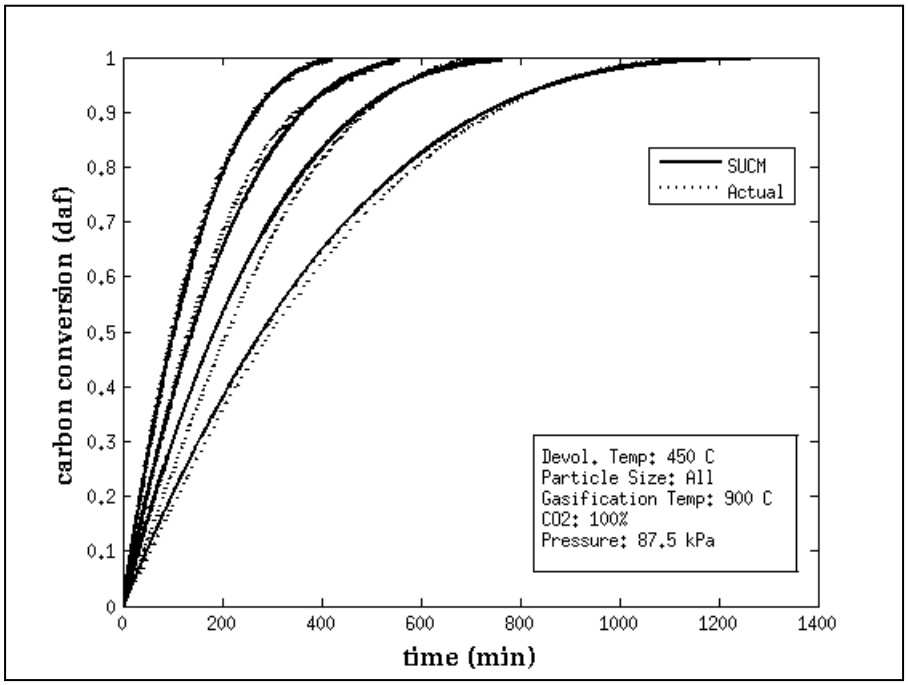

Figure 51: SUCM for different sized chars prepared at 450°C.

From Figure 51 it can be seen that the model gives a very good fit to the experimental results for the gasification of 5 mm and 10 mm particles (with R^2 values ranging from 0.99 to 0.98). The reaction rate constant was found to be: k'' = 5.5 x 10^{-7} m/s and k'' = 8.1 x 10^{-7} m/s for the 5 mm and 10 mm char particles respectively.

For the gasification of 20 mm particles, a reaction rate constant of k'' = 1.2 x 10^{-6} m/s was obtained, slightly over predicting the experimental conversion data. The same was found during the modelling of the 20 mm chars prepared at 700°C and 850°C (with R^2 values for 20 mm particles ranging from 0.98 to 0.96). Fitting the model to the gasification results for 40 mm char particles yielded again a very good fit (with a R^2 value of 0.99). A reaction rate constant of k'' = 1.6 x 10^{-6} m/s was obtained.

Investigating the CO_2 gasification of 5 different char types at temperatures between 850°C and 1000°C, Park & Ahn (2007) also obtained a good fit to experimental results using a shrinking particle model for char particle sizes in the range of 45-63 µm.

The rate constants obtained for the different particle sizes prepared at different devolatilisation temperatures are given in Table 18.

Table 18: Reaction rate constants at different experimental conditions.

Devolatilisation Temperature	Particle Size (mm)			
	5 mm	**10 mm**	**20 mm**	**40 mm**
450°C	5.5×10^{-7}	8.1×10^{-7}	12.2×10^{-7}	15.9×10^{-7}
700°C	5.6×10^{-7}	8.2×10^{-7}	11.4×10^{-7}	-
850°C	5.3×10^{-7}	8.0×10^{-7}	10.1×10^{-7}	-

From these results it can be seen that the reaction rate constant increases with an increase in particle diameter. This is not expected, since coal properties do not significantly change with particle size (Section 4.2). This increase in rate constants with particle size could be due to a combination of factors including temperature distributions inside the oven, the fragmentation of particles during the gasification procedure and possible packed bed effects that can occur during the gasification of the 5 mm and 10 mm particles.

The main reason for the variation in the determined reaction kinetic constant may be the increased fragmentation with larger particles. The SUCM is based on the assumption that spherical particles, with the associated surface area, are used. If larger particles are fragmented more, the surface area, and hence the conversion rate will increase. Furthermore the radial temperature profile inside the oven could result in larger particles experiencing slightly higher temperatures during gasification. This could, in turn, cause the elevated reaction rate. Due to the multiple particles used during the gasification of 5 mm and 10 mm particles, the packed bed effect could shield the inside particles from the higher temperature of the oven wall resulting in lower reaction rates.

Chapter 5: Conclusions and Recommendations

5. Conclusions

A large batch of ROM coal was used to obtain representative samples of different size fractions. The size fractions ranged from +3.35 mm to -53 mm. The different size fractions were used to investigate the influence of particle size and temperature on devolatilisation behaviour of coal. The resulting chars were then used to investigate the influence of particle size and devolatilisation conditions on the CO_2 gasification reactivity. The final gasification results were then modelled using the SUCM in the reaction controlled regime. From this study the following conclusions were drawn.

5.1. Coal characterisation

The four different size fractions were characterised in terms of proximate analysis, ultimate analysis and calorific value. From proximate analysis it was found that the volatile matter content of the samples was in the order of 21.7 ($\pm$ 1.1) % while the ash content was determined at 27.5 ($\pm$ 2.6) % over the size range. The ultimate analysis yielded a carbon content of 84.5 ($\pm$ 2.2) % for the investigated size ranges. The calorific value showed very little change over the particle size ranges and was found to be in the order of 21.9 ($\pm$ 0.9) MJ/kg. The SSNMR results from three different size fractions indicated that the coal has an aromatic carbon content of 74% and an aliphatic carbon content of 26%. Other SSNMR parameters either remained constant or varied slightly over the investigated size fractions. No specific trends with regards to particle size could be observed.

From characterisation results it was concluded that the chemical and structural properties of the coal investigated do not change significantly over the particle size ranges investigated.

5.2. Devolatilisation results

The results obtained from devolatilisation experiments indicate that both temperature and particle size play a significant role in the rate of devolatilisation. The results clearly indicate that larger particles take significantly longer times to devolatilise than smaller particles, mainly due to an increased heating time for large particles.

Investigating the devolatilisation of particles of similar size at different temperatures indicated that an increase in devolatilisation temperature does not only increase the final amount of volatile release but also the rate of mass loss, for all particle sizes.

5.3. Gasification results

The gasification results showed that for 5 mm and 10 mm particles, devolatilisation temperature does not have a significant effect on gasification reactivity. Some differences during the gasification of the 20 mm particle were, however, observed; these differences in reactivity could be caused by the use of single particles, or by increased fragmentation of the particles devolatilised at lower temperatures. The gasification results show that the particle size strongly influences gasification kinetics while devolatilisation conditions indirectly influence reactivity to a lesser extent.

5.4. Gasification modelling

The gasification results were successfully modelled using the shrinking unreacted core model in the reaction controlled regime. Using the calculated rate constants to model

actual results, a very good correlation was obtained for 5 mm, 10 mm and 40 mm particles. The model slightly over predicted the actual results for 20 mm particles, particularly for the chars prepared at 700°C and 850°C. The reaction kinetic constant that was obtained from the gasification experiments was found to increase with particle size. The non-spherical nature of the coal, together with fragmentation and possible temperature gradients in the particle and the oven could be a reason for this.

5.5. Recommendations

The work done during this investigation could well be supported by investigating the influence of devolatilisation temperature and particle heating rate on the degree of fragmentation occurring for large particles. A study to determine stable particle sizes at different reaction conditions could also be beneficial to the understanding of coal behaviour under various conditions. Further supportive studies on fragmentation and devolatilisation behaviour on different density samples could also be beneficial to large particle investigations as very little information on this topic was found in literature. The use of samples obtained from a “homogeneous” block of coal could more clearly highlight the effects of different conditions as particle property variations would be minimised. The samples for investigation could also be further homogenised by working with samples obtained from a narrow density cut.

A study that focuses on comparing the devolatilisation behaviour of powders with that of larger sized particles could be beneficial as this could help bridge the gap between the comparability of results found in literature for powders and large particles. The use of software such as Wipfrag or the image processing tool in Matlab can be considered to further investigate the degree of fragmentation of large particles.

In terms of characterisation, it is recommended that SSNMR analysis be done on both parent coal samples and the devolatilised samples as this was not in the scope of this investigation. Further analysis such as BET can be considered as additional characterisation experiments.

Other aspects that should be considered for investigation include an accurate particle temperature profile over a wide range of particle sizes, and the effect of heat transfer

between particles during the investigation of large particle devolatilisation as compared to using single particle experiments.

Furthermore, it may be insightful to investigate the influence of devolatilisation temperatures on CO_2 gasification where the gasification temperature is lower than the devolatilisation temperatures. Determining the stable particle size for large particle gasification could aid in determining the temperature effects without the effect of enhanced heat transfer due to fragmentation.

References

ADESANYA, B A & PHAM, H N. 1995. Mathematical modelling of devolatilization of large coal particles in a conventive environment. *Fuel*, 74(6):896-902.

AGARWAL, P K, GENETTI, W E & LEE, Y Y. 1984. Devolatilization of large coal particles. *Fuel*, 63:1748-1752.

ALONSO, M J, BORREGO, A G, ALVAREZ, D & MENÉNDEZ, R. 2001. A reactivity study of chars obtained at different temperatures in relation to their petrographic characteristics. *Fuel Processing Technology*, 69:257-272.

BORAH, R C, GHOSH, P & RAO, P G. 2008. Devolatilization of coals of North-Eastern India under fluidized bed conditions in oxygen-enriched air. *Fuel Processing Technology*, 89:1470-1478.

BOZKURT, Y, MISIRLIOGLU, Z, SINAG, A, TEKES, A T & CANEL, M. 2008. Behavior of chars from Bursa Mustafa Kemal Pasa Alpagut and Balikesir Dursunbey Cakirca lignite (Turkey) during non-catalytic and catalytic gasification. *Energy Sources, Part A*, 30:1797-1810.

BP. 2009. Statistical Review of World Energy 2009. Date of access: 15 Febuary 2010. <bp.com/statisticalreview>

BUNT, J R & WAANDERS, F B. 2008. Identification of the reaction zones ocuring in a commercial-scale Sasol-Lurgi FBDB gasifier. *Fuel*, 87:1814-1823.

BUNT, J R & WAANDERS, F B. 2009. Pipe reactor gasification studies of a South African bituminous coal blend. Part 1 - carbon and volatile matter behaviour as fanction of feed coal particle size reduction. *Fuel*, 88:585-594.

BUNT, J R & WAANDERS, F B. 2010. Trace element behaviour in the Sasol-Lurgi fixed-bed dry-bottom gasifier. Part 3 - The non-volatile elements: Ba, Co, Cr, Mn, and V. *Fuel*, 89:537-548.

BURNHAM, A K, OH, M S & CRAWFORD, R W. 1989. Pyrolysis of Argonne premium coals: Activation energy distributions and related chemistry. *Energy and Fuels*, 3(1):42-55.

CAKAL, G O, YUCEL, H & GURUZ, A G. 2007. Physical and chemical properties of selected Turkish lignites and their pyrolysis and gasification rates determine by thermogravimetric analysis. *J. Anal. Appl. Pyrolysis*, 80:262-268.

CHEN, C, HORIO, M & KOJIMA, T. 2000. Numerical simulation of entrained flow coal gasifiers. Part I: modeling of coal gasification in an entrained flow gasifier. *Chemical Engineering Science*, 55:3861-3874.

CHEN, C, HORIO, M & KOJIMA, T. 2001. Use of numerical modeling in the design and scale-up of entrained flow coal gasifiers. *Fuel*, 80:1513-1523.

CHEN, W, NAGARAJAN, G, ZHANG, Z, SHEN, B & FAN, L T. 1994. Stochastic modeling of devolatilization-induced coal fragmentation during fluidized-bed combustion. *Industrial and engineering chemistry research*, 33:137-145.

CLOKE, M, LESTER, E & BELGHAZI, A. 2002. Characterisation of the properties of size fractions from ten world coals and their chars produced in a drop-tube furnace. *Fuel*, 81:699-708.

COLLOT, A. 2006. Matching gasification technologies to coal properties. *International Journal of Coal Geology*, 65:191-212.

COUSINS, A, PATERSON, N, DUGWELL, D R & KANDIYOTI, R. 2006. An investigation of the reactivity of chars formed in fluidized bed gasifiers: The effect of reaction conditions and particle size on coal char reactivity. *Energy and Fuels*, 20:2489-2497.

DACOMBE, P, POURKASHANIAN, M, WILLIAM, A & YAP, L. 1999. Combustion-induced fragmentation behaviour of isolated coal particles. *Fuel*, 78:1847-1857.

DEVANATHAN, N & SAXENA, S C. 1987. Transport model for devolatilization of large nonplastic coal particles: The effect of secondary reactions. *Ind. Eng. Chem. Res.*, 26:539-548.

DU PLESSIS, R. 2007. *Influence of temperature on the pyrolysis of large coal particles*.

ENGLAND, T. 2002. Coal preperation in South Africa. Pietermaritzburg: Natal Witness Commercial Printers.

ERINCIN, D, SINAG, A, MISIRLIOGLU, Z & CANEL, M. 2005. Characterization of burning and CO2 gasification of chars from mixtures of Zonguldak (Turkey) and Australian bituminous coals. *Energy Conversion and Management*, 46:2748-2761.

EVERSON, R C, NEOMAGUS, H W J P, KAITANO, R, FALCON, R, VAN ALPHEN, C & DU CANN, V M. 2008. Properties of high ash char particles derived from inertinite-rich coal: 1. Chemical, structural and petrographic characteristics. *Fuel*, 87:3082-3090.

FENG, J, LI, W & XIE, K. 2004. Relation between coal pyrolysis and corresponding coal char gasification in CO2. *Energy Sources*, 26:841-848.

FLETCHER, T H, SOLUM, M S, GRANT, D M & PUGMIRE, R J. 1992. Chemical Structure of Char in the Transition from Devolatilization to Combustion. *Energy and Fuels*, 6:643-650.

GIBBINS-MATHAM, J & KANDIYOTI, R. 1988. Coal pyrolysis yields from fast and slow heating in a wire-mesh apparatus with a gas sweep. *Energy and Fuels*, 2(4):505-511.

GU, J, WU, S, ZHANG, X, WU, Y & GAO, J. 2009. CO2-gasification reactivity of different carbonaceous materials at elevated temperatures. *Energy Sources, Part A*, 31:232-243.

HANSON, S, PATRICK, J W & WALKER, A. 2002. The effect of coal particle size on pyrolysis and steam gasification. *Fuel*, 81:531-537.

HERSHKOWITZ, F. 1985. Mass transfer effects in coal conversion chemistry. *In*: SCHLOSBERG, Richard H, ed. *Chemistry of coal conversion*, New York and London: Plenum Press. 45-47 p.

HIGMAN, C & VAN DER BURGT, M. 2008. Gasification Processes. *In*: *Gasification - 2nd edition*, Gulf Professional Publishing. 91-182 p.

HODGE, E M, ROBERTS, D G, HARRIS, D J & STUBINGTON, J F. 2010. The significance of char morphology to the analysis of high-temperature char-CO2 reaction rates. *Energy and Fuels*, 24:100-107.

IEA. 2010. *Coal informatin 2010*. France.

IRFAN, M F, USMAN, M R & KUSAKABE, K. 2011. Coal gasification in CO2 atmosphere and its kinetics since 1948: A brief review. *Energy*, 36:12-40.

KIM, B, GUPTA, S, LEE, S, KIM, S & SAHAJWALLA, V. 2008. Devolatilization and cracking characteristics of Australian lumpy coals. *Energy and Fuels*, 22:514-522.

KOVACIK, G, CHAMBERS, A & OZUM, B. 1991. CO2 gasification kinetics of two alberta coal chars. *The Canadian Journal of Chemcial Engineering*, 69:811-815.

KRISTIANSEN, A. 1996. *Understanding coal gasification.* London.

KWON, T, KIM, S D & FUNG, D P C. 1988. Reaction kinetics of char - CO2 gasification. *Fuel*, 67:530-535.

LAZARO, M, MOLINER, R & SUELVES, I. 1998. Non-iothermal versus isothermal technique to evaluate kinetic parameters of coal pyrolysis. *Journal of Analytical and Applied Pyrolysis*, 47:111-125.

LEE, S H, KIM, S D & LEE, D H. 2002. Particle size reduction of anthracite coals during devolatilisation in a thermobalance reactor. *Fuel*, 81:1633-1639.

LEVENSPIEL, O. 1999. Fluid-particle reaction: Kinetics. *In*: *Chemical reaction engineering, 3rd edition*, USA: John Wiley and Sons. 566-586 p.

LIU, T, FANG, Y & WANG, Y. 2008. An experimental investigation into the gasification reactivity of chars prepared at high temperatures. *Fuel*, 87:460-466.

LIU, H, KANEKO, M, LUO, C, KATO, S & KOJIMA, T. 2004. Effect of pyrolysis time on the gasification reactivity of char with CO2 at elevated temperatures. *Fuel*, 83:1055-1061.

LIU, H, LUO, C, KANEKO, M, KATO, S & KOJIMA, T. 2003. Unification of gasification kinetics of char in CO2 at elevated temperatures with a modified random pore model. *Energy and Fuels*, 17:961-970.

LIU, H, LUO, C, KATO, S, UEMIYA, S, KANEKO, M & KOJIMA, T. 2006 a. Kinetics of CO2/char gasification at elevated temperatures Part I: Experimental results. *Fuel Processing Technology*, 87:775-781.

LIU, H, LUO, C, TOYOTA, M, UEMIYA, S & KOJIMA, T. 2006 b. Kinetics of CO2/char gasification at elevated temperatures. Part II: Clarification of mechanism through modelling and char characterization. *Fuel Processing Technology*, 87:769-774.

LIU, H, ZHU, H, KANEKO, M, KATO, S & KOJIMA, T. 2010. High-temperature gasification reactivity with steam of chars derived under various pyrolysis conditions in a fluidized bed. *Energy Fuels*, 24:68-75.

LUO, C, WATANABE, T, NAKAMURA, M, UEMIYA, S & KOJIMA, T. 2001. Gasification kinetics of coal chars carbonized under rapid and slow heating conditions at elevated temperatures. *Journal of Energy Resources Technology*, 123:21-26.

LU, L, SAHAJWALLA, V & HARRIS, D. 2000. Characteristics of Chars Prepared from Various Pulverized Coals at Different Temperatures Using Drop-Tube Furnace. *Energy and Fuels*, 14(4):869-876.

MANGENA, S J, BUNT, J R, WAANDERS, F B & BAKER, G. 2011. Identification of reaction zones in a commercial Sasol-Lurgi fixed bed dry bottom gasifier operation on North Dakota lignite. *Fuel*, 90:167-173.

MATSUI, I, KUNII, D & FURUSAWA, T. 1987. Study of char gasification by carbon dioxide. 1. Kinetic study by thermogravimetric analysis. *Ind. Eng. Chem. Res.*, 26:91-95.

MITCHELL, R E & AKANETUK, A E J. 1996. The impact of fragmentation on char converstion during pulverized coal combustion. (*In* Twenty-sixth symposium (International) on combustion. The combustion institute. p. 3137-3144.)

NEAVEL, R C. 1981. 192 vols. Coal structure and coal science: Overview and recommendations. *In*: GORBATY, M L & OUCHI, K, eds. *Coal structure*, Washington D.C.: American Chemical Society. 1 - 13 p.

OCHOA, J, CASSANELLO, M C, BONELLI, P R & CUKIERMAN, A L. 2001. CO2 gasification of Argentinean coal chars: a kinetic characterization. *Fuel Processing Technology*, 74:161-176.

PARK, H Y & AHN, D H. 2007. Gasification kinetics of five coal chars with CO2 at elevated pressures. *Korean J. Chem. Eng.*, 24(1):24-30.

PEELER, J P & POYNTON, H J. 1992. Devolatilization of large coal particles under fluidizes bed conditions. *Fuel*, 71:425-430.

PORADA, S. 2004. The reactions of formation of selected gas products during coal pyrolysis. *Fuel*, 83:1191-1196.

ROBERTS, D G, HARRIS, D J & WALL, T F. 2003. On the effects of high pressure and heating rate during coal pyrolysis on char gasification reactivity. *Energy and Fuels*, 17:887-895.

ROBERTS, D G, HODGE, E M, HARRIS, D J & STUBINGTON, J F. 2010. Kinetics of char gasification with CO2 under regime II conditions: Effects of temperature, reactant, and total pressure. *Energy and Fuels*, 24:5300-5308.

ROSS, D P, HEIDENREICH, C A & ZHANG, D K. 2000. Devolatilisation times of coal particles in fluidised-bed. *Fuel*, 79:873-883.

SASONGKO, D & STUBINGTON, J F. 1996. Significant factors affecting devolatilization of fragmenting, non-swelling coals in fluidized bed combustion. *Chemical engineering science*, 51(16):3909-3918.

SAWETTAPORN, S, BUNYAKIAT, K & KITIYANAN, B. 2009. CO2 gasification of Thai coal chars: Kinetics and reactivity studies. *Korean J. Chem. Eng.*, 26(4):1009-1015.

SCALA, F. 2011. Fluidized-bed combustion of single coal char particles: An analysis of the burning rate and of the primary CO/CO2 ratio. *Energy and Fuels*, 25(3):1051-1059.

SERIO, M A, HAMBLEN, D G, MARKHAM, J R & SOLOMON, P R. 1987. Kinetics of volatile product evolution in coal purolysis: Experiment and theory. *Energy and Fuels*, 1:138-152.

SETHI, N K, PUGMIRE, R J, FACELLI, J C & GRANT, D M. 1988. Quatitive determination of different carbon types in fusinite and anthracite coals from carbon-13 nuclear magnetic resonance chemical shielding line-shape analysis. *Analytical Chemistry*, 60:1574-1579.

SHINN, J H. 1984. From coal to single-stage and two-stage products: A reactive model of coal structure. *Fuel*, 63:1187-1196.

SOLOMON, P R & HAMBLEN, D G. 1985. Pyrolysis. *In*: SCHLOSBERG, Richard H, ed. *Chemistry of coal conversion*, New York and London: Plenum Press. 121-251 p.

SOLOMON, P R & SERIO, M A. 1994. Progress in coal pyrolysis research. *Prepr. Pap. Am. Chem. Soc. Div. Fuel Chem*, 39:69.

SOLOMON, P R, SERIO, M A & SUUBERG, E M. 1992. Coal pyrolysis: experiments, kinetic rates and mechanisms. *Progress in Energy and Combustion Science*, 18:133-220.

SOLUM, Mark S, PUGMIRE, Ronald J & GRANT, David M. 1989. 13C Solid -State NMR of Argonne Premium Coals. *Energy and Fuels*, 3:187-196.

SOLUM, Mark S, SAROFIM, Adel F, PUGMIRE, Ronald J, FLECTHER, Thomas H & ZHANG, Haifeng. 2001. 13C NMR Analysis of Soot Produced from Model Compounds and a Coal. *Energy and Fuels*, 15:961-971.

STOCK, L M. 1989. Coal pyrolysis. *Acc. Chem. Res.*, 22:427-433.

STREZOV, V, LUCAS, J A & WALL, T F. 2005. Effect of pressure on the swelling of density separated coal paticles. *Fuel*, 84:1238-1245.

STRUIS, R P, VAN SCALA, C, STUCKI, S & PRINS, R. 2002. Gasifcation reactivity of charcoal with CO2. Part I: Conversion and structural phenomena. *Chemical Engineering Science*, 57:3581-3592.

STUBINGTON, J F, HUANG, G & SCARONI, A W. 1991. Devolatilization of mm-size coal particles. *Fuel*, 70:1105-1108.

STUBINGTON, J F & LINJEWILE, T M. 1989. The effects of fragmentation on devolatilizatio of large coal particles. *Fuel*, 68:155-160.

STUBINGTON, J F, NG, K W K, MOSS, B & PEELER, P K. 1997. Comparison of experimental methods for determining coal particle devolatilization times under fluidized bed combustor consitions. *Fuel*, 76(3):233-240.

STUBINGTON, J F & SASONGKO, D. 1998. On the heating rate and volatile yield for coal particles injected into fluidised bed combusters. *Fuel*, 77:1021-1025.

STUBINGTON, J F & SUMARYONO. 1984. Release of volatiles from large coal particles in a hot fluidized bed. *Fuel*, 63:1013-1019.

SUGGATE, R P & DICKINSON, W W. 2004. Carbon NMR of coals: the effects of coal type and rank. *International Journal of Coal Geology*, 57:1-22.

TANG, L G, GUPTA, P R, SHENG, C D & WALL, T F. 2005. The estimation of char reactivity from coal reflectogram. *Fuel*, 84:127-134.

VAN DYK, J C. 2001. Development of an alternative laboratory method to determine thermal fragmentation of coal sources during pyrolysis in the gasification process. *Fuel*, 80:245-249.

VAN DYK, J C, KEYSER, M J & COERTZEN, M. 2006 b. Syngas production from South-African coal sources using Sasol-Lurgi gasifiers. *International Journal of Coal Geology*, 65:243-253.

VAN DYK, J C, MELZER, S & SOBIECKI, A. 2006 a. Mineral matter transformation during Sasol-Lurgi fixed bed dry bottom gasification - utilization of HT-XRD and FactSage modelling. *Minerals Engineering*, 19:1126-1135.

VAN DYK, J C & WAANDERS, F B. 2007. Manipulation of gasification coal feed in order to increase the ash fusion temperature of coal enabling the gasifiers to operate at higher temperatuers. *Fuel*, 86:2728-2735.

VAN HEEK, K H. 2000. Progress of coal science in the 20th century. *Fuel*, 79:1-26.

VAN NIEKERK, Daniel. 2008. *Structural elucidation, molecular representation and solvent interactions of vitrinite-rich and inertinite-rich South African coals - NWU internal research.*

VAN WYK, Dewalt. 2007. *Influence of temperature on the pyrolysis of large coal particles - NWU internal research*.

WILDEGGER-GAISSMAIER, A E & AGARWAL, P K. 1990. Drying and devolatilization of large coal particles under combustion conditions. *Fuel*, 69:44-52.

WILKIE, C A & HAWORTH, D T. 1978. The 13C-NMR solid state spectroscopy of various classes of coals. *Journal of inorganic and nuclear chemistry*, 40:1989-1991.

WORLD COAL INSTITUTE. *The coal resource: A comprehensive overview of coal 2010*.

WU, S, GU, J, ZHANG, X, WU, Y & GAO, J. 2008. Variation of carbon crystalline structures and CO2 gasification reactivity of Shenfu coal chars at elevated temperatures. *Energy and Fuels*, 22:199-206.

WU, Y, WU, S & GAO, J. 2009 a. A study on the applicability of kinetic models for Shenfu coal char gasification with CO2 at elevated temperatures. *Energies*, 2:545-555.

WU, Y, WU, S, GU, J & GAO, J. 2009 b. Differences in physical properties and CO2 gasification reactivity betweencoal char and petroleum coke. *Process Safety and Environmental Protection*, 87:323-330.

YANG, H, CHEN, H, JU, F, YAN, R & ZHANG, S. 2007. Influence of pressure on coal pyrolysis and char gasification. *Energy and Fuels*, 21:3165-3170.

YU, D, XU, M, SUI, J, LIU, X, YU, Y & CAO, Q. 2005. Effect of coal particle size on the proximate composition and combustion properties. *Thermochimica Acta*, 439:103-109.

ZAJDLIK, R, JELEMENSKY, L, REMIAROVA, B & MARKOS, J. 2001. Experimental and modelling investigations of single coal particle combustion. *Chemical engineering science*, 56:1355-1361.

ZHANG, L, HUANG, J, FANG, Y & WANG, Y. 2006. Gasification reactivity and kinetics of typical Chinese anthracite chars with steam and CO2. *Energy and Fuels*, 20:1201-1210.

ZHENG, L & FURINSKY, E. 2005. Comparison of Shell, Texaco, BGL and KRW gasifiers as part of IGCC plant computers simulations. *Energy Conversion and Management*, 46:1767-1779.

ZHU, W, SONG, W & LIN, W. 2008. Effect of the coal particle size on pyrolysis and char reactivity for two types of coal and demineralized coal. *Energy and Fuels*, 22:2482-2487.

Appendix A: Devolatilisation

In this section all the devolatilisation results are shown with regard to the multiple runs used to determine the calculated average. The effect of devolatilisation temperature and particle size on devolatilisation behaviour is also shown for all temperatures and particles sizes.

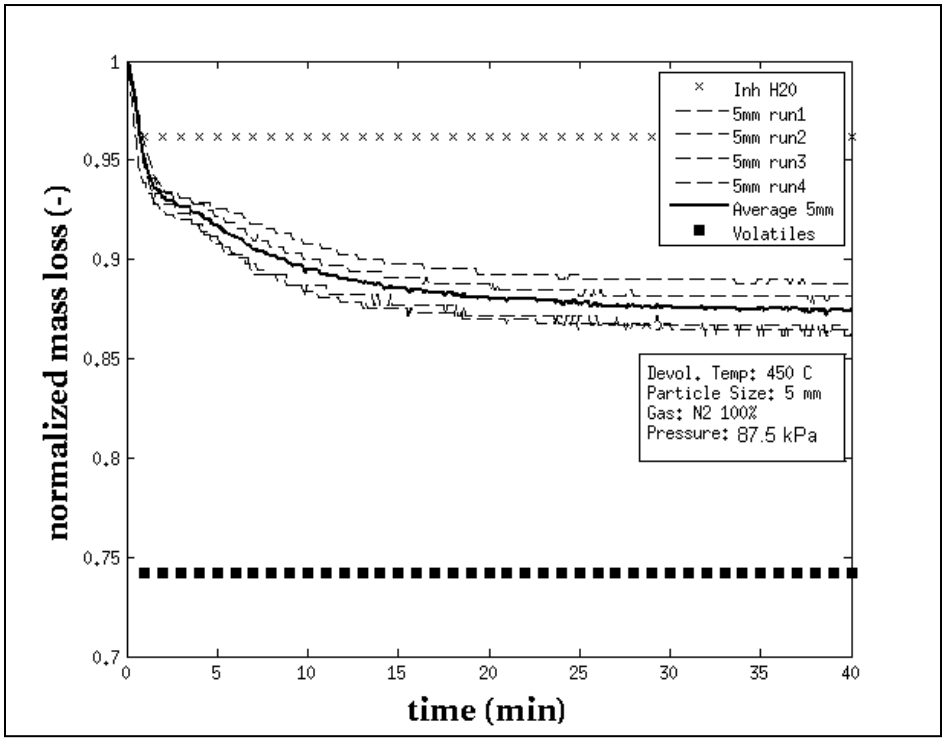

Figure A 1: Devolatilisation of 5 mm particle at 450°C

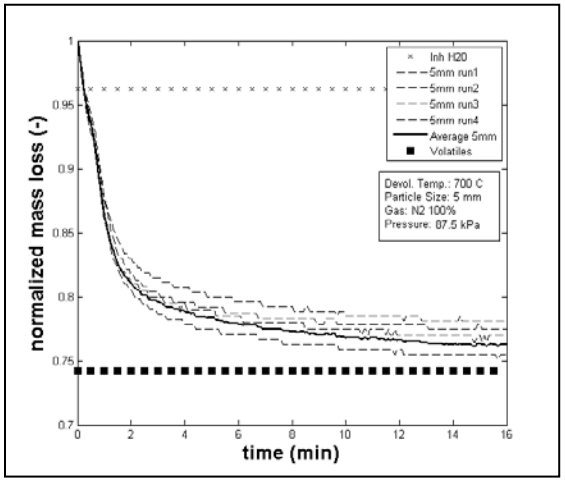

Figure A 2: Devolatilisation of 5 mm particle at 700°C.

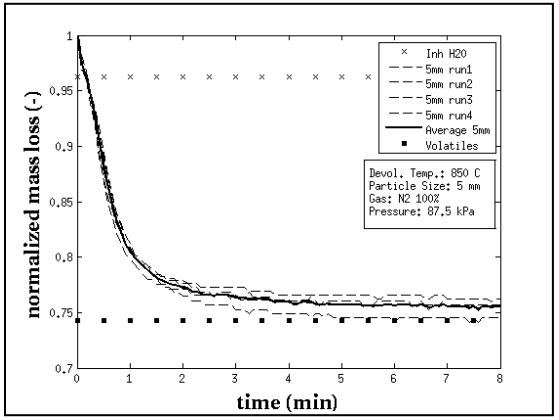

Figure A 3: Devolatilisation of 5 mm particle at 850°C.

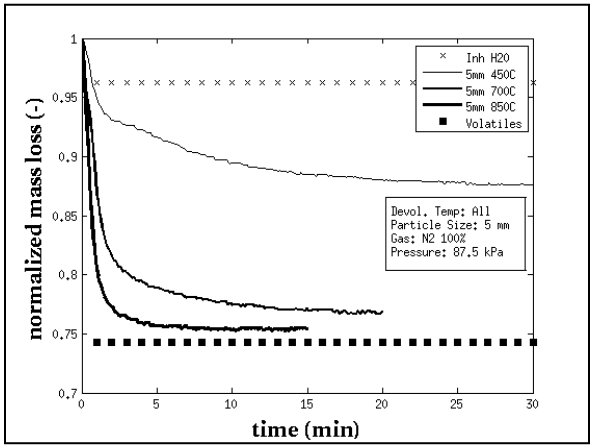

Figure A 4: Devolatilisation of 5 mm particle at different temperatures.

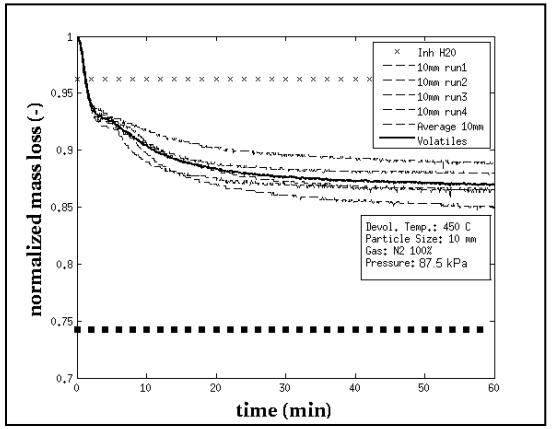

Figure A 5: Devolatilisation of 10 mm particles at 450°C.

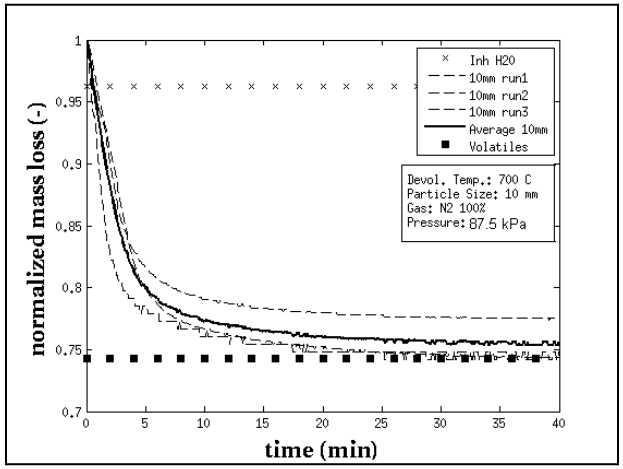

Figure A 6: Devolatilisation of 10 mm particles at 700°C.

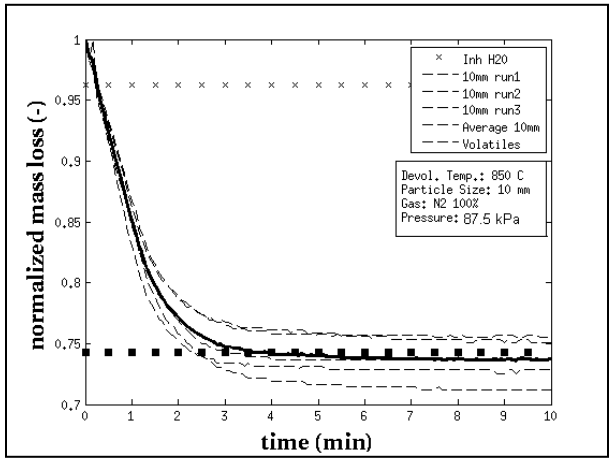

Figure A 7: Devolatilisation of 10 mm particles at 850°C.

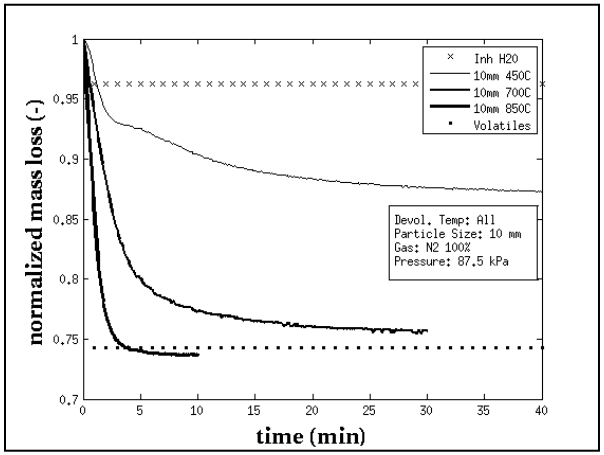

Figure A 8: Devolatilisation of 10 mm particles at different temperatures.

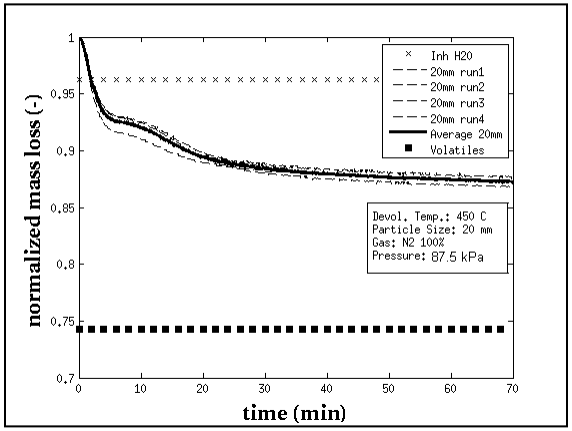

Figure A 9: Devolatilisation of 20 mm particles at 450°C.

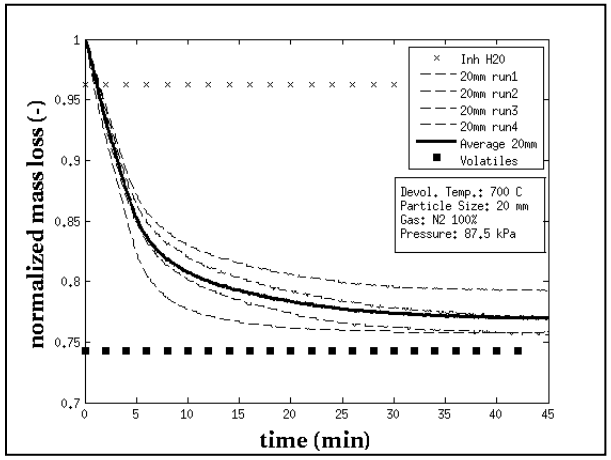

Figure A 10: Devolatilisation of 20 mm particles at 700°C.

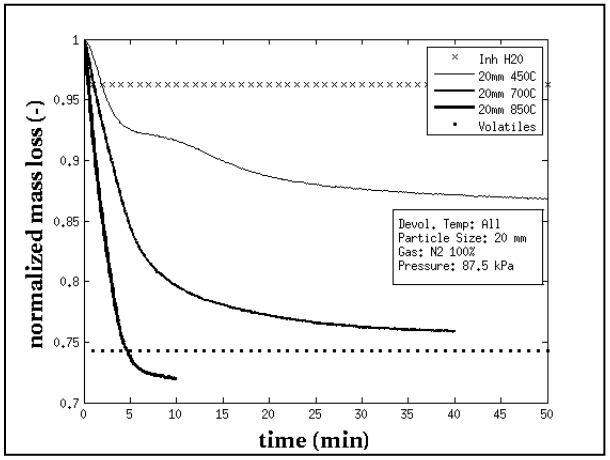

Figure A 12: Devolatilisation of 20 mm particles at different temperatures.

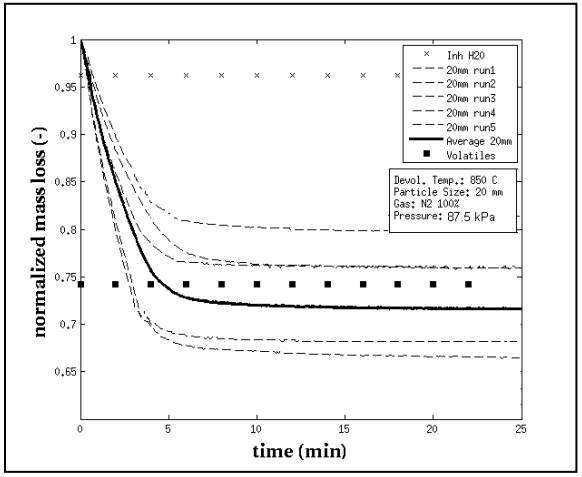

Figure A 11: Devolatilisation of 20 mm particles at 850°C.

Figure A 13: Devolatilisation of 40 mm particles at 450°C.

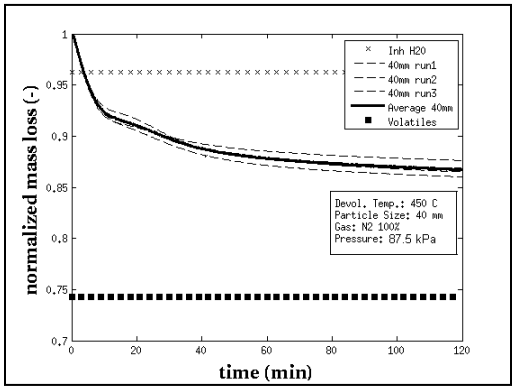

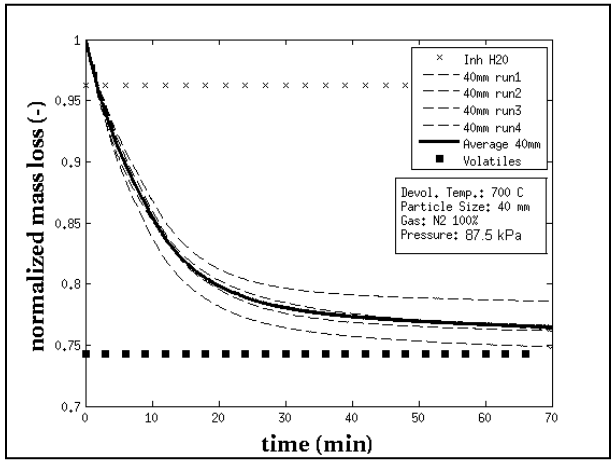

Figure A 14: Devolatilisation of 40 mm particles at 700°C.

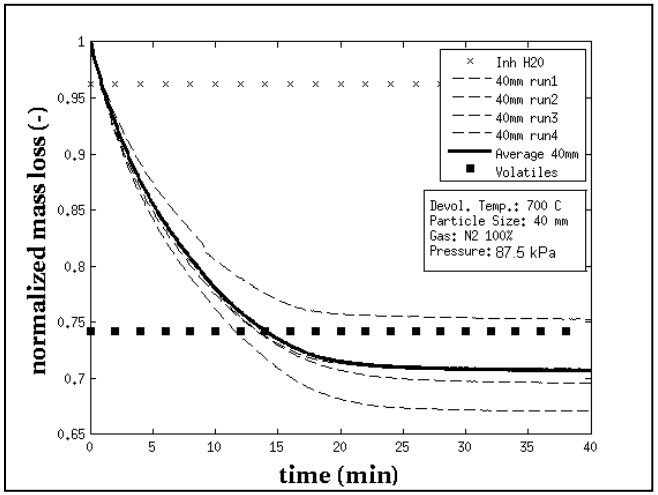

Figure A 15: Devolatilisation of 40 mm particles at 850°C.

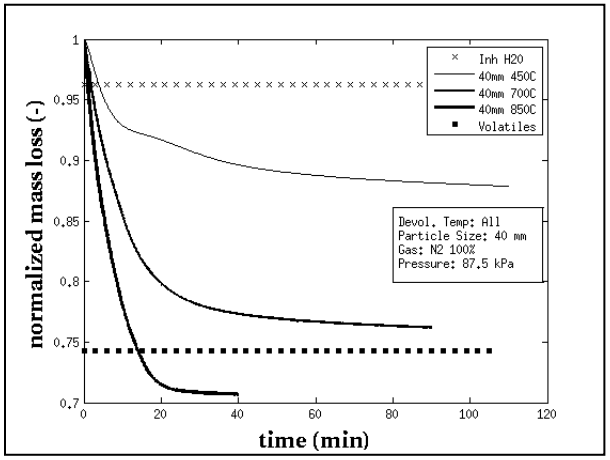

Figure A 16: Devolatilisation of 40 mm particle at different temperatures.

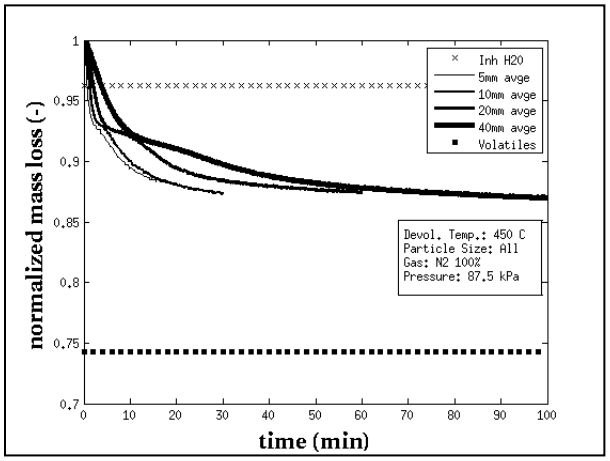

Figure A 17: Devolatilisation at 450°C for different particle sizes.

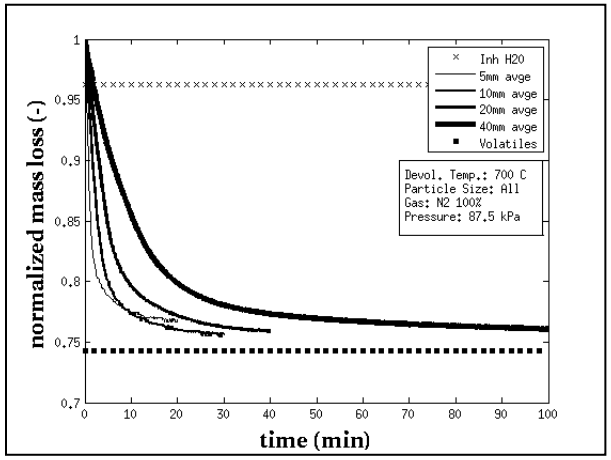

Figure A 18: Devolatilisation at 700°C for different particle sizes.

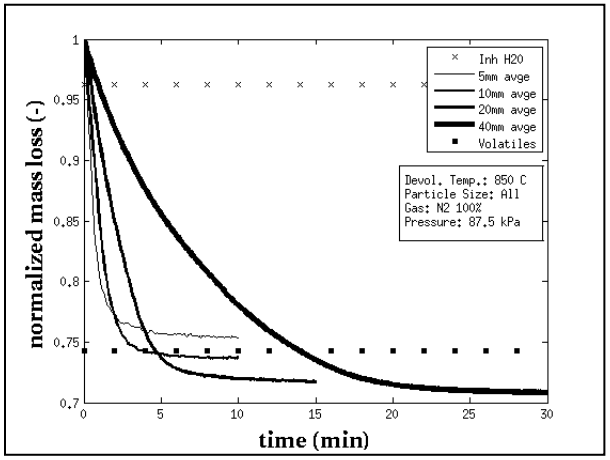

Figure A 19: Devolatilisation at 850°C for different particle sizes.

Appendix B: Gasification

In this section all the gasification results are shown with regard to the multiple runs used to determine the calculated average. The effect of devolatilisation temperature and particle size on the gasification kinetics is also shown for all temperatures and particles sizes.

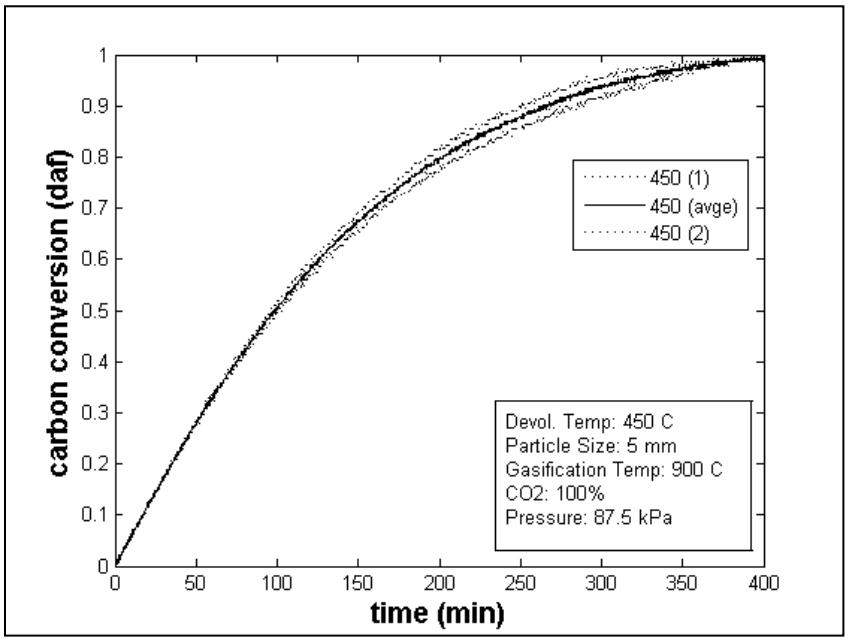

Figure B 1: Gasification of 5 mm particle prepared at 450°C.

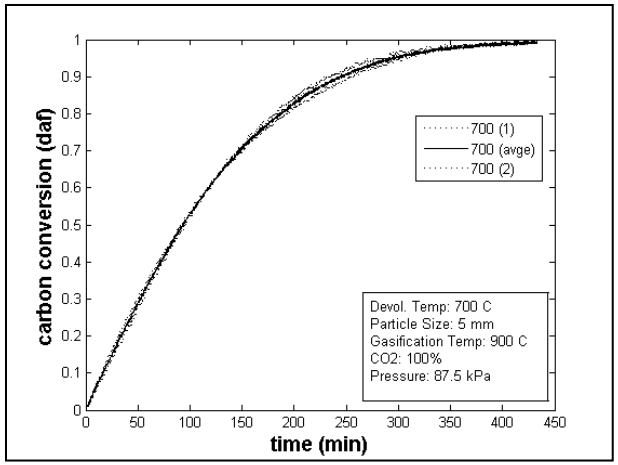

Figure B 2: Gasification of 5 mm particles prepared at 700°C.

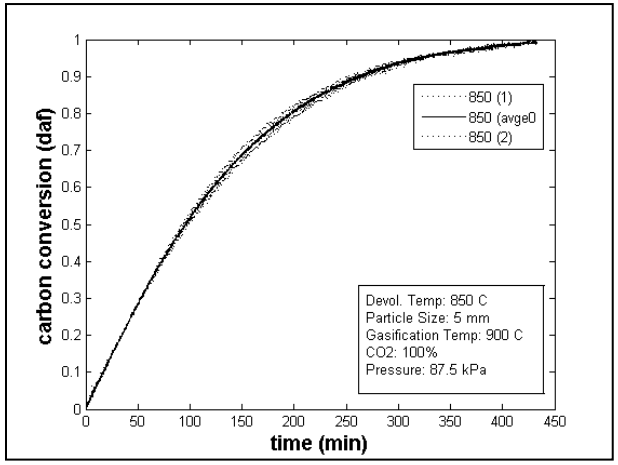

Figure B 3: Gasification of 5 mm particles prepared at 850°C.

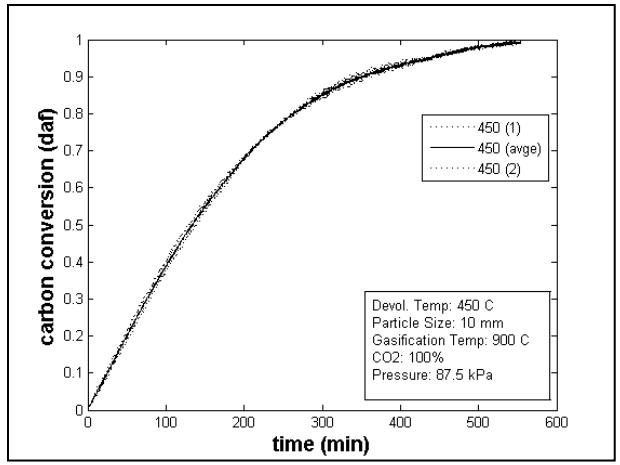

Figure B 4: Gasification of 10 mm particles prepared at 450°C.

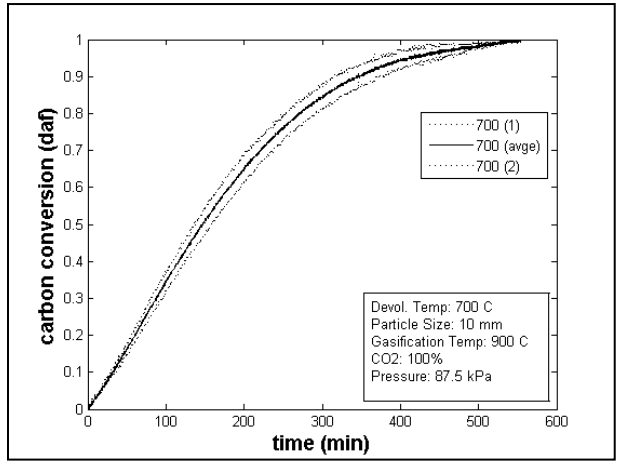

Figure B 5: Gasification of 10 mm particles prepared at 700°C.

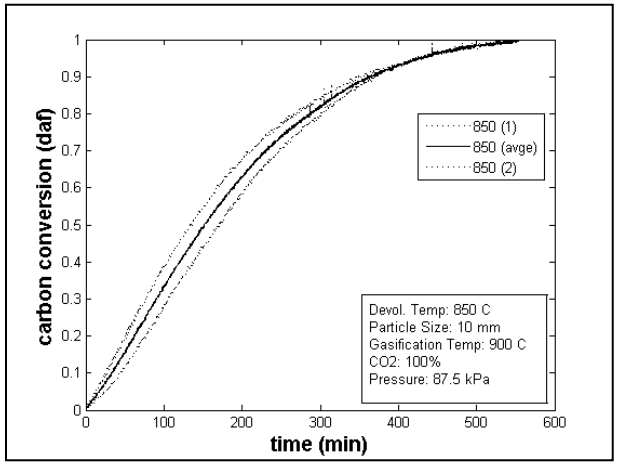

Figure B 6: Gasification of 10 mm particles prepared at 850°C.

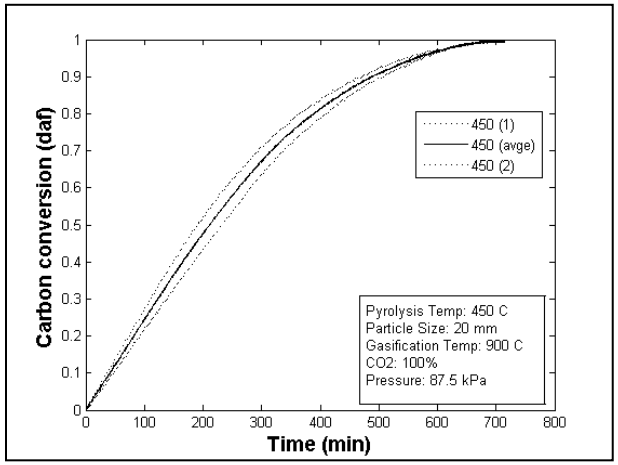

Figure B 7: Gasification of 20 mm particles prepared at 450°C.

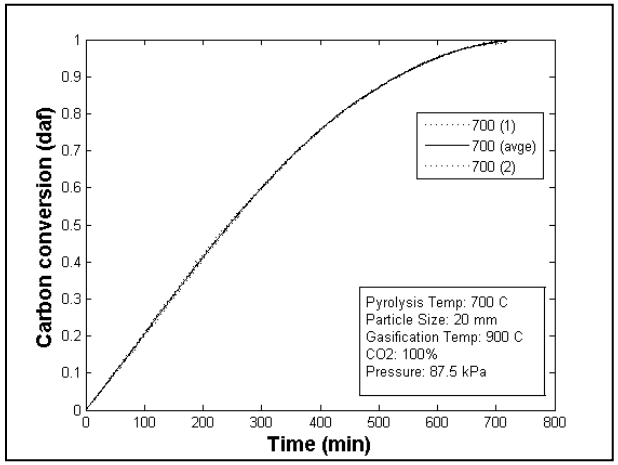

Figure B 8: Gasification of 20 mm particles prepared at 700°C.

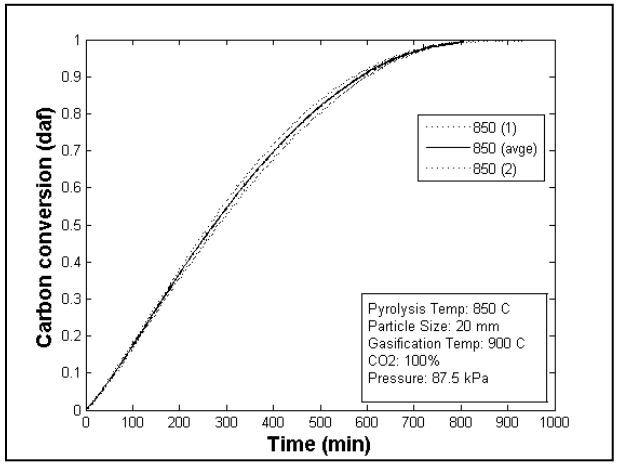

Figure B 9: Gasification of 20 mm particles prepared at 850°C.

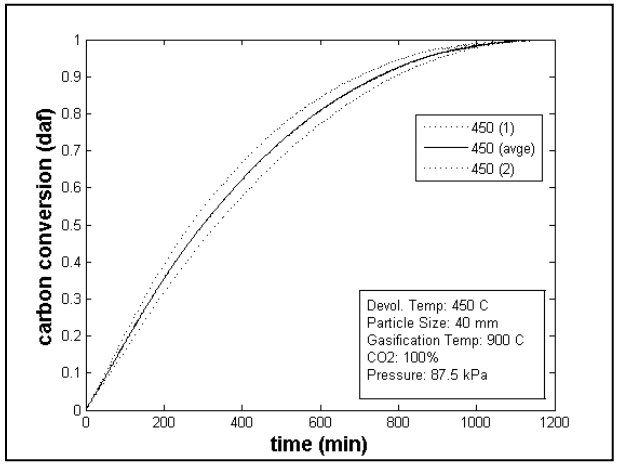

Figure B 10: Gasification of 40 mm particles prepared at 450°C.

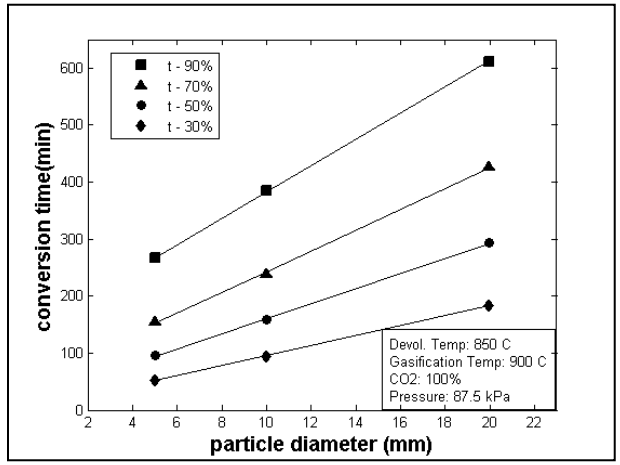

Figure B 12: Influence of particle size on time to reach 30%, 50%, 70% and 90% conversion for particles devolatilised at 850°C.

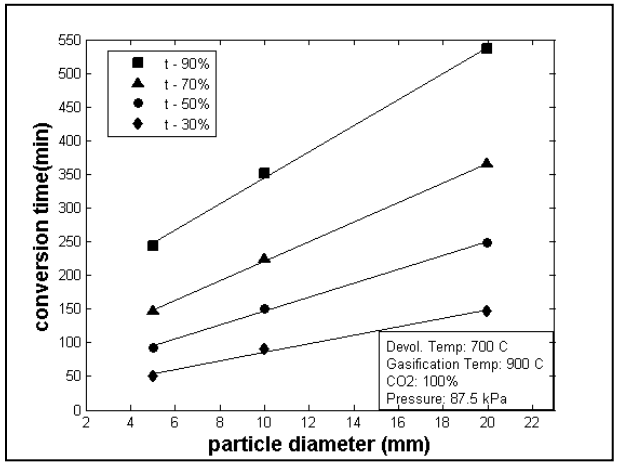

Figure B 11: Influence of particle size on time to reach 30%, 50%, 70% and 90% conversion for particles devolatilised at 700°C.

Appendix C: Modelling

In this section the modelled gasification data are shown with regard to the SUCM for all devolatilisation temperatures as well as particle sizes.

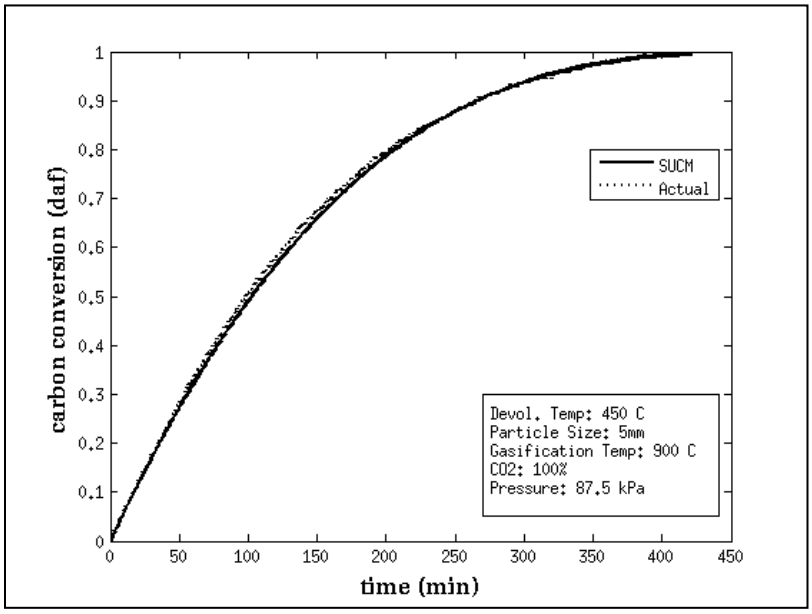

Figure C 1: SUCM for 5 mm particles prepared at 450°C.

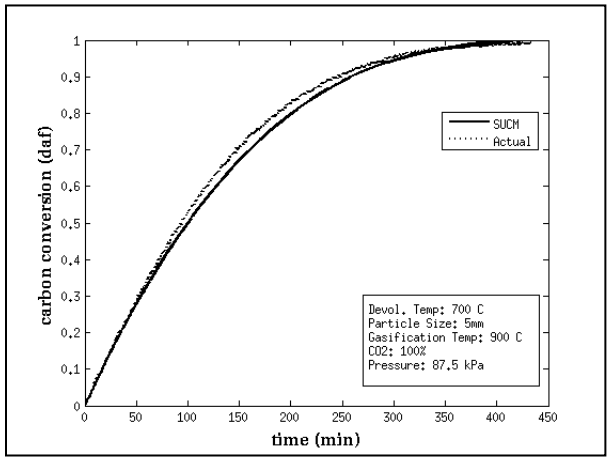

Figure C 2: SUCM for 5 mm particles prepared at 700°C.

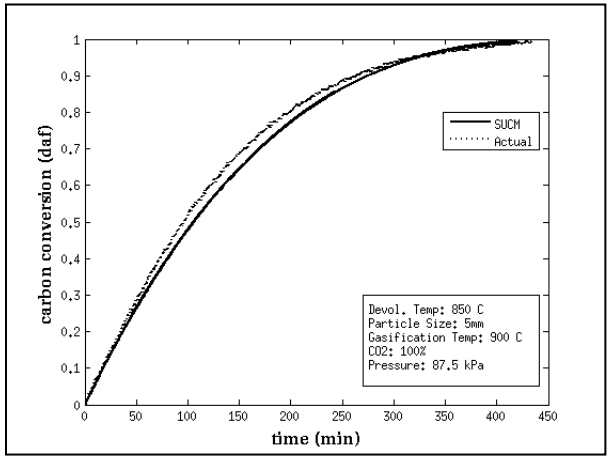

Figure C 3: SUCM for 5 mm particles prepared at 850°C.

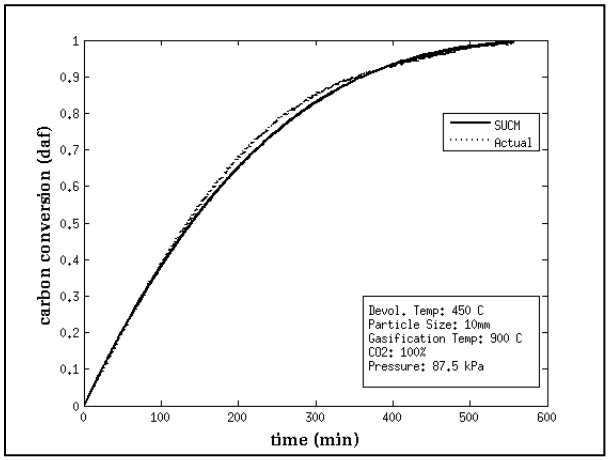

Figure C 4: SUCM for 10 mm particles prepared at 450°C.

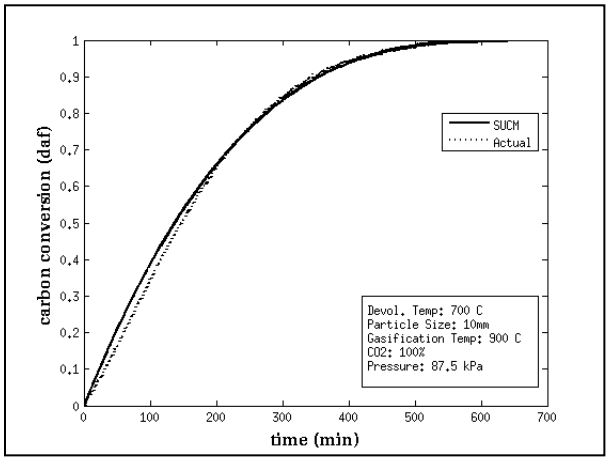

Figure C 5: SUCM for 10 mm particles prepared at 700°C.

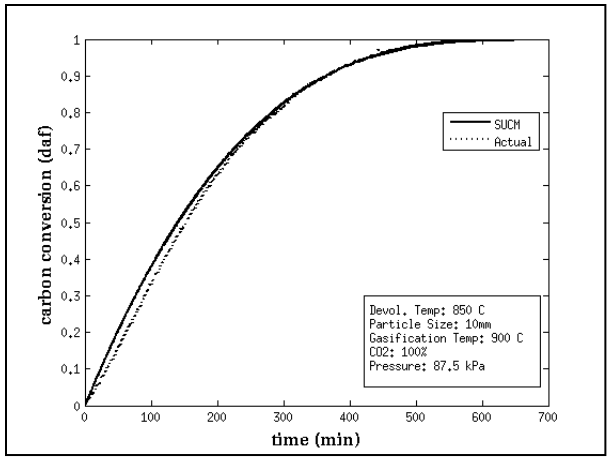

Figure C 6: SUCM for particles prepared at 850°C.

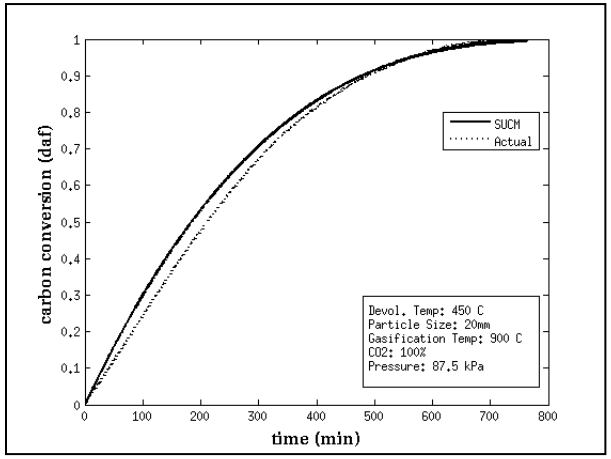

Figure C 7: SUCM for 20 mm particles prepared at 450°C.

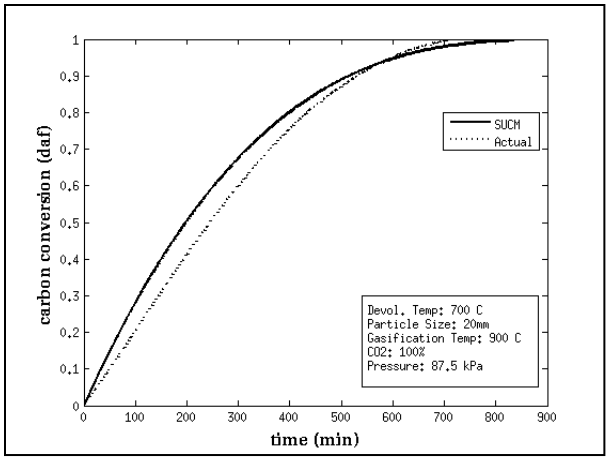

Figure C 8: SUCM for 20 mm particles prepared at 700°C.

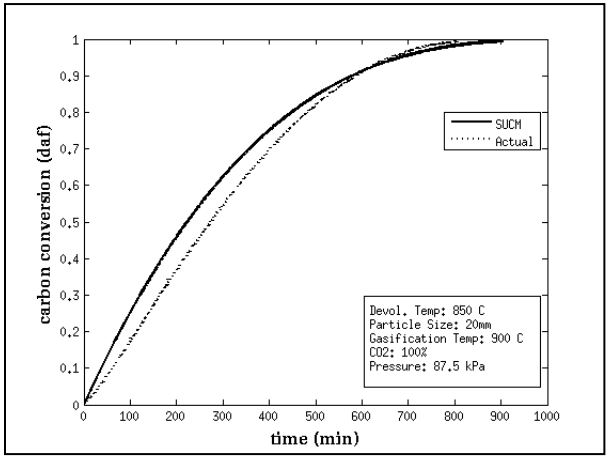

Figure C 9: SUCM for 20 mm particles prepared at 850°C.

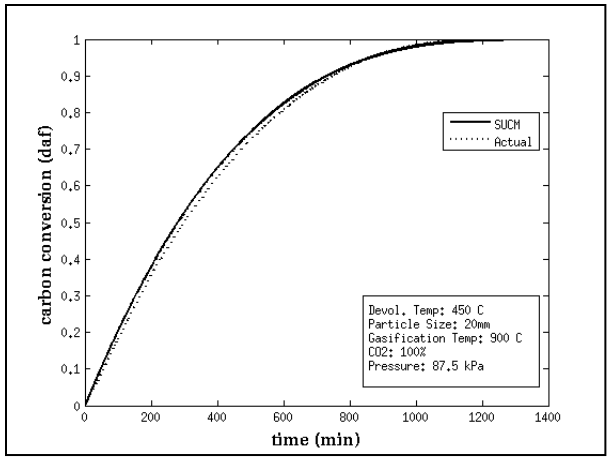

Figure C 10: SUCM for 40 mm particles prepared at 450°C.